

Development and evaluation of a motorcycle riding simulator for low speed maneuvering

Grottoli, M.

DOI

[10.4233/uuid:8f654bb3-e951-4bc7-a303-50adf79f8155](https://doi.org/10.4233/uuid:8f654bb3-e951-4bc7-a303-50adf79f8155)

Publication date

2021

Document Version

Final published version

Citation (APA)

Grottoli, M. (2021). *Development and evaluation of a motorcycle riding simulator for low speed maneuvering*. [Dissertation (TU Delft), Delft University of Technology].
<https://doi.org/10.4233/uuid:8f654bb3-e951-4bc7-a303-50adf79f8155>

Important note

To cite this publication, please use the final published version (if applicable).
Please check the document version above.

Copyright

Other than for strictly personal use, it is not permitted to download, forward or distribute the text or part of it, without the consent of the author(s) and/or copyright holder(s), unless the work is under an open content license such as Creative Commons.

Takedown policy

Please contact us and provide details if you believe this document breaches copyrights.
We will remove access to the work immediately and investigate your claim.

DEVELOPMENT AND EVALUATION OF A MOTORCYCLE RIDING SIMULATOR FOR LOW SPEED MANEUVERING

MARCO GROTTOLO



**DEVELOPMENT AND EVALUATION OF A
MOTORCYCLE RIDING SIMULATOR FOR LOW SPEED
MANEUVERING**

DEVELOPMENT AND EVALUATION OF A MOTORCYCLE RIDING SIMULATOR FOR LOW SPEED MANEUVERING

Dissertation

for the purpose of obtaining the degree of doctor
at Delft University of Technology
by the authority of the Rector Magnificus, Prof.dr.ir. T.H.J.J. van der Hagen,
chair of the Board for Doctorates,
to be defended publicly on Monday 19, April 2021 at 17:30 o'clock

by

Marco GROTTO

Master of Science in Mechatronics and Robotics,
Politecnico di Milano, Italy,
born in Taranto, Italy

This dissertation has been approved by the promotor.

Composition of the doctoral committee:

Rector Magnificus	chairperson
Dr.ir. R. Happee	Delft University of Technology, promotor
Prof.dr.ir. M. Mulder	Delft University of Technology, promotor

Independent members:

Prof.dr.ir. D.A. Abbink	Delft University of Technology
Prof.dr.ir. H. Vallery	Delft University of Technology
Prof.dr. H.H. Bülthoff	Max Planck Institute Tübingen Eberhard Karls Universität Tübingen, Germany
Dr.ir. T. Tamarozzi	Siemens Digital Industries Software, Belgium
Dr.ir. A.L. Schwab	Delft University of Technology



This research has been funded by the European Union's Seventh Framework Programme through the international consortium MOTORIST (Motorcycle Rider Integrated Safety) agreement No. 608092.

Keywords: Motorcycle Dynamics, Riding Simulator, Motion Cueing, Motion perception

Printed by: Ipskamp

Cover by: Original design by Emanuele and Edoardo Boccanfuso

Copyright © 2021 by Marco Grottoli

ISBN 978-94-6421-323-2

An electronic version of this dissertation is available at:
<http://repository.tudelft.nl/>.

*One never notices what has been done;
one can only see what remains to be done.*

Marie Skłodowska Curie

CONTENTS

Summary	xi
Abbreviations	xv
Symbols	xvii
1 Introduction	1
1.1 Driving simulators	2
1.2 Motorcycle riding simulators	3
1.3 Gap analysis	7
1.4 Scope of the thesis	10
1.5 Thesis structure	13
I Motorcycle simulator development: vehicle model and motion cueing	17
2 Motorcycle multibody model validation for Human-in-the-Loop simulations	19
2.1 Introduction	20
2.2 Methods	20
2.2.1 Motorcycle model	20
2.2.2 Rider balance assist	24
2.2.3 Lateral dynamics controller	26
2.2.4 Model validation	27
2.3 Results and discussion	29
2.4 Conclusions.	34
2.5 Acknowledgment	34
3 Objective evaluation of prediction strategies for optimization-based motion cueing	35
3.1 Introduction	36
3.2 Methods	37
3.2.1 Motion perception	37
3.2.2 Vehicle maneuvers	38
3.2.3 Predictive Motion Cueing Algorithm	39
3.2.4 Dependent variables	44
3.3 Results	47
3.3.1 Motion quality indicators	47
3.3.2 Motion cueing mechanisms	52
3.3.3 Workspace usage.	54
3.4 Discussion	55
3.5 Conclusions.	57
3.6 Acknowledgement	58

II	Motorcycle simulator evaluation: behavioral fidelity and perceived realism	59
4	Emergency braking at intersections: A motion-base motorcycle simulator study	61
4.1	Introduction	62
4.2	Method	63
4.2.1	Participants	63
4.2.2	Apparatus	63
4.2.3	Stimuli	66
4.2.4	Procedure	69
4.2.5	Measures.	70
4.3	Results	71
4.3.1	Simulator sickness and experienced workload	71
4.3.2	Effect of visual stimuli on riders' speed and braking performance	72
4.3.3	Comparison of braking performance between the motion and no-motion configurations	76
4.4	Discussion	76
4.5	Conclusions and recommendations	80
4.6	Supplementary material	80
5	Motorcycle simulator subjective and objective validation for low speed maneuvering	81
5.1	Introduction	82
5.2	Method	83
5.2.1	Riding scenario	83
5.2.2	Motion cueing	84
5.2.3	Dependent measures	86
5.2.4	Participants	91
5.2.5	Riding simulator	91
5.2.6	Procedure	92
5.3	Results	93
5.3.1	Replacing the HMD with a screen	93
5.3.2	Time histories comparison with real measurements	95
5.3.3	Riding performance metrics and realism.	95
5.3.4	Simulator presence	99
5.3.5	Simulator sickness	101
5.4	Discussion	101
5.4.1	Simulator evaluation.	101
5.4.2	Effect of simulator motion	102
5.4.3	Considerations on visualization technologies	103
5.5	Conclusions.	103
5.6	Acknowledgment	103
6	Discussion and Conclusions	105
6.1	Main findings	106
6.1.1	Part I: Motorcycle simulator development	106
6.1.2	Part II: Motorcycle simulator evaluation	107

6.2	Discussion	108
6.2.1	Usability of the high fidelity motorcycle model.	108
6.2.2	Evaluation of optimization-based motion cueing	109
6.2.3	Human-in-the-loop evaluation of the riding simulator	110
6.3	Conclusions.	111
6.4	Recommendations	112
A	Motorcycle multibody model	115
A.1	Introduction	116
A.2	Reference frames	116
A.3	Three-point (PQR) method	116
A.4	Bodies properties	117
A.5	Model topology	117
B	Adaptive filter-based motion cueing algorithm	121
B.1	Introduction	122
B.2	Reference frames	122
B.3	Map In	123
B.4	High-Pass linear.	124
B.5	Low-Pass linear	124
B.6	High-Pass rotational	125
B.7	Adaptive algorithm	126
B.8	Platform kinematics.	126
	References	127
	Acknowledgements	141
	Curriculum Vitae	143
	List of Publications	145

SUMMARY

Driving simulators have been extensively used over the last decades and technological advancements have propelled their development for cars, trucks and other vehicles with four (or more) wheels. This dissertation focuses on the use of driving simulators for two-wheeled vehicles and in particular on the development and evaluation of a motorcycle riding simulator for low speed maneuvering. The reason to focus on low speed maneuvers is related to the unstable nature of motorcycles at low speeds. A dedicated riding simulator could be used to train riders to cope with vehicle instabilities and develop active safety systems that can help them to maintain the vehicle balanced and avoid falling.

Existing riding simulators adopt simplified vehicle models to simulate motorcycle dynamics. In some cases, advanced non-linear models are adopted, but their validation is not always sufficiently described for the simulator application. Once the model has been integrated in the complete simulator, the results of its real-time simulation are used to provide feedback to the simulator rider through the cueing systems. Motion cueing is particularly interesting due to the peculiar vehicle dynamics of two wheelers. Different approaches are found in literature, however the applied motion cueing methods are not based on understanding of human motion perception. Finally, the riding simulator should also be validated for its usage in the specific application domain and its fidelity and behavioral validity are often neglected.

In this thesis, specific aspects of development and validation of a riding simulator for low speed maneuvering are investigated. It addresses the following research objectives:

1. Analysis of the usability of a high fidelity motorcycle model for the reproduction of low speed longitudinal and lateral maneuvers,
2. Evaluation of optimization-based motion cueing and the adopted prediction strategy for the reproduction of low speed longitudinal and lateral maneuvers, and
3. Evaluation of riding simulator realism when reproducing longitudinal and lateral maneuvers at low speed.

The first two research objectives are related to development aspects of riding simulator, and each objective has been addressed in a separate chapter. Chapter 2 presents the development and validation of a high fidelity motorcycle model, in combination with powertrain, braking system and tires. A specific set of longitudinal and lateral maneuvers at low speed has been performed on an instrumented motorcycle. The experimental results have been used to update and validate the developed motorcycle model in the speed range between 0 and 10 meters per second. Two dedicated controllers have been developed and coupled with the motorcycle model to stabilize it during the transition from and to standstill, and to steer the motorcycle for the reproduction of lateral

maneuvers. Results show that the developed model accurately reproduced longitudinal and lateral accelerations that were measured on the actual vehicle, with the steering controller introducing a lag in the lateral acceleration. The model was also integrated in a riding simulator for human-in-the-loop simulations.

Chapter 3 addresses the second research objective on the evaluation of optimization-based motion cueing algorithms. The investigation focuses on the usability of such cueing algorithms for the reproduction of low speed maneuvers. For practical reasons, four-wheeled vehicles were studied first. An optimization-based motion cueing algorithm was developed and the adoption of two prediction strategies was evaluated. The first prediction strategy, *oracle*, assumes perfect knowledge of future vehicle motion, it cannot be used for driver-in-the-loop simulations and it is considered as a reference to evaluate the best motion cueing quality that can be achieved. The second strategy, *constant*, ignores changes in the future reference and assumes a constant reference equal to last vehicle status. To evaluate the effects of the adopted prediction strategy, motion cueing quality indicators have been defined to quantify correlation, delay and absolute difference with respect to the reference motion to reproduce on the simulator. As expected, the results show that the ideal prediction provides the best motion cueing quality, managing the use of the limited workspace by coordinating multiple motion cueing mechanisms. The analysis of the results also provides indications of what should be improved for the development of advanced prediction strategies for optimization-based motion cueing algorithms.

The second part of this thesis is dedicated to the third research objective on the evaluation of simulator realism, where two experiments were carried out on a motion based riding simulator for its evaluation in reproducing longitudinal and combined longitudinal and lateral dynamics maneuvers. For both experiments, the motorcycle model presented in Chapter 2 was adopted, after integration in the riding simulator. In Chapter 4 only longitudinal dynamics maneuvers were performed. The simulator evaluation, and the effect of added physical motion, was carried out by analyzing rider's behavior and the assessment of simulator presence. Results show that the 12 participants were able to accelerate from 0 to 13.9 meters per second and brake to standstill without falling. The addition of simulator motion did not have significant influence on the task performed, but it had a significant positive influence on simulator presence.

In Chapter 5, another experiment with 12 participants was performed to validate the riding simulator for both longitudinal and lateral dynamics maneuvers in the speed range between 0 and 10 meters per second. Participants were asked to reproduce the same maneuvers that were used to validate the motorcycle model. Results show that the participants were able to reproduce the maneuvers without falling or losing balance, with the turning maneuver resulting often in large path deviation. Overall, the simulator realism measured was rated to be sufficient, with good agreement between simulator and experimental results. The addition of physical simulator motion had a limited, positive, influence on braking performance and on simulator presence, particularly on the feeling of being involved in the virtual environment.

This thesis addresses the three research objectives regarding development and validation of riding simulators for low speed maneuvering. With respect to the first objective, a validated high fidelity motorcycle model with dedicated control strategies can

be used in a riding simulator for the reproduction of low speed longitudinal and lateral maneuvers. This allows future applications of riding simulators for the subjective evaluation of model modifications before the availability of physical prototypes, and the possibility to evaluate safety systems to support riders. On the second objective of this thesis, it can be concluded that the adoption of optimization-based motion cueing algorithms has the potential to improve motion cueing quality. To benefit from this potential, dedicated prediction strategies need to be investigated to accurately estimate future vehicle motion. Finally, in relation to the third objective of this thesis, the developed riding simulator provides a sufficient level of realism for the reproduction of longitudinal and lateral maneuvers at low speeds, while the addition of physical motion provides minor positive effects on riding performance and perceived simulator realism. In conclusion, the presented simulator shows that riding simulators can be used for research and development applications at very low speeds, including from and to standstill.

ABBREVIATIONS

ABS	Anti-lock Braking Systems
ADAS	Advanced Driver-Assistance Systems
CC	Cubic Centimeter
COG	Center of Gravity
CVT	Continuously Variable Transmission
DIL	Driver-In-the-Loop
DOF	Degrees of Freedom
ECU	Electronic Control Unit
HMD	Head Mounted Display
HP	High-Pass
HuIL	Human-in-the-Loop
IMU	Inertial Measurement Unit
LP	Low-Pass
MCA	Motion Cueing Algorithm
MISC	Misery Scale
MPC	Model Predictive Control
NCBF	Non-Centroidal Body Fixed
PTW	Powered Two Wheeler
rpm	revolutions per minute
VR	Virtual Reality

SYMBOLS

Symbol	Unit	Description
N	kgms^{-2}	Newton, measurement unit of force
<i>x</i>	m	Position
<i>v</i>	ms^{-1}	Velocity
<i>a</i>	ms^{-2}	Acceleration
<i>g</i>	ms^{-2}	Gravitational acceleration
ω	rads^{-1}	Rotational velocity
$\boldsymbol{\omega}$		Vector of rotational velocities
α	rads^{-2}	Rotational acceleration
$\boldsymbol{\alpha}$		Vector of rotational accelerations
<i>t</i>	s	Time
<i>F</i>	N	Force
F		Vector of orthogonal forces
<i>T</i>	Nm	Torque
M		Vector of orthogonal torques
<i>I</i>	kgm^2	Moment of inertia
I		Moment of inertia tensor

1

INTRODUCTION

1.1. DRIVING SIMULATORS

DRIVING simulators have been in use since the 1960s and technological advances of the last decades propelled their use in different domains for cars, trucks and other vehicles with four (or more) wheels. Currently, driving simulators are used in engineering for the development of new vehicles and control systems, but also from a psychological and medical perspective, to train and understand drivers. The functional elements used in a driving simulator are shown in Figure 1.1. The simulation computer processing block includes all computations required to compute vehicle motion relative to the environment, considering driver control actions, aerodynamics and road surface inputs. This block provides inputs to the sensory feedback generation block which produces sensory cueing commands or inputs to the sensory display device block. Given displayed sensory cues, the human operator (driver) senses this information and, based on training and experience, produces control inputs that are fed back to the simulation computer processing block. In Virtual Reality (VR) applications using Head Mounted Display (HMD), head orientation must also be provided to the simulation computer processing block.

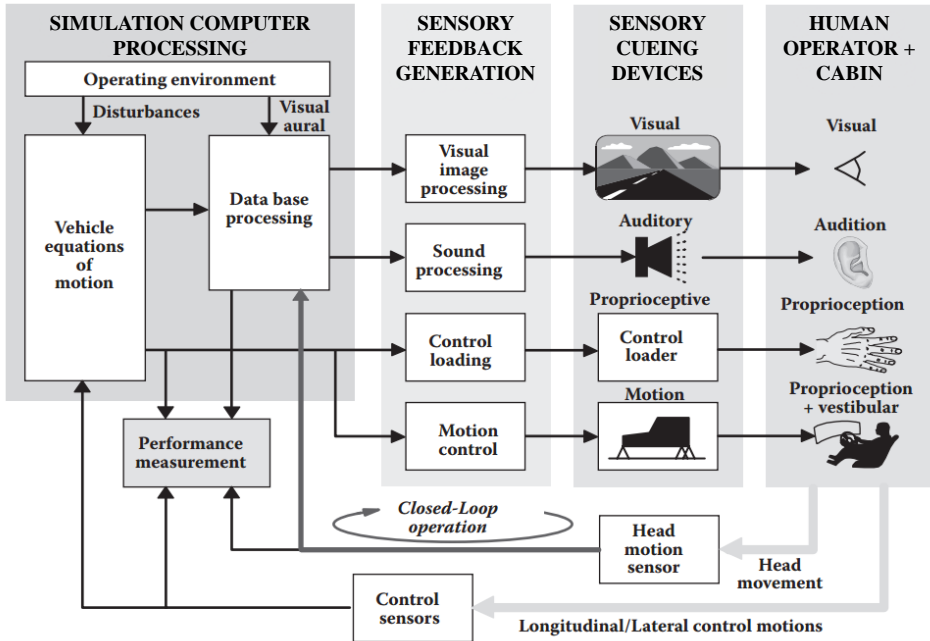


Figure 1.1: Functional elements of a driving simulator [56].

The major elements of a typical driving simulator are: cueing systems (visual, auditory, proprioceptive, and physical motion), vehicle dynamics, computational power, physical mock-up, measurement algorithms and data processing and storage.

Cueing systems are responsible for the stimulation of driver sensory and perceptual systems. In each of these systems the appropriate stimulus resulting from the drivers

control inputs must be computed and then accurately presented to the driver in real-time. Some cues, such as the steering feel, are a direct consequence of the driver's control actions and the resulting vehicle response. Other cues, like motion, are a function of the vehicle response to driver's input with the addition of independent inputs, such as vehicle-road interactions, aerodynamic forces and additional disturbances. Visual and auditory cues result from driver-vehicle interactions, but also have significant independent inputs provided by typical roadway elements (e.g., traffic, pedestrians, and traffic control devices) in the driving scenarios.

Vehicle dynamics are also critical to the development of driving simulators, together with vehicle-driver interaction, the effects of controls, the presentation of driving scenarios (road profiles, traffic control devices, traffic and pedestrians and roadside objects) and sensors and measurement algorithm. These aspects together represent important factors to achieve a valid representation of the driving environment.

Driving simulators have been developed in the automotive industry for many different types of vehicles and with various purposes. This dissertation focuses specifically on the use of driving simulators for two-wheeled vehicles.

1.2. MOTORCYCLE RIDING SIMULATORS

IN this section, some of the most advanced research simulators developed specifically for motorcycles are summarized. A complete list of riding simulators and their cueing systems that have been analyzed in this study is reported in Table 1.1.

The first driving simulator for a two-wheeled vehicle found in literature was developed by Honda, starting from 1988 and presented in [162]. This simulator adopted a motorcycle mock-up with seven actuators used to control 5 Degrees of Freedom (DOF) (lateral, roll, pitch, yaw and steering) with a projection screen and stereo sound generation. The simulator included a motorcycle model with 4 DOF. However, the motorcycle simulator was not usable due to the methodology adopted to render the roll motion and the steering feeling. The reproduction of roll motion by means of the physical mock-up made the riders unable to control the motorcycle model due to the lack of centrifugal force that compensates the lateral acceleration. It was also found that the rider had the tendency to steer in the direction of the turn, making it very difficult to maneuver in the intended direction.

After 1990, Honda developed a second prototype, with an actuated mock-up able to reproduce roll, pitch and yaw motion. An improved vehicle model was implemented, able to reproduce different maneuvers (i.e., slalom, lane change and obstacle avoidance) and riding conditions (i.e., riding at low speed and riding with cross wind) [89]. Finally, in 2002, Honda commercialized a new version of their riding simulator, with a 6 DOF motion platform, actuated steering and a HMD for visualization [22], see Figure 1.2. Although the Honda simulator represents the first advanced riding simulator, the adopted motorcycle model was based on simplified equations and a detailed subjective evaluation was not found in literature.

Another advanced riding simulator was developed by the PERCRO Laboratory of the School of Advanced Studies of Pisa. Their MORIS (Motorcycle Rider Simulator) simulator was presented in 2003. Similarly to the Honda simulator, they also adopted a 6 DOF motion system, but instead of a HMD they used a large projection screen. The MORIS

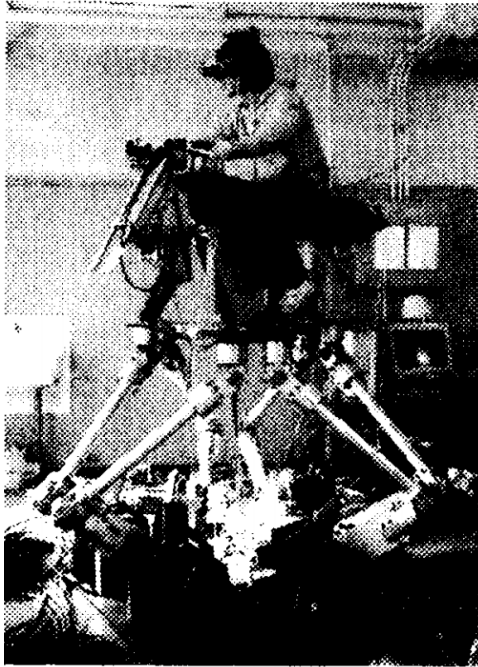


Figure 1.2: Motorcycle riding simulator developed by Honda [22].

simulator is shown in Figure 1.3. This simulator was specifically designed as an engineering tool to be used by the motorcycle manufacturer to evaluate vehicle design modifications [52, 51]. A subjective evaluation was conducted with 20 subjects. Each subject had a 20 minutes trial without training to freely ride the motorcycle. The results showed a good overall sense of realism without symptoms of motion sickness [50]. Also this simulator adopted a simplified vehicle model, while additional details were reported on the adopted washout Motion Cueing Algorithm (MCA) [2].

In the early 2000s, a research group of the Mechanical Engineering Department of the University of Padua presented a first prototype of a riding simulator [30]. By 2011, they published the development and validation of their motorcycle simulator for rider training and for the development of innovative devices to improve rider safety. The mechanical mock-up was able to reproduce motion in 5 DOF: roll, pitch, yaw, lateral and steering. The visualization setup included a 180 degrees projection screen with a 5.1 surround system for the reproduction of acoustic cues. The simulator is shown in Figure 1.4. For the first time, the simulator adopted a non-linear motorcycle multibody model with 14 DOF [33, 31]. The results of the simulation of the motorcycle model were also compared with data measured on a real motorcycle for both slalom and cornering maneuvers [31]. Subjective evaluation was also performed with 20 subjects reproducing a set of maneuvers, including longitudinal, lateral and combined longitudinal and lateral dynamics. The results of the vehicle model simulation were comparable with experimental data and the subjective evaluation resulted to be satisfactory.



Figure 1.3: Motorcycle riding simulator developed during the MORIS project by the PERCRO Laboratory of the School of Advanced Studies of Pisa [50].



Figure 1.4: Motorcycle riding simulator developed by the University of Padua [32].



Figure 1.5: DESMORI simulator developed at the Würzburger Institut für Verkehrswissenschaften (WIVW) [160].

The DESMORI simulator, see Figure 1.5, was developed at the Würzburger Institut für Verkehrswissenschaften (WIVW). This simulator introduces a series of improvements with respect to the previously developed simulators. Similar to the MORIS simulator, it uses a real motorcycle mounted on a 6 DOF motion platform as simulator mock-up, where the original motorcycle controls are used to measure rider's input to apply on the motorcycle model. Additional features introduced by this simulator are: a visualization system with multiple projectors and a cylindrical screen for wide field of view, a force sensor used to measure the roll torque that the rider applies to the motorcycle by shifting his/her weight on the vehicle and small screens used to reproduce rear view mirrors and motorcycle dashboard. Furthermore, the rider was provided with a customized vest connected to a rope towing mechanism actuated to provide proprioceptive feedback of acceleration. The motorcycle model adopted in this simulator has a similar complexity to what was integrated in the simulator of the University of Padua, but it is based on a commercially available software dedicated for real-time simulation of 2-wheeled vehicles [160]. Objective comparison of model simulation results with experimental data was not reported. Subjective evaluation was carried out with progressive increment of cueing system starting with only visual and adding (one by one) auditory, proprioceptive and motion. The effects of visual and acoustic cues achieved high ratings, while proprioceptive and motion cueing were attributed a medium to low influence on simulator realism.

Another motorcycle simulator was developed by Cruden, using a Ducati motorcycle as mock-up, with instrumentation mounted to measure rider's input of throttle, brakes, clutch, gear shift, steering torque sensor and rider's body position sensor. In this simula-



Figure 1.6: Motorcycle riding simulator developed by Cruden [155].

tor, the visualization of the virtual environment is provided using a HMD, while acoustic feedback is provided by a surround system. The motorcycle model is based on Cruden proprietary software, but no objective comparison with experimental data is reported. This simulator was subjectively evaluated for speed perception and path following, in the speed range between 50 and 120 kmh⁻¹. The results show a satisfactory level of riding performance and simulator presence. The rider's body position sensors resulted to be significant to reduce sickness when no motion was applied, while the addition of motion cueing influenced both riding performances and subjective evaluation [155, 156].

Table 1.1 provides an overview of riding simulators and their cueing systems. The table includes information about motion, steering, visual and sound systems used in the analyzed simulators. We can see that in terms of adopted motion system, most of the riding simulators are able to reproduce three or more DOF of motion. When only a few are reproduced, typically rotations are preferred. When only 1 DOF was selected, it was always the motorcycle roll angle. Regarding steering feedback, most of the simulators use active steering, with an electric motor applying torque at the handlebar. Only two simulators do not have active steering, but they still adopt elastic components to passively provide torque at the handlebar. Several simulators use projection systems or screens as visualization device, only two of them use HMD. All simulators have a sound system to provide acoustic cues.

1.3. GAP ANALYSIS

DURING the evolution of research oriented riding simulators, one of the aspects that has evolved over the years is the vehicle model adopted. Early riding simulators adopted simplified vehicle models, mostly based on linear equations of motion capable to reproduce the dynamics of a two wheeler for a specific speed. An important leap forward was done by the University of Padua with dedicated work in motorcycle mod-

Table 1.1: Overview of the riding simulators for research and development with respect to their cueing systems.

Simulator	Motion system (vestibular)	Steering actuation (proprioceptive)	Visualization system (visual)	Sound system (acoustic)
Honda [22]	6 DOF	Yes	HMD	Sound available
MORIS [50]	6 DOF	Yes	Large projection screen	Sound available
University of Padua [34]	4 DOF (roll, pitch, yaw, lateral)	Yes	Large projection screen	Surround system
IFSTTAR [112]	3 DOF (roll, pitch, yaw)	Yes	3 screens setup	Surround system
University of Nottingham [143]	1 DOF	Yes	Large projection screen	Surround system
Monash University [133]	3 DOF (roll, pitch, vertical)	No	Single screen	Stereo sound
WIVW static I [160]	1 DOF (passive roll)	No	Medium size flat projection screen	Stereo sound
WIVW static II [159]	1 DOF (passive roll)	Yes	3 screens setup	Stereo sound
DESMORI [160]	6 DOF	Yes	Large curved projection screen	Headphones integrated in helmet
BMW Motorrad [74]	6 DOF	Yes	Large flat projection screen	Surround system
Cruden [155, 156]	6 DOF	Yes	HMD	Headphones integrated in HMD
MOTORIST (this thesis)	6 DOF	Yes	HMD or screen	Headphones integrated in helmet

eling and real-time simulation [33]. This model is based on multibody theory and can be used to simulate the non-linear behaviors of a two wheeler, both at unstable and stable speeds. Such models can also be used to calculate the steering torque that the rider would feel at the handlebar while riding the vehicle. Although this work represented a great improvement in motorcycle modeling, many simulators kept using simplified models. Some riding simulators even adopted models of four wheels vehicles, inverting and amplifying the roll motion computed by the model to imitate the behavior of a two wheeler [143, 133]. Such models approximate the vehicle motion, but do not provide an accurate reproduction of the dynamics of an actual two wheeler. More recent riding simulators started to adopt advanced motorcycle vehicle models, with solutions based on proprietary software [160, 74, 156].

In most of the analyzed simulators, the validation of the adopted vehicle model for the maneuvers to be reproduced on the simulator is not reported. In cases where the model was validated against experimental data, the validation was typically performed for maneuvers at velocities above 10 m s^{-1} . Although some of these simulators have been used to investigate maneuvers starting from standstill, most of them focused on the reproduction of maneuvers with vehicle velocities above 10 m s^{-1} , avoiding the issues associated with the reproduction of the intrinsic unstable nature of two-wheeled vehicles at very low speed.

The solution of the vehicle model provides the necessary information to render the vehicle motion to the rider of the simulator. This is achieved by means of a control algorithm responsible to generate a reference signal for the motion system of the simulator. As reported in the riding simulators overview, most of the advanced riding simulators adopt a 6 DOF motion system to provide physical roll to the riders of the simulator. When a subset of DOF was chosen, the preference was always given to rotations and if only 1 DOF was selected it was always the motorcycle roll angle. Given the possibility to control the physical motion of the simulator, it is crucial to understand how to control it. For this reason, MCAs are adopted to compute how the motion system should be controlled starting from the integration of the vehicle's equations of motion.

Early simulators adopted classical washout MCAs, derived from aircraft and four-wheeled vehicles simulators. The simulators using a four-wheeled vehicle model controlled the motion system to implement the inverted roll angle obtained from the vehicle simulation (i.e., lean left in a left turn and vice versa). In one study [75], a comparison between a washout based MCA and a simplified approach is presented. The washout based motion cueing adopted a high pass filter to extract the high frequency component of the roll motion that was rendered using the motion system, while the low frequency content was rendered using visual cue. The result showed that the riders of the simulator preferred the simplified approach, where the computed roll angle of the motorcycle was split in two equal parts and reproduced with physical simulator roll in the direction of the turn and visualization roll in the opposite direction. Thereby, the physical motion rendered is reduced to a half of the computed roll angle, while the remaining part was rendered by rotating the visual horizon in the opposite direction, resulting in a total roll equal to the value computed by the vehicle simulation. Another study focused on the combination of visual and motion information in a simulator study where riders could choose visual and physical roll during a turn with given radius and at a specific speed

[102]. In the latter study, the physical roll of the simulator was limited and the rider could adjust the visual roll to find the best compromise. Results show that the participants could be divided in two groups, some preferred more physical roll and other more visual roll. Another recent study [156] combined a washout MCA with a direct workspace management algorithm. Here the motorcycle roll angle computed by the vehicle model is scaled to 25% and then filtered with a first order low-pass filter. Results show that this algorithm was preferred to a no motion condition with improved simulator presence and better performances in the lane keeping maneuver. The reported literature shows the relevance of physical and visual motion cueing in particular for roll. However the applied motion cueing methods are not based on understanding of human motion perception.

Independently from the motorcycle model and the MCA adopted by the simulator, it is important to understand how the overall system is perceived by the subject of a simulator study in comparison with their real life experience. All the studies mentioned in the previous section largely focused on the development aspects of motorcycle riding simulators. Most studies report subjective evaluation [22, 50, 34, 143, 133, 160, 74, 156], analyzed with a dedicated experiment with subjects performing a set of maneuvers. Out of these studies, only some reported the occurrence of motion sickness [50, 133, 160, 74, 156]. Only two studies investigated the effects of physical motion [160, 156], which significantly improved simulator presence, but the magnitude of these improvements ranked last with respect to visual, acoustic and proprioceptive cues.

In summary, in this thesis three research gaps are identified. The first is on motorcycle modeling for the simulation of low speeds maneuvers. Detailed models are available in literature, but the issues related to two-wheelers instability at low speeds hamper the use of these models, and favors the adoption of simplified vehicle models in riding simulators. The second gap identified is the rendering of physical motion in combination with visual cues. Studies analyzed from literature have tried to address this challenge by combining physical and visual motion, however the development of a MCA based on human motion perception could provide a valid alternative. Finally, the third research gap investigated is the validation of the riding simulator for low speed maneuvers. Simulator validation is a crucial aspect for the adoption of riding simulators, but it is often overseen. The scope and the research objectives of this thesis addressing these gaps are described in the next section.

1.4. SCOPE OF THE THESIS

THIS thesis focuses on the development and evaluation of a motorcycle riding simulator for low speed maneuvering. The reason to focus on low speed maneuvers is related to the unstable nature of motorcycles at low speeds. A dedicated riding simulator could be used to train riders to cope with vehicle instabilities and develop active safety systems that can help riders to maintain the vehicle balanced and avoid falling. The research objectives (RO) of this thesis are introduced below and highlighted in text boxes.

Research Objective 1

Analysis of the usability of a high fidelity motorcycle model for the reproduction of low speed longitudinal and lateral maneuvers.

The first effort presented is the development, validation and fidelity of the motorcycle model used in a riding simulator. The model provides all information for the generation of artificial cues (visual, motion, haptic, acoustic, etc.) and therefore, an accurate vehicle model in the relevant range of applications is necessary [54]. Previous studies have already addressed the modeling of a motorcycle for different purposes, from the study of vehicle stability [139] to the development of control systems [110, 99]. Ref. [33] focused on an accurate motorcycle model implementation to be used on a riding simulator and its successful validation with experimental data. Nevertheless, all these studies focused on motorcycle model validation and usage for velocities above 10 ms^{-1} .

This thesis deals specifically with low speed maneuvering of motorcycles, presenting the development of a high fidelity model based on multibody dynamics coupled with models of motorcycle sub-systems such as: engine, transmission, clutch, brakes and tires. In contrast with car driving simulators, where a four-wheeled vehicle remains always stable, a two-wheeled vehicle becomes unstable at low speed hampering the usage of riding simulators for low speed maneuvering. Another difference between four-wheeled and two-wheeled vehicles is in the way that a turning maneuver is performed. A four-wheeled vehicle rolls in the opposite direction of the turn, with the occupant of the vehicle perceiving a centrifugal force pushing him or her out of the turn. In contrast, a two-wheeled vehicle leans into the turn, balancing the lateral force with a component of the gravitational acceleration, leaving only a vertical component of the force pushing the rider on the vehicle seat. This thesis presents novel control techniques to keep the motorcycle model stable at very low speeds, virtually replacing the foot on the ground used by the rider of a real motorcycle and allowing the use of the model on a riding simulator. The presented model is validated with experimental data acquired on a real motorcycle, for a set of longitudinal and lateral dynamics maneuvers.

Research Objective 2

Evaluation of optimization-based motion cueing and the adopted prediction strategy for the reproduction of low speed longitudinal and lateral maneuvers.

The second effort presented in this thesis is related to the MCA adopted to render motion to the rider of the simulator. One of the most commonly used MCAs is known as the classical washout algorithm [135, 127, 128]. Classical MCAs are based on filters, where linear accelerations and angular velocities are first scaled and then high-pass filtered to remove constant signal content (washout). In addition, low-pass filters are used for longitudinal and lateral accelerations, where tilt coordination is adopted to use gravitational acceleration to reproduce sustained accelerations. These algorithms present some limitations. The tuning process is not trivial and it is often subjective. Different approaches have been studied to objectively tune the parameters of classical MCAs by following a specific process [59] or by optimizing a set of dedicated objective metrics of

motion cueing quality [15, 17]. Nevertheless, the results obtained from these techniques can still be improved by further subjective tuning. The tuning process of classical MCAs is specific to the set of maneuvers to reproduce on the motion simulator. Since classical MCAs do not include knowledge of the motion system's limitation, the tuning process must be repeated if the set of maneuvers changes. Otherwise, the trajectory obtained by the classical MCA could be exceeding the physical boundaries of the motion system. More recently, another approach based on optimization has become popular [37, 49, 3, 57]. Unlike filter-based MCAs, the optimization-based approach uses Model Predictive Control (MPC) to compute an optimal solution, within system limitations, using an internal model of the motion system to predict the future system response [126, 103, 154, 13]. This new approach takes into account motion system limitations and the tuning is achieved with weighting factors on linear and rotational motion cues. The optimization-based MCA has shown multiple advantages with respect to the classical algorithm, both in terms of workspace usage and subjective evaluation, when the vehicle trajectory is completely known in advance (passive driving) [24]. However, other challenges are introduced with the usage of predictive MCA. Compared to the classical MCA, this algorithm requires more computational time to solve an optimization problem at each time step of the algorithm, making it more challenging to adopt for more common Driver-In-the-Loop (DIL) simulations (active driving). Another aspect to consider is that the predictive MCA requires a future reference of the motion to reproduce on the simulator to compute a prediction of the system response. When using the predictive MCA in DIL simulations, assumptions regarding the future reference signals must be made. Previous studies have already addressed the issue of providing a future reference for the predictive MCA. For example, the vehicle motion recorded on a circuit is used to provide a better reference for future laps [11], or a neural network is trained using simulated data to predict the future reference motion [107]. However, it remains unclear how the prediction strategies adopted influence the quality of the motion cueing.

In this thesis a study has been conducted to understand the potential of optimization based MCAs when different prediction strategies are adopted. The first strategy corresponds to the ideal case in which the future motion to be reproduced on the simulator is known, as if it could be perfectly predicted. This cannot be applied for active driving but represents the perfect strategy which is expected to best reproduce the reference motion and therefore it is assumed here as a reference. The second strategy assumes a constant motion as future reference, ignoring every possible variations from the current status. For practical reasons the MCA study in Chapter 3 focused on four-wheeled vehicles. Chapter 6 outlines the perspective of MCA for motion cueing in two-wheelers.

Research Objective 3

Evaluation of riding simulator realism when reproducing longitudinal and lateral maneuvers at low speed.

Achieving a sufficient level of simulator realism remains a challenge. Previous studies have presented the development and evaluation of riding simulators for rider training, evaluation of vehicle design changes and development of active safety systems, but all of them focused on motorcycle maneuvering at high speed (i.e., above 10 ms^{-1}), where

the motorcycle vehicle dynamics become stable [138]. The riding simulator realism for low speed maneuvering is investigated in this thesis with a specific focus on the speed range between 0 and 10 ms^{-1} and evaluated with respect to motion cueing.

To investigate the third research objective of this thesis, a motion based riding simulator has been developed, the MOTORIST simulator [19], shown in Figure 1.7. The physical mock-up is based on a Piaggio Beverly motorcycle instrumented to measure rider's input of throttle, brakes and steer. No gear shift or clutch control are present on the motorcycle, as it has a Continuously Variable Transmission (CVT) with a multi disk centrifugal clutch. The front wheel of the motorcycle was replaced by an electric motor to provide torque feedback on the handlebar. Motion cueing is provided with a 6 DOF motion system while visual cues are provided using either an HMD integrated in the motorcycle helmet, or a 22 inch screen placed in front of the simulator. Acoustic cues are provided with stereo speakers integrated in the helmet.

1.5. THESIS STRUCTURE

THIS thesis is divided in two parts, see Figure 1.8. In the first part, the motorcycle simulator development is discussed, and is comprised of Chapters 2 and 3. In the second part, the simulator evaluation results are described, and is comprised of Chapters 4 and 5. The chapters from two to five contain the main contributions, mostly based on peer-reviewed scientific publications in conferences and journals.

Chapter 2 describes the development of the motorcycle model. The presented model also includes engine, transmission, brakes and tires. A specific set of longitudinal and lateral maneuvers previously performed on a real motorcycle are used to validate the vehicle dynamics in the speed range between 0 and 10 ms^{-1} . This chapter is based on conference publication [66] and it is related to the first research objective.

Chapter 3 presents an objective evaluation of optimization based MCA with different prediction strategies. Dedicated metrics are used to evaluate the influence of the adopted prediction strategy on motion cueing quality and motion system workspace utilization. This chapter is based on the journal publication [68] and it is related to the second research objective.

Chapter 4 is related to the usability and validity of the riding simulator in an experiment related to rider hazard anticipation. The reproduced scenario includes only longitudinal maneuvers reproduced with the motorcycle model presented in Chapter 2 (based on the journal publication [95]). In Chapter 5, the validation of the riding simulator for both longitudinal and lateral maneuvers is presented. Together, these chapters address the third research objective.

The final chapter provides an overall discussion of the results and final conclusions. Details on the developed motorcycle model (Chapter 2) and the adopted motion cueing algorithm (Chapters 4 and 5) are in Appendices A and B, respectively.



Figure 1.7: MOTORIST motorcycle riding simulator adopted in this thesis.

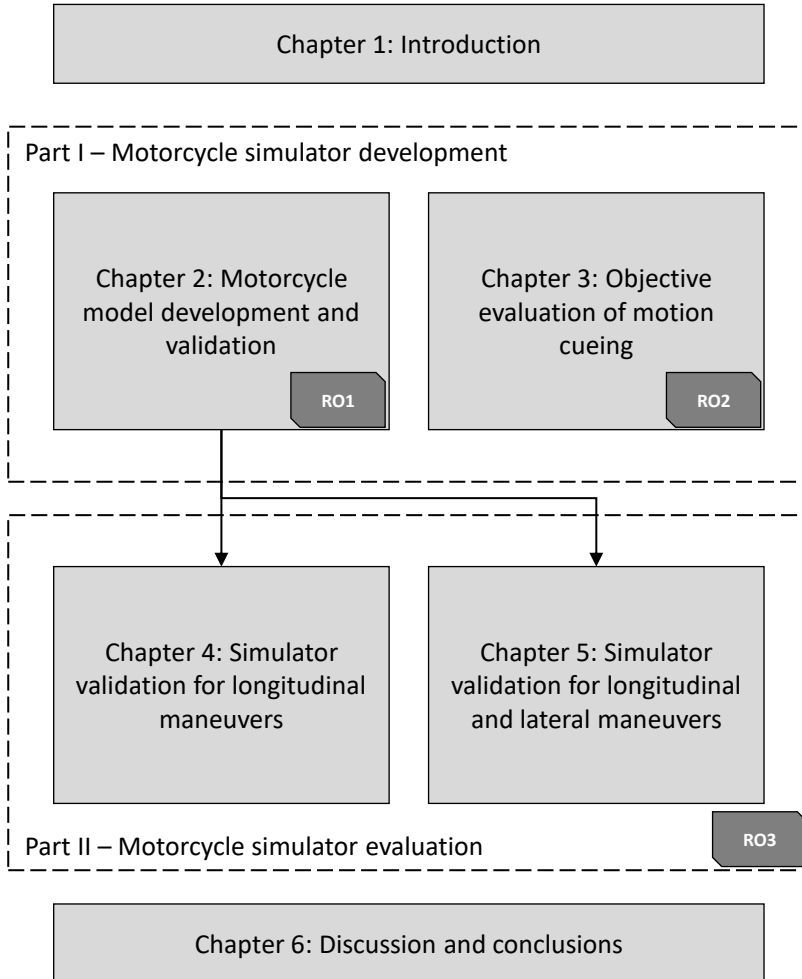


Figure 1.8: Graphical representation of thesis structure.

I

MOTORCYCLE SIMULATOR DEVELOPMENT: VEHICLE MODEL AND MOTION CUEING

2

MOTORCYCLE MULTIBODY MODEL VALIDATION FOR HUMAN-IN-THE-LOOP SIMULATIONS

Driving simulators are widely used for research and training for vehicles with four or more wheels. Simulators for two-wheeled vehicles, such as motorcycles, are not as common. This chapter presents the development of a multibody motorcycle model and its validation in the speed range between 0 and 10 m s^{-1} for use in a riding simulator. One of the difficulties for the realization of a riding simulator is given by the unstable nature of motorcycles at low velocity. This instability has been previously addressed using highly simplified vehicle models. In this work an alternative approach is presented, where the lateral dynamics of the motorcycle model are augmented (stabilized) only for velocities below 3 m s^{-1} . Whereas previous models employ simplified dynamics of the powertrain, in this chapter detailed models of engine, clutch and variable transmission are adopted. The model has been validated using measurements obtained with an instrumented motorcycle. Results show accurate reproduction of the motorcycle dynamics for both longitudinal and lateral dynamics. The motorcycle model is integrated in a riding simulator for human-in-the-loop simulations with positive subjective evaluation results.

This chapter as been published as:

Marco Grottooli, Francesco Celiberti, Anne van der Heide, Yves Lemmens, and Riender Happee. "Motorcycle multibody model validation for Human-in-the-Loop simulation". In: *Driving Simulation & Virtual Reality Conference & Exhibition*. 2019.

2.1. INTRODUCTION

DRIVING simulators are extensively used in a great variety of studies in research and training for cars, trucks and other ground vehicles with four or more wheels. In such simulators, the driver input actions drive a vehicle model which is solved in real-time. The output of the model simulation is used to provide artificial cues (visual, motion, haptic, acoustic, etc.) of the vehicle responses to the driver. The fidelity of the model strongly influences the accuracy of these cues and therefore, the realism that can be reached by the simulator. In order to guarantee the usability of simulator, it is crucial that the vehicle model captures the dynamics of the vehicle in the range of the tasks at hand, to allow the driver to experience as closely as possible the real vehicle behavior, independently of the cueing apparatus.

In the context of two-wheeled vehicles, riding simulators can be beneficial for the purpose of training riders to cope with the complex motorcycle dynamics, particularly at low speed, when the vehicle instability becomes more difficult to simulate properly. The reproduction of such scenarios on a riding simulator is known to be a challenge which hampers the usability of riding simulators at low velocities.

Previous studies have already addressed the modeling of a motorcycle for the study of vehicle stability [139] and for the development of control systems [110, 99]. Another study [33] focused on an accurate, yet efficient, motorcycle model implementation to be used on a riding simulator. It presented a detailed description of the implemented motorcycle model, together with a validation by comparison with experimental data acquired with an instrumented motorcycle. In all the presented maneuvers, the motorcycle model showed very good agreement with the experimental data. Nevertheless, the lowest speed reached by the motorcycle in all presented maneuvers was 10 m s^{-1} . In addition, only a simplified model of the motorcycle's powertrain was implemented, where a simple proportional controller was used to compute the traction or braking torques at the wheels, to match the longitudinal velocity measured during experimental testings.

This chapter describes the validation of a high fidelity multibody model of a motorcycle, including engine, clutch and transmission, for a human-in-the-loop riding simulator in the speed range between 0 and 10 m s^{-1} . The following research questions will be addressed:

- Is the implemented model able to properly reproduce the dynamics of a real motorcycle?
- Can this model be integrated in a riding simulator for a realistic reproduction of the maneuvers performed on the real motorcycle?

2.2. METHODS

2.2.1. MOTORCYCLE MODEL

THE motorcycle considered in this study is a 300 Cubic Centimeter (CC) Piaggio Beverly scooter with variable transmission and independently actuated brakes. This particular type of motorcycle has been chosen due to its popularity, especially in urban environments. The motorcycle model presented has already been introduced in a previous study with the goal of reproducing low speed dynamics [72]. In another study

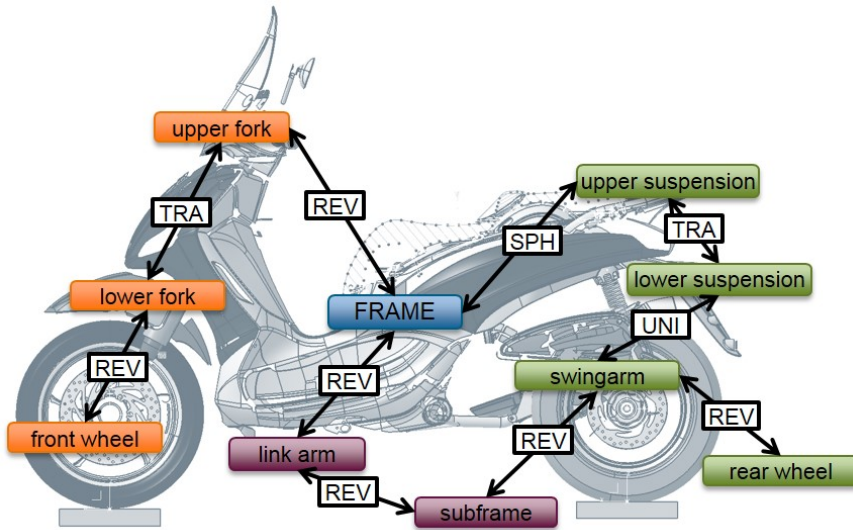


Figure 2.1: Motorcycle model scheme. Only the main bodies are represented. The connection blocks represent the type of ideal joint connecting the bodies. REV: revolute joint, TRA: translational joint, UNI: universal joint, SPH: spherical joint.

this motorcycle model has been integrated in a complete motorcycle simulator [19]. The model has two components: the dynamic model and the motorcycle subsystems.

DYNAMIC MODEL

The motorcycle dynamic model is responsible for reproducing the pure dynamics of the mechanism and is realized by applying the theory of multibody systems [79, 136]. The model includes 16 rigid bodies connected with 17 joints. The resulting DOF of the model are 13. A simplified scheme of the motorcycle model's bodies and their connections is presented in Figure 2.1. Details on the methodology used to model the vehicle and additional details are reported in Appendix A. In addition, a mass of 80 kg has been rigidly connected to the center of gravity of the motorcycle frame, to reproduce the rider. A simplification is made here, by neglecting the effect of rider body motions on the dynamics of the motorcycle. The inputs to the model are: the tire forces and torques, the steering torque, traction and braking torques applied at the wheels. The suspension forces are computed using realistic stiffness and damping curves obtained from the motorcycle manufacturer.

MOTORCYCLE SUBSYSTEMS

The modeled subsystems are: engine, CVT, clutch, final gear and brakes. These subsystems have been modeled using Simcenter Amesim.

Engine model

The engine model uses a look-up table generated from data available from the motorcycle manufacturer to compute the engine torque from engine speed and throttle han-

idle position. The relation between the throttle handle position and the power output is controlled by the Electronic Control Unit (ECU) of the vehicle via a mapping function, which is embedded in the look-up table in this model. In idle condition, the engine is designed to output 1.5 Nm of torque at the speed of 1,500 revolutions per minute (rpm). This torque is balanced by internal engine friction due to the rotation. The input to the model is the rider's throttle command and the outputs are the engine speed and torque. The engine model is connected to the CVT as shown in Figure 2.2.

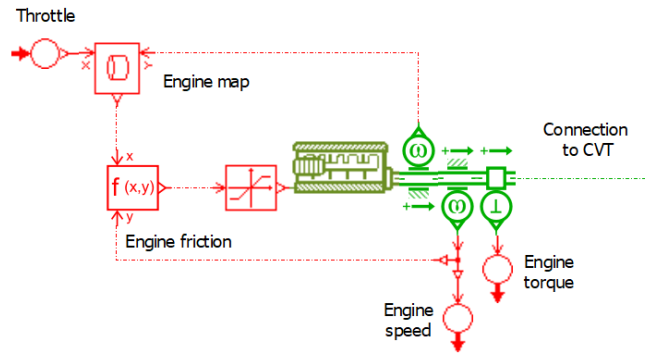


Figure 2.2: Engine model scheme. The input to the model is the rider's throttle and the output is connected to the Continuously Variable Transmission (CVT).

CVT model

The CVT consists of two pulleys connected by a belt. The driving pulley connects the CVT to the engine side, while the driven pulley is connected to the output shaft of the CVT. Both pulleys can move axially to change the radius at which the belt gets in contact with the pulleys and therefore changing the gear ratio. The CVT model used is based on a previous study [105], using the following assumptions:

- The belt and the pulleys have no mass,
- The belt moves only in axial direction,
- The belt is considered to be rigid, and
- There are no power losses in the transmission.

Using these assumptions the model is reduced to the balance between three forces acting on the system. From the equilibrium of these three forces, the axial displacement of the driven pulley can be computed and used to calculate the gear ratio of the CVT. The CVT model represents the connection between the engine and the clutch, as shown in Figure 2.3. It requires as input the engine speed and it gives as output the CVT ratio and the clutch shaft speed.

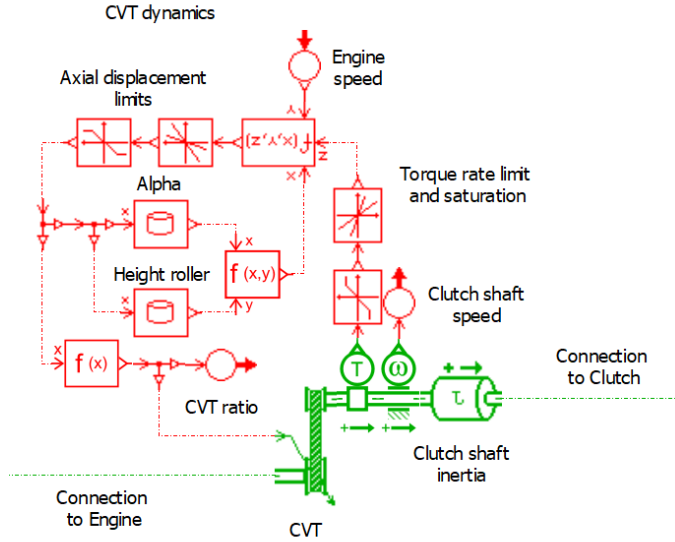


Figure 2.3: Continuously Variable Transmission (CVT) model scheme. The model connects the engine to the clutch. It takes the engine speed as input and it outputs the CVT ratio and the clutch shaft speed.

Clutch

The multi disk clutch is modeled using a rotary Coulomb friction model with hyperbolic tangent. The transition between opened and closed clutch happens at a certain pre-defined engine speed. In between there is a hyperbolic tangent Coulomb friction. The friction torque transmitted by the clutch is computed as follows:

$$T_{clutch} = s T_{Coulomb} n_{plates} \tanh\left(2 \frac{v_{rel}}{v_{trsh}}\right),$$

where s is a dimensionless signal between zero and one that controls the opening and closing of the clutch depending on the engine speed, $T_{Coulomb}$ is the maximum Coulomb friction torque expressed in Nm for one clutch plate, n_{plates} is the number of plates in the clutch, v_{rel} is the relative angular velocity between the driven pulley and the rear wheel, to neglect friction torque when the angular velocity are equal. Finally, v_{trsh} is defined as the relative angular velocity for which the friction applied is equal to 95 % of the maximum friction. Both v_{rel} and v_{trsh} must be expressed in the same dimension of rotational velocity. In this case rpm are adopted. The model receives the clutch shaft speed as input and it outputs the clutch engagement signal, a dimensionless signal between 0 and 1 that indicates no clutch engagement or full engagement, respectively. The clutch model is connected between the CVT and the final gear, as shown in Figure 2.4.

Final gear and brakes

The final gear is a constant gear ratio between the output shaft of the clutch and the rear

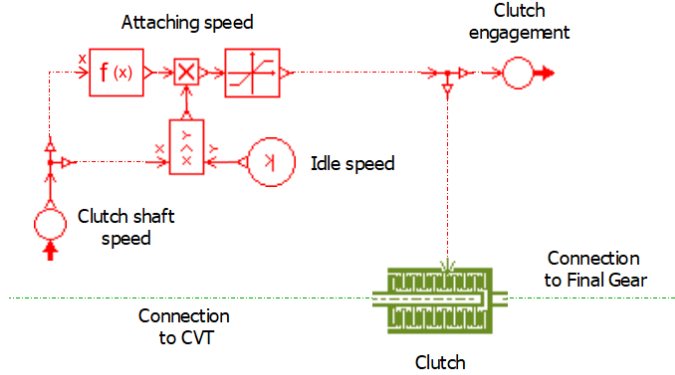


Figure 2.4: Clutch model scheme. The input to the model is the clutch shaft speed and the output is the clutch engagement. The model connects the CVT to the final gear.

wheel of the motorcycle. The total transmission ratio between the engine and the wheel is computed as follows:

$$\tau_{total} = \tau_{CVT} \tau_{final},$$

where τ_{total} is the total transmission ratio of the transmission, τ_{CVT} is the transmission ratio of the CVT and τ_{final} is the constant gear ratio of the final gear. All gear ratios are dimensionless.

In order to model the braking system, the rider's braking input actions on the front and rear brakes are scaled and then multiplied by the hyperbolic tangent of the front and rear wheel velocity, respectively. This function allows to neglect the braking torque applied at the wheels when the vehicle is not moving.

The inputs for the combined final gear and brakes model are the rider's braking input on front and rear brake and the velocity of the front and rear wheel. The outputs are the torques applied to the front and rear wheels of the dynamic model of the motorcycle. The model is also connected to the clutch, see Figure 2.5.

Tires

Tires are another crucial component of the motorcycle model and they have been modeled using the semi-empirical non-linear magic formula dedicated for motorcycle suitable for camber angles up to 30 degrees [41]. The tire model and the magic formula parameters for the motorcycle tires are taken from a previous study [48], where the calculation of the longitudinal and lateral forces, as well as the aligning moment of the tire, is based on the assumption of pure slip.

2.2.2. RIDER BALANCE ASSIST

Due to the unstable nature of the motorcycle model at low velocities, a dedicated control algorithm has been developed for two purposes. First, it keeps the motorcycle upright also at low speed and second, it stabilizes the steer when the rider releases it. Depend-

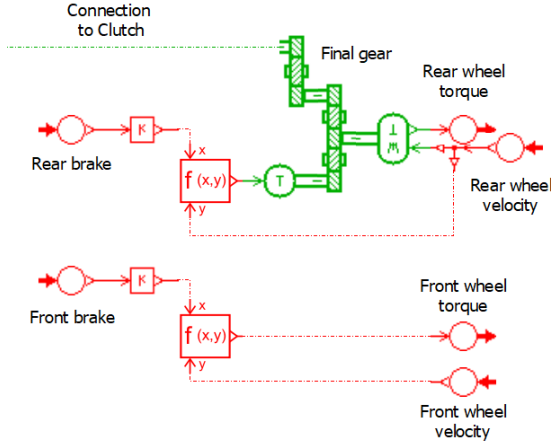


Figure 2.5: Final gear and brakes model scheme. The final gear model is connected to the clutch and receives the rear wheel velocity as input from the dynamic model of the motorcycle. The output is the rear wheel traction torque to apply on the dynamic model. The inputs for the brakes are the rider's braking actions on the front and rear brake levers and the outputs are the front and rear braking torques to apply on the dynamic model.

ing on the velocity of the vehicle, the implemented controller provides input forces and torques to support the motorcycle and to keep it balanced, while its effect is canceled above a certain speed.

On a real motorcycle, the rider keeps the vehicle upright at standstill by simply placing a foot on the ground. On the simulated motorcycle, the force exerted by the rider's foot can be replaced by a force applied in lateral direction at the Center of Gravity (COG) of the motorcycle. The magnitude of this force is computed with a proportional-derivative controller, which aims at keeping the roll angle of the motorcycle ϕ at zero. The stabilizing force F_{COG} applied at the COG is computed as follows:

$$F_{COG} = k_{P_{COG}} \phi + k_{D_{COG}} \dot{\phi},$$

where $k_{P_{COG}}$ is the proportional coefficient of the controller expressed in N rad^{-1} , $k_{D_{COG}}$ is the derivative coefficient of the controller expressed in $\text{N}/(\text{rad/s})$, ϕ and $\dot{\phi}$ are expressed in rad and rad s^{-1} , respectively.

In a similar way, also the steering angle is controlled by the balance assist, where another proportional-derivative controller is used compute a steering torque to keep the steering angle δ at zero. The steering torque control action T_{steer} is computed as follows:

$$T_{steer} = k_{P_{steer}} \delta + k_{D_{steer}} \dot{\delta},$$

where $k_{P_{steer}}$ is the proportional coefficient of the controller expressed in Nm rad^{-1} , $k_{D_{steer}}$ is the derivative coefficient of the controller expressed in $\text{Nm}/(\text{rad/s})$, δ and $\dot{\delta}$ are expressed in rad and rad s^{-1} , respectively.

These control actions are applied to the simulated motorcycle model at low speed, but when the velocity increases, they are no longer required and their effect should be canceled. In order to achieve this results, a dimensionless gain is computed which goes from 1 to 0 depending on the vehicle speed v :

$$gain = \begin{cases} 1, & v < v_{full\ assist} \\ \frac{1}{2} + \frac{1}{2} \cos\left(\pi \frac{v - v_{full\ assist}}{v_{part\ assist} - v_{full\ assist}}\right), & v_{full\ assist} \leq v \leq v_{part\ assist} \\ 0, & v > v_{part\ assist} \end{cases}$$

where $v_{full\ assist}$ is the maximum speed at which the balance assist applies the full control action and $v_{part\ assist}$ is the minimum speed at which no assist is applied to the motorcycle model. The values adopted for these speed values are 0.5 and 3 m s⁻¹ respectively.

2.2.3. LATERAL DYNAMICS CONTROLLER

In order to steer the motorcycle model, a steering torque needs to be applied. In a previous study [33], the steering torque was computed from the measured steering torque in the experiments with the addition of a proportional controller on the measured roll angle. This approach requires a measure of steering torque during the experiment, which is difficult, since it requires invasive modifications of the motorcycle's steering column. In another study [139] the steering torque to be applied to the model is computed with a proportional-integral-derivative controller on the desired motorcycle roll angle. Both solutions cannot be directly applied to a motorcycle simulator, however, since the maneuver to be reproduced is not defined a priori, but rather a consequence of the (unknown) rider's actions. The solution proposed in this chapter is based on the approach presented in a previous work [110], where some modifications have been made in order to make the lateral controller usable for a motorcycle simulator.

The steering angle imposed by the rider is used, together with the vehicle speed, to compute a reference roll angle, which is then used to compute the steering torque that is applied to the motorcycle model. The reference roll angle is computed under the assumption of steady state turn. In this condition the forces applied on the motorcycle are the gravity, the centrifugal force and the forces exerted by the tire. A scheme of these forces is shown in Figure 2.6, where m is the mass of the motorcycle, g is the gravitational acceleration, v is the motorcycle velocity, r is the curvature radius, F_y and F_z are the lateral and vertical components of the tire force.

In this condition the reference roll angle is obtained from the balance between the centrifugal and the gravitational forces:

$$\phi_{ref} = \arctan\left(\frac{v^2}{r g}\right)$$

The steering angle δ is directly imposed by the rider and used to define the curvature radius:

$$\frac{1}{r} = \frac{w}{\cos\epsilon \cos\delta},$$

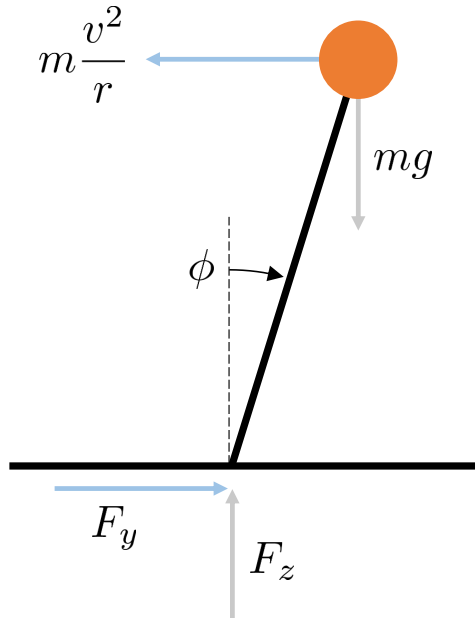


Figure 2.6: Balance of forces acting on a motorcycle in steady state cornering.

where w is the motorcycle wheelbase and ϵ is the motorcycle caster angle.

The reference roll angle computed is used in a proportional-derivative controller to compute the steering torque to apply to the motorcycle model. In addition, a derivative controller is used to introduce some damping on the steering to smoothen the action of the previous controller. The total steering torque τ is computed as follows:

$$\tau = P_{\phi} (\phi_{ref} - \phi) + D_{\phi} \dot{\phi} + D_{\delta} \dot{\delta},$$

where P_{ϕ} is the proportional coefficient of the controller expressed in Nm rad^{-1} , D_{ϕ} is the derivative coefficient of the controller expressed in $\text{Nm}/(\text{rad/s})$ and D_{δ} is the derivative coefficient (or damping) added to the steering column expressed in $\text{Nm}/(\text{rad/s})$.

2.2.4. MODEL VALIDATION

THE model has been validated with data collected on a real motorcycle instrumented with: inertial measurement unit, steering and throttle encoders, brake pressure sensors and wheel speed sensors [82]. Dedicated maneuvers have been performed for both longitudinal and lateral dynamics for different magnitudes of acceleration and deceleration [18].

Acceleration maneuvers have been performed starting from stand still and accelerating to 30 or 50 km h^{-1} in 30 m. The braking maneuvers started always with an acceleration from standstill to 30 km h^{-1} and a straight path of 15 m at constant speed. Then, the

rider was instructed to reach a full stop at a given distance, indicated on the track with cones. The braking distances measured were: 4.5, 5.5, 7.5, 12 and 25 m. For the lateral dynamics, a constant turn with a radius of 10.5 m was performed. For this maneuver, the rider was instructed to perform the turn at a constant speed of 25 km h^{-1} . These maneuvers will be indicated here with the following abbreviations:

- A30: acceleration from standstill to 30 km h^{-1} ,
- A50: acceleration from standstill to 50 km h^{-1} ,
- B25: braking from 30 km h^{-1} to standstill in 25 m,
- B12: braking from 30 km h^{-1} to standstill in 12 m,
- B7.5: braking from 30 km h^{-1} to standstill in 7.5 m,
- B5.5: braking from 30 km h^{-1} to standstill in 5.5 m,
- B4.5: braking from 30 km h^{-1} to standstill in 4.5 m, and
- U25: constant turn with 10.5 m radius performed at 25 km h^{-1} .

In order to perform the model validation simulations, the rider inputs measured on the real instrumented motorcycle were applied to the simulated model. Due to model uncertainties, a scaling function was applied to throttle and braking input in order to accurately reproduce the validation maneuvers in terms of measured velocity and acceleration profiles.

For the throttle input, a linear scaling was initially assumed, but the results showed that for low throttle values the resulting acceleration was too low, while for higher throttle the acceleration was too high. In order to correct this behavior, a non-linear scaling function was adopted. The braking pressure was measured on the instrumented scooter at both front and rear brake calipers. To convert the measured input to a braking torque applied on the motorcycle model the following relation was used:

$$T_{brake} = p_{brake} A_{caliper} r_{disk},$$

where T_{brake} is the braking torque applied to the motorcycle model in N m, p_{brake} is the measured pressure at the brake calipers expressed in Pa, $A_{caliper}$ is the area in m^2 of the caliper where the pressure was measured and r_{disk} is the radius of the braking disk expressed in m.

The steering angle measured on the real motorcycle was used as input for the lateral dynamics controller of the motorcycle model.

For the validation of the lateral dynamics maneuver U25, a proportional controller was implemented on the motorcycle model in order to follow the longitudinal speed of the motorcycle that was measured during the testing. Since longitudinal and lateral dynamics are coupled, by minimizing the differences in longitudinal direction with the speed controller, the comparison would only show differences due to the lateral dynamics of the motorcycle.

2.3. RESULTS AND DISCUSSION

THE results for all the maneuvers are available on an on-line repository [67]. In the remainder of this chapter only some representative results are presented.

The selected acceleration maneuver is A50, and results are shown in Figure 2.7. In this maneuver, the motorcycle model starts from standstill, which is possible thanks to the balance assist, then it accelerates reproducing the longitudinal velocity and acceleration measured on the real vehicle. At the beginning of the maneuvers the transition from zero speed and acceleration happens in a smooth way due to the speed-dependent gain that allows for a gradual transition from assisted to free ride. The value of the speed-dependent gain of the rider balance assist is represented in the picture with a gray shadow. Where the shadow is in dark gray color, the value of the gain is equal to one, the gradient color represent the transition from one to zero and where the shadow is not visible the gain is zero, meaning that the motorcycle model does not receive any input from the balance assist.

Results of the simulation of the engine and the transmission are also shown. The engine torque, as well as the engine rpm starts to increase as the throttle input increases. The clutch starts to engage and transmits more of the engine torque to the rear wheel. When the clutch is fully engaged, the rpm starts to increase until the balance of forces in the CVT results in a different transmission ratio. Thanks to the transmission, the torque provided by the engine remains constant during the acceleration.

The results for the selected braking maneuvers are presented in Figures 2.8 and 2.9 for maneuvers B25 and B4.5, respectively. For these maneuvers, the motorcycle model starts again from standstill and accelerates to a constant speed, then the actual braking maneuver starts. The amplitude of vehicle deceleration is always matched, especially in the initial phase of the braking maneuvers. Toward the end of the maneuver, when the speed approaches zero, the balance assist acts on the motorcycle model, smoothening the transition to standstill. Also in these figures, the value of the gain of the balance assist is represented by a gray shadow in the areas where the assist is active on the motorcycle model. Again, the engine and the transmission work together to speed up the motorcycle in the acceleration phase. When the throttle is released and the brakes are pulled, the CVT ratio starts to decrease until it reaches its minimum, then the clutch starts to disengage, until the motorcycle model reaches the standstill. It is also worth noticing how the brake input is divided between the front and rear brakes (indicated with FB and RB, respectively). In maneuver B25, the deceleration is very low and the rider uses both brakes equally. In maneuver B4.5, the braking is quite aggressive, and the front brake almost reaches its maximum value.

Results for the lateral dynamics maneuver U25 are shown in Figure 2.10. The results obtained with the motorcycle model correlate with the measured data, although a lag is introduced in the lateral acceleration of the motorcycle model due to the lateral dynamics controller. It is significant to notice that the roll angle reached during this maneuver is almost 30° for both the simulated and the real motorcycle.

Results obtained from the motorcycle model simulations appear much smoother than the measured data. This represents an advantage to the usage of the motorcycle model for the validation of dedicated motorcycle motion cueing algorithm in a human-in-the-loop riding simulator, as reduction of jerk motion is crucial to increase the quality

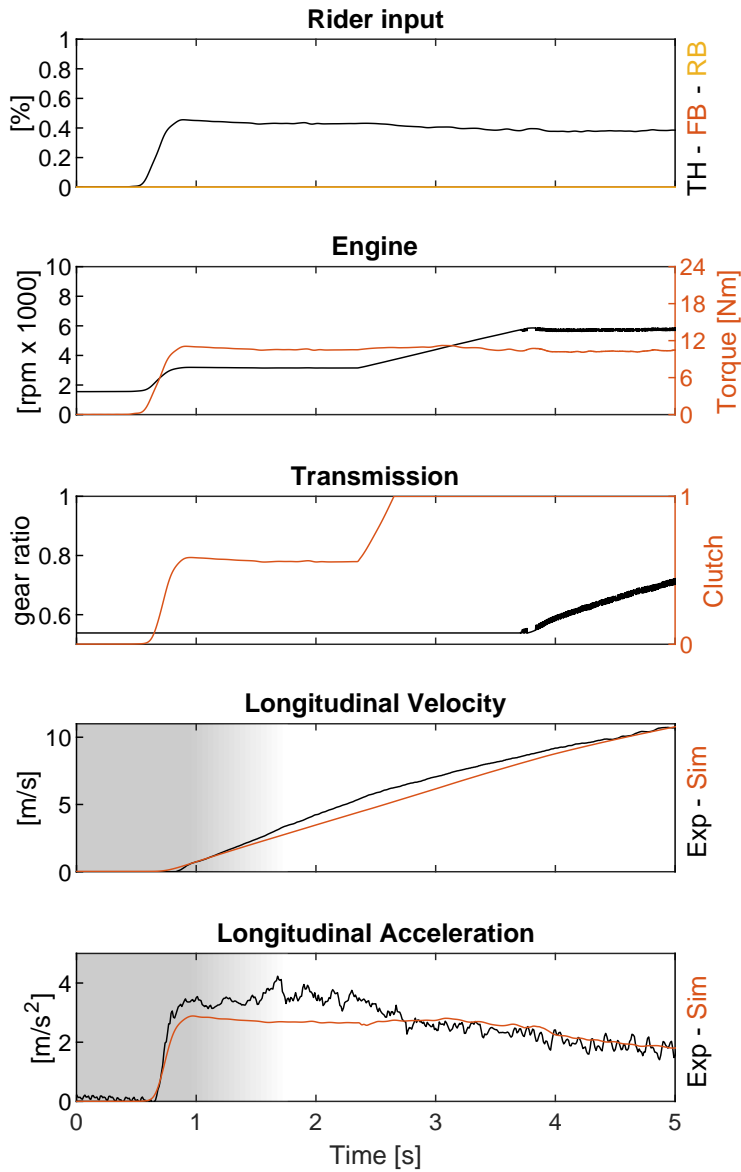


Figure 2.7: Maneuver A50. Comparison between model simulation (red in the two bottom plots) and measurements on a real motorcycle (black in the two bottom plots). TH: throttle, FB: front brake, RB: rear brake.

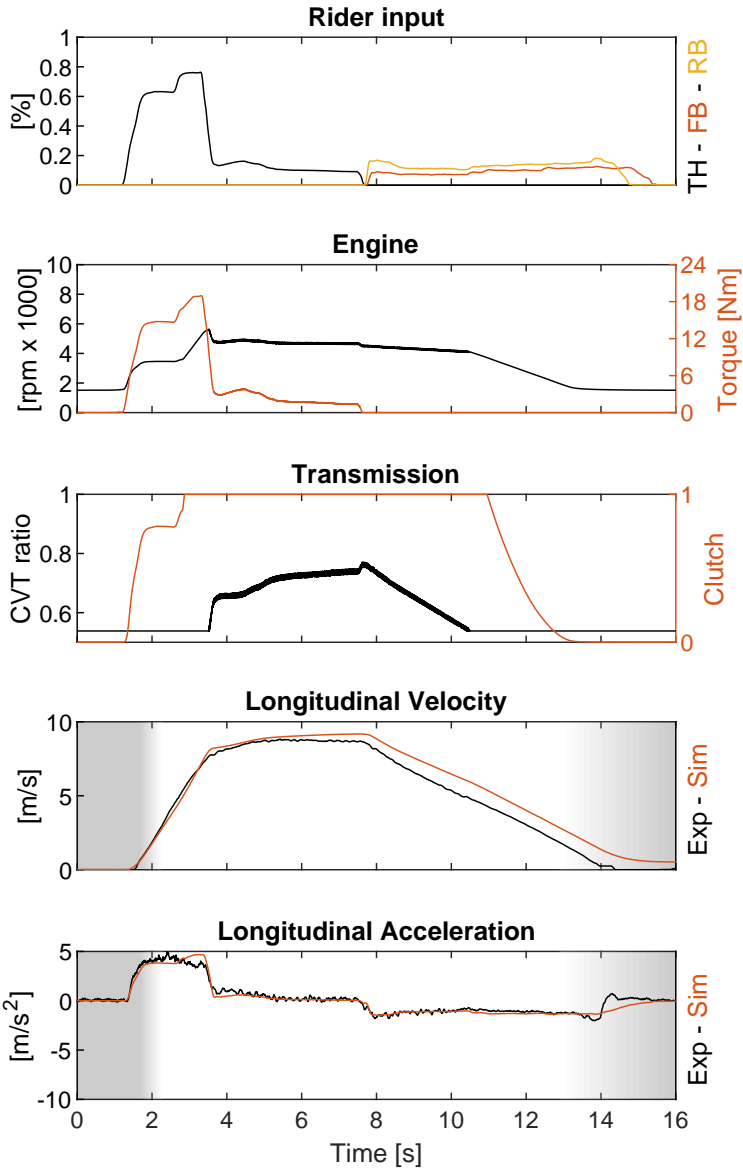


Figure 2.8: Maneuver B25. Comparison between model simulation (red in the two bottom plots) and measurements on a real motorcycle (black in the two bottom plots). TH: throttle, FB: front brake, RB: rear brake.

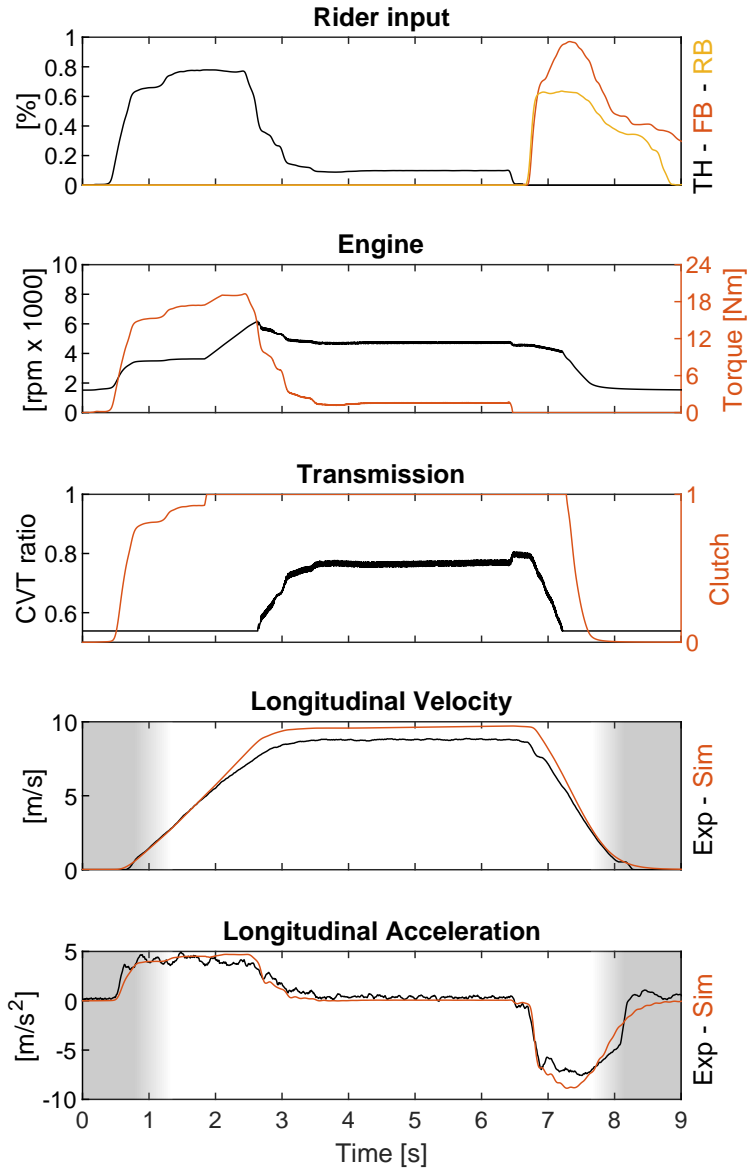


Figure 2.9: Maneuver B4.5. Comparison between model simulation (red in the two bottom plots) and measurements on a real motorcycle (black in the two bottom plots). TH: throttle, FB: front brake, RB: rear brake.

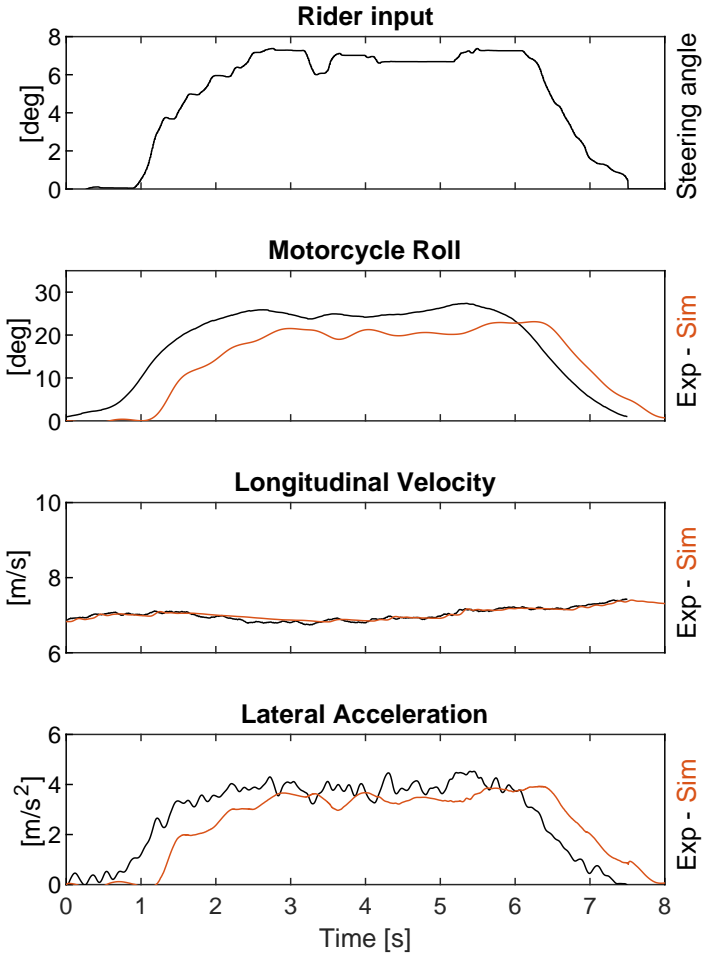


Figure 2.10: Maneuver U25. Comparison between model simulation (red in the two bottom plots) and measurements on a real motorcycle (black in the two bottom plots).

of the perceived motion [142].

The presented model has been integrated in a riding simulator and tested by a few subjects in order to evaluate the realism of the riding feeling. After a few minutes of practice, all subjects reported positively on their perceived realism and were well able to start from standstill and ride at low speed.

2.4. CONCLUSIONS

A motorcycle multibody model, in combination with engine and transmission models, has been implemented and validated together with two control strategies for low-speed stability and lateral dynamics. From the combined analysis of acceleration and braking maneuvers it is possible to conclude that the results of the motorcycle model correlate well with the measured data on an instrumented motorcycle in the speed range between 0 and 10 ms^{-1} , with longitudinal accelerations up to 5 ms^{-2} in acceleration and 8 ms^{-2} in braking. On the lateral dynamics, the model results in a lag in lateral acceleration due to the lateral controller. Nevertheless, the value of lateral acceleration in steady turning is matched up to 4 ms^{-2} .

The model presented in this study has also been integrated in a complete riding simulator for human-in-the-loop simulations and has been evaluated by a few subjects. Further investigations are required to conclude on the subjective perception of the riding feelings. The presented model will be also used for the reproduction of the validation maneuvers for the investigation of a dedicated motion cueing algorithm for riding simulators.

2.5. ACKNOWLEDGMENT

THIS work has been funded by the European Union's Seventh Framework Programme through the international consortium MOTORIST (Motorcycle Rider Integrated Safety) agreement No. 608092. Initial results were published in the MOTORIST Deliverable 2.1 [18]. The authors would like to acknowledge Pedro Huertas-Leyva, Giovanni Savino and Lorenzo Berzi from the University of Florence for their support during the measurements on the instrumented motorcycle.

3

OBJECTIVE EVALUATION OF PREDICTION STRATEGIES FOR OPTIMIZATION-BASED MOTION CUEING

Optimization-based motion cueing algorithms based on model predictive control have been recently implemented to reproduce the motion of a car within the limited workspace of a driving simulator. These algorithms require a reference of the future vehicle motion to compute a prediction of the system response. Assumptions regarding the future reference signals must be made in order to develop effective prediction strategies. However, it remains unclear how the prediction of future vehicle dynamics influences the quality of the motion cueing. In this study two prediction strategies are considered. Oracle: the ideal prediction strategy that knows exactly what the future reference is going to be. Constant: a prediction strategy that ignores every future change and keeps the current vehicle's linear accelerations and angular velocities constant. The two prediction strategies are used to reproduce a sequence of maneuvers between 0 and 50 km h⁻¹. A comparative analysis is carried out to objectively evaluate the influence of the prediction strategies on motion cueing quality. Dedicated indicators of correlation, delay and absolute error are used to compare the effects of the adopted prediction on simulator motion. Also the motion cueing mechanisms adopted by the different conditions are analyzed, together with the usage of simulator workspace. While the constant strategy provided reasonable cueing quality, the results show that knowledge of the future vehicle trajectory reduces the delay and improves correlation with the reference trajectory, it allows the combined usage of different motion cueing mechanisms and increases the usage of workspace.

This chapter has been published as: Marco Grotto, Diane Cleij, Paolo Pretto, Yves Lemmens, Riender Happee, and Heinrich H. Bülthoff. "Objective evaluation of prediction strategies for optimization-based motion cueing". In: *SIMULATION* 95.8 (Dec. 2018), pp. 707–724. DOI: [10.1177/0037549718815972](https://doi.org/10.1177/0037549718815972).

3.1. INTRODUCTION

MOTION Cueing Algorithms (MCAs) are used in driving simulators to provide inertial motion to the user of the simulator. The motion obtained from the vehicle dynamic simulation is adjusted by the MCA to fit the limited workspace of the simulator motion system. To achieve this goal, different algorithms have been developed in the past decades. One of the most commonly used MCAs is known as the classical algorithm [135, 127, 128]. Classical MCAs are based on filters, where linear accelerations and angular velocities are first scaled and then high-pass filtered to remove constant signal content (washout). In addition, low-pass filters are also used for longitudinal and lateral accelerations, where tilt coordination is adopted to use gravitational acceleration to reproduce sustained accelerations. These algorithms present some limitations. The tuning process is not trivial and it is often subjective. Different approaches have been studied to objectively tune the parameters of classical MCAs by following a specific process [59] or by optimizing a set of dedicated objective metrics of motion cueing quality [15, 17]. Nevertheless, the results obtained from these techniques can still be improved by further subjective tuning. The tuning process of classical MCAs is specific to the set of maneuvers to reproduce on the motion simulator. Since classical MCAs do not include knowledge of the motion system's limitation, the tuning process must be repeated if the set of maneuvers changes. Otherwise, the trajectory obtained by the classical MCA could be exceeding the physical boundaries of the motion system. More recently another approach based on optimization has become popular [37, 49, 3, 57]. Unlike filter-based MCAs, the optimization-based approach uses MPC to compute an optimal solution, within system limitations, using an internal model of the motion system to predict the future system response [126, 103, 154, 13]. This algorithm will be referred here as predictive MCA. This new approach takes into account motion system limitations and the tuning is achieved with weighting factors on linear and rotational motion cues. The predictive MCA has shown multiple advantages with respect to the classical algorithm, both in terms of workspace usage and subjective evaluation, when the vehicle trajectory is completely known in advance (passive driving) [24]. However, other challenges are introduced with the usage of predictive MCA. Compared to the classical MCA, this algorithm requires more computational time to solve an optimization problem at each time step of the algorithm, making it more challenging to adopt for more common DIL simulations (active driving). Another aspect to consider is that the predictive MCA requires a future reference of the motion to reproduce on the simulator to compute a prediction of the system response. When using the predictive MCA in DIL simulations, assumptions regarding the future reference signals must be made. Previous studies have already addressed the issue of providing a future reference for the predictive MCA. For example, the vehicle motion recorded in a circuit is used to provide a better reference for future laps [11], or a neural network is trained using simulated data to predict the future reference motion [107]. However, it remains unclear how the prediction strategies adopted influence the quality of the motion cueing. In this study, two prediction strategies are considered. The first strategy corresponds to the ideal case in which the future motion to be reproduced on the simulator is known, as if it could be perfectly predicted. This cannot be applied for active driving but represents the perfect strategy which is expected to reproduce at best the reference motion and therefore it is assumed here as a

reference. The second strategy assumes a constant motion as future reference, ignoring every possible variations from the current status. It can be expected that the results for this strategy will be sub-optimal with respect to the first one. The scenario used to compare the results of the two prediction strategies is the reproduction on a motion based simulator of a sequence of maneuvers in an urban-like environment. The simulations are performed offline and the future reference for the few seconds ahead is passed to the predictive MCA at each time step, as if it would be for a DIL simulation. The simulator motion computed with the considered prediction strategies is analyzed and compared with the reference motion.

The goal of this study is to objectively evaluate the influence of the adopted prediction strategy on motion cueing quality. The analysis carried out should also determine whether it is worth investing in an improved prediction strategy to obtain a better motion cueing quality.

3.2. METHODS

3.2.1. MOTION PERCEPTION

The main role of the MCA is to reproduce the simulated vehicle motion as accurately as possible for the simulator user. In the process of motion perception, humans use visual, vestibular and proprioceptive organs to detect motion direction and rate of change. The vestibular system is located in the inner ear and consists of semicircular canals and otolith organs, which sense angular and linear motion respectively. More specifically, the otolith organs detect specific forces, which result from summation of acceleration in space and gravity. Thus, the specific forces \mathbf{f} can be expressed as in Equation 3.1, where \mathbf{a}_{ng} indicates the non-gravitational accelerations and \mathbf{g} indicates the gravitational acceleration.

$$\mathbf{f} = \mathbf{a}_{ng} - \mathbf{g} \quad (3.1)$$

Therefore, humans are unable to discriminate between linear accelerations and the component of gravitational acceleration that occurs when the head is tilted with respect to the gravity vector [135]. This effect can be exploited in motion simulators, allowing to reproduce sustained accelerations by simulator tilt. The use of tilt angles is limited to 20 - 30 deg (Aubert effect), which limits the maximum possible acceleration simulated via tilt coordination to 0.5 g [129]. The use of tilt coordination generates additional motion in the rotational channels, in order for this false motion not to be noticed, the tilt rate should be limited to the angular velocity perception threshold. Different values of this threshold can be found in literature, a unique value is difficult to identify given also the subjective nature and the dependency from the simulation scenario (active/passive driving). In this study a value of 3 deg/s is considered [113, 114]. Humans require additional sensory information (i.e. visual, proprioceptive) in order to discriminate between acceleration and tilt [146].

A vestibular system model is not considered here, in this study the goal of the MCA is to reproduce on the motion simulator the specific forces and the angular velocities obtained from a vehicle dynamics simulation. The predictive MCA computes the optimal simulator motion and predicts the associated perceived motion of the driver on the

Table 3.1: Maximum longitudinal acceleration (a_x), lateral acceleration (a_y), maximum yaw rate (ω_z) and maximum significant frequency content of the considered vehicle maneuvers.

Maneuver	a_x [m s^{-2}]	a_y [m s^{-2}]	ω_z [deg/s]	[Hz]
A	2	-	-	0.4
B	3	-	-	0.4
CT	-	2	10	0.2
DLC	-	± 1	± 5	0.3
BCTA	± 1	2	10	0.2

simulator. Vehicle specific forces and angular velocities are used as reference motion for the predictive MCA in order to minimize the difference between the motion on the simulator and in the real vehicle.

3.2.2. VEHICLE MANEUVERS

The maneuvers to reproduce on the motion based simulators are selected in an urban-like scenario between 0 and 50 km h^{-1} . The simulated vehicle performs the following maneuvers:

- A: accelerating from 0 to 50 km h^{-1}
- B: braking from 50 to 0 km h^{-1}
- CT: constant turn at 50 km h^{-1}
- DLC: double lane change at 50 km h^{-1}
- BCTA: braking from 50 to 30 km h^{-1} while entering the turn and accelerating from 30 to 50 km h^{-1} while exiting the turn

The maneuvers have been selected to explore typical longitudinal, lateral and combined motion scenarios. In particular A and B are purely longitudinal maneuvers, while CT and DLC are purely lateral. In addition, BCTA has been chosen to evaluate the combined longitudinal and lateral dynamics. A description of these maneuvers in terms of maximum accelerations and significant frequency content is given in Table 3.1. The frequency spectrum of the vehicle motion is computed and the maximum significant frequency of each maneuver is considered as the frequency above which the amplitude of the signal's spectrum is below 10% of its maximum. The vehicle dynamic simulations have been performed with a time step of 1 ms using CarSim TM (Mechanical Simulation Corporation). The selected vehicle was a mid-size sedan and it was autonomously driven over a pre-defined path at a controlled speed. The simulation was performed off-line and the results have been filtered to remove the high frequency content of the vehicle motion using a zero-phase low-pass 4th order Butterworth filter with cut-off frequency of 12.6 rad s^{-1} .

3.2.3. PREDICTIVE MOTION CUEING ALGORITHM

The MCA adopted in this study is based on MPC. This advanced control technique uses a simplified model of the system under control, i.e. motion system used in dynamic simulators, to predict the future system's response and optimize the control action to achieve optimal tracking performances within system limitations. The motion system considered for this study is a 6 DOF hexapod [144] with a linear actuator stroke of 0.533 m and resulting single DOF limits reported in Table 3.2.

In order to define the equations of motion of the considered motion system, the following frames of reference are defined:

- Inertial Frame (IF): fixed to the ground and placed at the center of the hexapod fixed base
- Platform Frame (PF): placed at the center of the hexapod moving base
- Head Frame (HF): positioned at the head center of the simulator user

The non-linear equations of motion of the system have been derived, considering the moving platform as a single rigid body with mass m and inertia tensor \mathbf{I} . The rigid body is subject to three orthogonal forces \mathbf{F} and three orthogonal torques \mathbf{M} applied at the center of mass. The complete equations of motion are reported in Equation 3.2.

$$\begin{cases} \dot{\mathbf{p}} = \mathbf{v} \\ \dot{\mathbf{q}} = \frac{1}{2} E^T \boldsymbol{\omega} \\ \dot{\mathbf{v}} = \frac{\mathbf{F}}{m} + \mathbf{g} \\ \dot{\boldsymbol{\omega}} = \mathbf{I}^{-1} (\mathbf{M} - \boldsymbol{\omega} \times \mathbf{I} \boldsymbol{\omega}) \end{cases} \quad (3.2)$$

With:

$$E = \begin{bmatrix} -q_1 & q_0 & q_3 & -q_2 \\ -q_2 & -q_3 & q_0 & q_1 \\ -q_3 & q_2 & -q_1 & q_0 \end{bmatrix} \quad (3.3)$$

Where \mathbf{p} and \mathbf{v} are respectively the position and the velocity of the center of mass expressed in IF, \mathbf{q} is the vector of the orientation quaternions and $\boldsymbol{\omega}$ the rotational velocity vector expressed in PF.

In order to proceed to the full problem statement, the state vector \mathbf{x} and the input vector \mathbf{u} of the controlled system are defined.

$$\mathbf{x} = \begin{bmatrix} \mathbf{p} \\ \mathbf{q} \\ \mathbf{v} \\ \boldsymbol{\omega} \end{bmatrix} \quad \mathbf{u} = \begin{bmatrix} \mathbf{F} \\ \mathbf{M} \end{bmatrix} \quad (3.4)$$

Table 3.2: Motion system single degree of freedom limits.

DOF	Position		Velocity	Acceleration
x	-0.423 m	0.540 m	$\pm 0.8 \text{ m s}^{-1}$	$\pm 7 \text{ m s}^{-2}$
y	-0.432 m	0.432 m	$\pm 0.8 \text{ m s}^{-1}$	$\pm 7 \text{ m s}^{-2}$
z	-0.306 m	0.324 m	$\pm 0.55 \text{ m s}^{-1}$	$\pm 10 \text{ m s}^{-2}$
Roll	-20.25 deg	20.25 deg	$\pm 33.5 \text{ deg/s}$	$\pm 245 \text{ deg/s}^2$
Pitch	-23.85 deg	20.70 deg	$\pm 36.5 \text{ deg/s}$	$\pm 245 \text{ deg/s}^2$
Yaw	-23.40 deg	23.40 deg	$\pm 39.5 \text{ deg/s}$	$\pm 498 \text{ deg/s}^2$

The system is also subject to constraints, and the MPC allows to include them in the optimization problem. As a result, the computed motion trajectory will be optimized while still remaining within system limitations.

The main physical constraint comes from the system's actuators, which are limited within a certain range of motion. This limitation is expressed as an inequality constraint, where the actuator length is bounded between minimum (\mathbf{L}_{\min}) and maximum values (\mathbf{L}_{\max}). The lengths of the actuators can be computed solving the hexapod inverse kinematics [132], as shown in Equation 3.5.

$$\mathbf{L}_i = \|\mathbf{R}(\mathbf{q}) \mathbf{T}_i + \mathbf{p} - \mathbf{B}_i\| \quad \text{for } i = 1, \dots, 6 \quad (3.5)$$

Where \mathbf{L}_i is the length of the i_{th} actuator, \mathbf{T}_i and \mathbf{B}_i are the coordinate vectors of the actuator's mounting points on the moving and fixed base respectively. The expression is non-linear due to the presence of the rotation matrix $\mathbf{R}(\mathbf{q})$.

$$\mathbf{R}(\mathbf{q}) = \begin{bmatrix} 1 - 2q_2^2 - 2q_3^2 & 2(q_1 q_2 - q_0 q_3) & 2(q_1 q_3 + q_0 q_2) \\ 2(q_1 q_2 + q_0 q_3) & 1 - 2q_1^2 - 2q_3^2 & 2(q_2 q_3 - q_0 q_1) \\ 2(q_1 q_3 - q_0 q_2) & 2(q_2 q_3 + q_0 q_1) & 1 - 2q_1^2 - 2q_2^2 \end{bmatrix} \quad (3.6)$$

The constraint (Equation 3.5) is linearized with respect to the state vector.

$$\mathbf{L} \approx \mathbf{M}_k \mathbf{x}_k + \mathbf{Q}_k \quad (3.7)$$

Where \mathbf{M}_k is the Jacobian matrix of the vector \mathbf{L} with respect to the state vector \mathbf{x}_k , and \mathbf{Q}_k is the constant term of the linear approximation. Both \mathbf{M}_k and \mathbf{Q}_k are updated at each time step using the current state vector \mathbf{x}_k and included in the optimal control problem formulation.

Together with the actuators' length constraint also the single DOF motion limitation has been included in the optimization problem. This constraint somewhat reduces the usable platform workspace, but was considered anyway for extreme caution.

As introduced in Section 3.2.1, vehicle linear accelerations and angular velocities are considered as the target reference for the MPC controller. The aim of the controller is to reproduce the perceived motion as would occur in the real vehicle, but keeping the

simulator motion within its physical limitations. The output function expresses the perceived motion in terms of specific forces \mathbf{f} and angular velocities $\boldsymbol{\omega}$ on the simulator in HF, where the frame is indicated in the quantity subscription. The relevant quantities are first written in PF (Equation 3.8), where also the angular acceleration vector $\boldsymbol{\alpha}$ is defined.

$$\begin{aligned}\mathbf{f}_{PF}(\mathbf{x}, \mathbf{u}) &= \mathbf{R}^T (\mathbf{g} - \dot{\mathbf{v}}) \\ \boldsymbol{\omega}_{PF}(\mathbf{x}) &= \boldsymbol{\omega} \\ \boldsymbol{\alpha}_{PF}(\mathbf{x}, \mathbf{u}) &= \dot{\boldsymbol{\omega}}\end{aligned}\quad (3.8)$$

Next, the same quantities can be expressed in HF by means of the rotation matrix from PF to HF (${}^{HF}\mathbf{R}_{PF}$) and the translation vector from HF to PF (${}^{PF}\mathbf{r}_{HF}$). The definition of the output quantities in HF is reported in Equation 3.9.

$$\begin{aligned}\mathbf{f}_{HF}(\mathbf{x}, \mathbf{u}) &= {}^{HF}\mathbf{R}_{PF} [\mathbf{f}_{PF}(\mathbf{x}, \mathbf{u}) + \\ &\quad - \boldsymbol{\alpha}_{PF}(\mathbf{x}, \mathbf{u}) \times {}^{PF}\mathbf{r}_{HF} - \boldsymbol{\omega}(\mathbf{x}) \times (\boldsymbol{\omega}(\mathbf{x}) \times {}^{PF}\mathbf{r}_{HF})] \\ \boldsymbol{\omega}_{HF}(\mathbf{x}) &= {}^{HF}\mathbf{R}_{PF} \boldsymbol{\omega}_{PF}(\mathbf{x})\end{aligned}\quad (3.9)$$

As a result, the system output vector \mathbf{y} is defined in vector form as follows:

$$\mathbf{y}(\mathbf{x}, \mathbf{u}) = \begin{bmatrix} \mathbf{f}_{HF}(\mathbf{x}, \mathbf{u}) \\ \boldsymbol{\omega}_{HF}(\mathbf{x}) \end{bmatrix}\quad (3.10)$$

The system's equations of motion and output equations are then discretized and converted to a discrete-time dynamic model using the direct multiple shooting method [43].

The complete non-linear constrained optimization problem is formulated as in Equation 3.11. The MPC controller solves this problem at each time step. The implementation has been done in Matlab (The MathWorks, Inc.) and the quadratic programming problem is solved by a separate solver (qpOASES [53]).

$$\begin{aligned}\text{minimize} \quad & \sum_{k=0}^{N-1} I_k(\mathbf{x}_k, \mathbf{u}_k) + I_N(\mathbf{x}_N) \\ \text{subject to} \quad & \mathbf{x}_0 = \tilde{\mathbf{x}}_0 \\ & \mathbf{x}_{k+1} = A_k \mathbf{x}_k + B_k \mathbf{u}_k \\ & \mathbf{x}_{\min} \leq \mathbf{x}_k \leq \mathbf{x}_{\max} \\ & \mathbf{L}_{\min} \leq \mathbf{M}_k \mathbf{x}_k + \mathbf{Q}_k \leq \mathbf{L}_{\max} \\ & \mathbf{x}_{\min, N} \leq \mathbf{x}_N \leq \mathbf{x}_{\max, N} \\ & \mathbf{u}_{\min} \leq \mathbf{u}_k \leq \mathbf{u}_{\max}\end{aligned}\quad (3.11)$$

With $k = 0, \dots, N-1$. Where:

$$\begin{aligned}I_k(\mathbf{x}_k, \mathbf{u}_k) &= \|\hat{\mathbf{y}}_k - \mathbf{y}(\mathbf{x}_k, \mathbf{u}_k)\|_{W_y}^2 + \|\hat{\mathbf{x}}_k - \mathbf{x}_k\|_{W_x}^2 + \\ &\quad + \|\hat{\mathbf{u}}_k - \mathbf{u}_k\|_{W_u}^2 \\ I_N(\mathbf{x}_N) &= \|\hat{\mathbf{x}}_N - \mathbf{x}_N\|_{W_{x_N}}^2\end{aligned}\quad (3.12)$$

The optimization problem in Equation 3.11 is defined to minimize the cost function expressed by the two terms I_k and I_N defined in Equation 3.12. The term I_k of the cost function is defined as a sum of weighted squared norms of the difference between the vector quantities and their references over the prediction horizon of N time steps from 0 to $N - 1$, while the term I_N includes only the final states cost expressed as weighted squared norm of the difference between the final state vector and its reference. Both terms include the reference values which are defined over the prediction horizon before to solve the optimization problem. These references are: $\hat{\mathbf{y}}_k$, $\hat{\mathbf{x}}_k$, $\hat{\mathbf{u}}_k$ and $\hat{\mathbf{x}}_N$, which represent the reference trajectory for system output, state, input and final state respectively. The inclusion of these terms in the cost function has different meanings. For instance, by giving a null reference to the state over the prediction horizon a behavior similar to a washout filter would be obtained, where the MCA tries to keep the hexapod in its central position. For this study, this effect will not be considered and therefore the reference state $\hat{\mathbf{x}}_k$, as well as the respective weights W_x , will be set to zero. The addition of a null reference for input and final state in the cost function stabilizes the system. The stabilization effects are controlled by setting the associated weights. In this study, the references for both $\hat{\mathbf{u}}_k$ and $\hat{\mathbf{x}}_N$ are set to zero over the prediction horizon. The weights on the input are $1e-3$ for the linear accelerations and $1e-1$ for the angular velocities, while the weights on the final states are $1e1$ for all the states. The remaining term is the reference trajectory for the system output $\hat{\mathbf{y}}_k$, which needs to be defined at each time step in order to optimize the control action. The definition of the output reference is not only necessary to numerically solve the control problem, but the accuracy of future reference will also affect the performances of the algorithm. For example, if the reference includes changes derived from a particular maneuver to reproduce on the simulator, the algorithm will know it in advance and it will make use of this knowledge to improve the results. The output reference is defined by the prediction strategy. In this study, two different prediction strategies were compared: *oracle* and *constant*.

PREDICTION STRATEGIES

The first prediction strategy considered for this study is the ideal strategy that is able to predict with perfect accuracy the future vehicle motion. This strategy will be referred here with the name *oracle* (due to its “prophetic” capabilities in predicting the future [91]). Clearly, this strategy cannot be adopted in an active driving simulation but it is considered as a reference to evaluate the best possible motion cueing quality achievable with the predictive MCA. In order to implement the *oracle* strategy, linear accelerations and angular velocities resulting from the vehicle dynamic simulations must be known a priori. At each time step, and for the length of the prediction horizon, the corresponding signals are extracted from the fully known motion and provided to the predictive MCA.

The second strategy adopted in this study does not consider any assumptions on future vehicle behavior and, at each time steps, simply holds the current value of linear accelerations and angular velocities that results from the vehicle simulation. This strategy will be referred as *constant*. Contrary to the *oracle*, this strategy can be adopted for active driving simulation, but the resulting motion cueing quality is expected to be lower.

PREDICTION HORIZON LENGTH

An important aspect of the future prediction is given by the length of the prediction horizon. The further the algorithm can see in the future, the sooner it will respond to a future change. On the other hand, a longer prediction horizon would result in a very high computational cost. In a previous study [108] a Genetic Algorithm was adopted to optimize the length of the control and prediction horizon of the MPC. In another study [90] a model was developed to evaluate the relation between prediction horizon length and performance of the predictive MCA in terms of reduction of cost function. In the last study, the cost value obtained with a certain prediction length $c(h)$ was compared with the cost obtained with an infinite prediction c_∞ . A parametric model was developed and it is reported here in Equation 3.13.

$$\frac{c(h)}{c_\infty} - 1 = \left(\frac{h}{a}\right)^{-k} \quad (3.13)$$

Where a and k are characteristic parameters depending on the considered scenario. The results showed that for a urban-like scenario the characteristic time a for which the cost is twice the value with infinite horizon is 3.3 seconds and the cost decrease factor k is equal to 2. In this study a prediction horizon of 5 seconds is considered, which is roughly 1.5 times the characteristic time and would result in a cost value of approximately 1.4 times the cost with infinite horizon. The choice of 5 seconds of prediction, together with the selected time step of 0.1 seconds, results in an horizon length N equal to 50 and a total number of control parameters to optimize equal to 300. The implementation adopted in this study does not allow real time performances for a problem of this size. In order to improve the performance to real time, a different implementation could be adopted using more efficient programming language and/or optimization algorithm.

WEIGHTING FACTOR OPTIMIZATION

The motion cueing quality that can be achieved with the predictive MCA depends on the accuracy of the predicted motion that is provided to the MPC algorithm at each time step. The MPC algorithm aims at reproducing the given reference signals where the tracking performances are influenced by the weighting factors associated with each motion channel. In the considered problem formulation, the weighting factors associated with the perceived motion are the six non zero terms of the diagonal matrix W_y . Finding the optimal values of these weights is not trivial and it can strongly influence the results of the predictive MCA. Using the same set of weights for both prediction strategies might be unfair for the comparison of the obtained motion cueing results. Therefore an optimization of the weights is performed with the aim of finding the best possible set for each prediction strategy. The weights are initialized with values taken from literature [90, 24] and reported in Table 3.3, where the different order of magnitude is to account for the ratio between specific forces - in ms^{-2} - and angular velocities - in rads^{-1} - for typical maneuvers [90]. The simulator motion obtained with *oracle* and *constant* strategies for the entire sequence of maneuvers is used to compute the error with respect to the vehicle motion. The error is computed separately for linear (e_f) and rotational motion (e_w) and combined in the cost function reported in Equation 3.14, where the error on the rotational motion is multiplied by a factor of 100 to account for the different order of magnitude.

Table 3.3: Initial and optimized weighting factors on specific forces and angular velocities of the predictive MCA.

Weight	Specific forces			Angular velocities		
	f_x	f_y	f_z	ω_x	ω_y	ω_z
<i>Oracle</i>						
Initial	1	1	1	100	100	100
Optimal	3.021	1.101	3.031	100.310	101.239	100.574
<i>Constant</i>						
Initial	1	1	1	100	100	100
Optimal	1.000	1.579	1.579	100.013	100.000	100.000

$$\underset{W_y}{\text{minimize}} \quad \|e_f(W_y)\|^2 + 100 \|e_\omega(W_y)\|^2 \quad (3.14)$$

A wider optimization loop is defined in order to find the optimal value of W_y which minimizes the cost function computed over the whole sequence of maneuvers. The optimization is performed using an interior point method [8] with a step tolerance of $1e-10$. The optimal weighting factors are reported in Table 3.3. It can be noticed that the optimized weighting factors for the angular velocities are very similar to the initial values for both prediction strategies, therefore these weights could have been neglected in the optimization. On the other hand, the weights for specific forces differs between *oracle* and *constant*. In particular, the lowest weight for the *oracle* strategy is on f_y while the lowest for *constant* is on f_x . This difference can be related to many aspects, including the amplitude of the reference signals - maximum value of f_x higher than f_y - and the capability of each prediction strategy to obtain a feasible solution.

3.2.4. DEPENDENT VARIABLES

The influence of the prediction strategy on the simulator motion is analyzed in three different aspects: 1) analysis of motion quality indicators, 2) analysis of cueing mechanism usage 3) analysis of workspace usage.

MOTION QUALITY INDICATORS

A previous study [59] categorizes motion cueing errors into three types: false cues, scaling or missing cues and phase errors. Each of these cueing errors influences the motion cueing quality in a different way. In order to account for these influences when analyzing the results of the predictive MCA, it is necessary to identify some metrics to quantify the effects of each error.

Shape and scaling errors have been addressed in previous studies [60, 55], where scaling factors were adopted for the MCA and used to separate the contribution of the scaling from the shape error. In another study [125], a more general approach was introduced based on signal correlation to analyze the error introduced only by the signals' shape. The detection threshold of phase errors introduced by the MCA have been also studied [61] and in particular for pitch and yaw motion a phase error threshold of 22 deg/s was identified [87]. A complete knowledge of these phase error thresholds for

every motion channels would give the possibility to evaluate what is the maximum acceptable signal delay that will not be perceived. Unfortunately, these values are not yet known.

In a more recent article [16], dedicated indicators for motion signal correlation, scaling and delay were defined. These indicators have been proven to correlate well with the subjective cueing quality measured in a human-in-the-loop experiment and they will be considered here to study the impact of the prediction strategy on motion cueing quality. The indicators have been slightly modified with respect to their original definition [16] and are described in detail in the following paragraphs.

Correlation Coefficient (CC). Measures the signals' linear correlation. It provides a measure of similarity for the shape of the signal resulting from the MCA with respect to the reference signal. The CC is defined as the maximum value of cross-correlation between the motion resulting from the MCA and the reference motion over all delays. For normalization purpose it is divided by the maximum auto-correlation of the reference signal and therefore it is defined in the range $[0, +1]$, where 1 represents perfect correlation and 0 represents no correlation. The CC is computed for the longitudinal and lateral accelerations as well as for the yaw rate, as these are the only motion channels with significant signal power in car driving maneuvers. The other motion channels mainly contain parasitic motion, due to for example tilt coordination. In the latter case, only very poor correlation is expected.

Delay Indicator (DI). This indicator measures the delay between the reference signal and the signal resulting from the MCA. The indicator's value is obtained by computing the signal cross-correlation and extracting the value of signal delay that maximizes the cross-correlation. This delay is identified as DI and it is defined in the range $[0, +\infty)$. Also in this case, the indicator is used only for longitudinal and lateral accelerations, as well as for the yaw rate. Since the other motion channels do not have significant signal power, the correlation with the reference signal is not meaningful. As mentioned above, for the yaw rate, the phase error detection threshold is known and equal to 22 deg [87]. For each maneuver where the yaw rate is significant, the phase error threshold is divided by the maximum significant frequency content of each maneuver to compute the value of DI that corresponds to the phase error detection threshold. This value of DI represents the maximum signal delay that can not be perceived.

Absolute Difference (AD). This indicator represents the error between the reference signal and the result of the MCA. It is defined as the area of the error signal divided by the area of the reference signal. This definition is adopted for the analysis of the longitudinal and lateral accelerations and for the yaw rate. For the analysis of pitch and roll rate, the AD is defined as the area of the absolute rate above the angular velocity perception threshold of 3 deg/s [113]. With this modification, the AD differs from zeros only if the pitch and roll rate passes the perception threshold, assuming that below that value, the motion will not be perceived.

MOTION CUEING MECHANISMS

The analysis of the indicators gives a very important and quantifiable measurement of motion cueing quality. Similarly to a previous study [24], an analysis of motion cueing mechanisms provides insight to understand how the cueing quality is affected by the

prediction strategy. The motion cueing mechanisms that will be analyzed in this study are presented below.

Tilt coordination. This technique is often used to reproduce sustained linear acceleration with limited workspace motion simulators. The principle is to tilt the simulator in order to use a component of the gravitational acceleration to reproduce longitudinal or lateral acceleration. This mechanism is not explicitly included in the predictive MCA, but it could still be adopted as a result of the optimization.

Prepositioning. This motion cueing mechanism is intended to maximize the simulator motion in a certain direction. The simulator moves towards the extreme of the available workspace to make use of the full motion envelope in the direction needed to reproduce accurately a certain maneuver.

Velocity buffering. This mechanism can be interpreted as the equivalent of prepositioning in velocity and it has been first identified in previous studies [24]. The simulator is moved at a certain velocity in opposite direction with respect to the one needed. At the same time the perceived motion is compensated by tilt coordination, which compensates for the acceleration that is used to generate the linear velocity. When the maneuver begins, the simulator is already moving and can be accelerated in the opposite direction for a longer time.

WORKSPACE USAGE

A crucial limitation for motion simulators is the limited workspace available. The predictive MCA offers the possibility to include the system's constraints in the optimization problem and therefore it makes optimal usage of the available workspace. When changing the adopted prediction strategy, a different motion cueing quality is expected, together with a different usage of the simulator workspace. To determine whether the differences in motion cueing quality between prediction strategies are related to a more effective usage of simulator workspace, a dedicated analysis will be performed. In particular, the use of the actuators' length and motion envelope will be analyzed and compared.

The length of each actuator is computed for the full sequence of maneuvers. In order to analyze how the prediction strategy makes use of the actuators' length, the interquartile range is used. This quantity is normally adopted in statistics as a measure of variability and it is computed as the difference between 75th and 25th percentiles [109]. In this study it will be assumed that a higher interquartile range would represent a wider use of the full actuator length and therefore a more effective usage of the simulator workspace.

Another aspect to notice is the use of the motion system workspace. In this study, the motion obtained for the full sequence of maneuvers with the considered prediction strategies will be analyzed separately for displacement and orientation coordinates. For the analysis of the linear displacement, the sequence of X-Y-Z coordinates can be visualized as a set of points in the Euclidean space. The convex hull of the sets of points obtained by each prediction strategies is computed and its volume calculated. The obtained volumes can be compared with each other and with the complete position workspace, which is the X-Y-Z space that can be reached with every possible orientation of the motion system. A similar analysis is performed for the orientation coordinates. The Roll-Pitch-Yaw coordinates obtained by each prediction strategy for the entire sequence

of maneuvers is used to compute the convex hull. The volumes computed are again compared to each other and to the complete orientation workspace, which is the Roll-Pitch-Yaw space that can be reached with every possible position of the motion system. In this analysis it is inferred that a higher volume of the computed convex hull indicates a larger usage of the simulator workspace.

3.3. RESULTS

To compare the results obtained by the MCA with different prediction strategies, the motion quality indicators are computed and analyzed in Section 3.3.1. The use of different motion cueing mechanisms is presented in Section 3.3.2. Finally, the influence of the adopted prediction strategy on simulator workspace usage is shown in Section 3.3.3.

3.3.1. MOTION QUALITY INDICATORS

The first analysis of the resulting simulator motion depending on the adopted prediction strategy is carried out using the indicators defined in Section 3.2.4.1. To clarify the analysis, the maneuvers involving similar dynamics are grouped together in three sets defined as follows:

- Longitudinal dynamics: Acceleration (A) and Braking (B)
- Lateral dynamics: Constant Turn (CT) and Double Lane Change (DLC)
- Combined longitudinal/lateral dynamics: Braking while entering the turn and accelerating while exiting the turn (BCTA)

For each maneuver set, the most relevant motion channels are considered for the calculation of the indicators.

LONGITUDINAL DYNAMICS

For the longitudinal dynamic maneuvers, the most relevant motion channels are longitudinal acceleration and pitch rate.

The results for the acceleration maneuver are shown in Figure 3.1. The longitudinal acceleration obtained with the *oracle* strategy is very similar to the vehicle motion, while the *constant* strategy fails to reproduce the sustained acceleration at the beginning of the maneuver resulting in a missing cue, and at the end of the maneuver providing a false acceleration cue. The CC indicator reflects the differences in the signal shape. The CC is 0.95 for the *oracle* strategy while it is 0.87 for the *constant*. The distorted acceleration signal obtained with the *constant* strategy also results in a delayed cue. In fact, the obtained DI value for the *constant* strategy is 0.86 seconds, while the DI for the *oracle* is 0.11 seconds. In terms of absolute difference, the acceleration obtained with the *oracle* is very close to the reference motion and therefore the AD is 0.10. For the *constant* strategy, due to the different shape of the signal, the difference with the reference is higher, resulting in a value of AD of 0.33. Regarding the pitch rate, the *constant* strategy keeps the resulting signal at zero until the beginning of the maneuvers, then the angular velocity rapidly increases above the perception threshold. The *oracle* strategy, knowing the

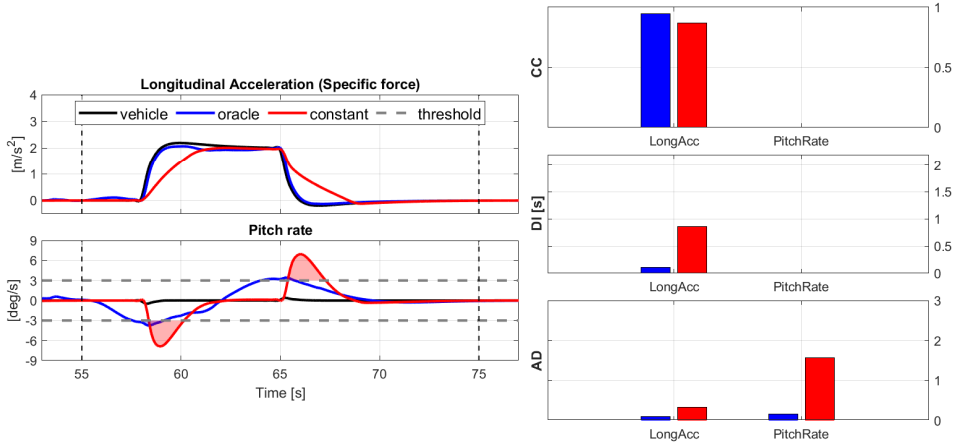


Figure 3.1: Resulting motion, and corresponding motion quality indicators, for the acceleration maneuver A. The results are shown compared to the vehicle motion. Also the rotational velocity perception threshold of 3 deg/s is represented for reference.

future reference in advance, starts using the angular velocity before the beginning of the maneuvers, resulting in a smoother signal which barely passes the perception threshold. The quantification of this effect is provided by the AD indicator, which is 0.17 for the *oracle* strategy and 1.56 for the *constant* strategy.

Similar results for the braking maneuver are shown in Figure 3.2. This maneuver is more aggressive than the acceleration and therefore the differences between the two strategies are more evident. The shape of the acceleration signal for the *oracle* still follows the reference motion, with only a small reduction of motion amplitude. The indicators computed for the *oracle* reflect the motion results, with CC of 0.92, DI of 0.10 seconds and AD of 0.18. For the *constant*, the resulting motion differs from the reference. The signal shape is distorted, resulting again in false and missing cues, with an overall delayed acceleration cue. The results of the indicators for the *constant* strategy confirms the analysis of the motion signal, with CC of 0.77, DI of 1.03 seconds and a value of AD of 0.33. For the pitch rate, the signal obtained by the *oracle* strategy is again smooth but in this case it passes the perception threshold. The *constant* strategy results in a signal that is above the perception threshold for less time than the *oracle*, but with higher amplitude. The results obtained for the AD are the highest of all maneuvers, with a value of 1.73 for the *oracle* and 2.66 for the *constant*.

LATERAL DYNAMICS

For the lateral dynamic maneuvers, lateral acceleration is the most relevant motion channel, together with roll rate and yaw rate.

The results obtained for the constant turn maneuver are shown in Figure 3.3. The lateral acceleration obtained by both prediction strategies follows the reference motion quite well, with an evident difference only in the timing of the signals. In fact, the motion obtained with the *oracle* starts and ends together with the reference, while the *constant*

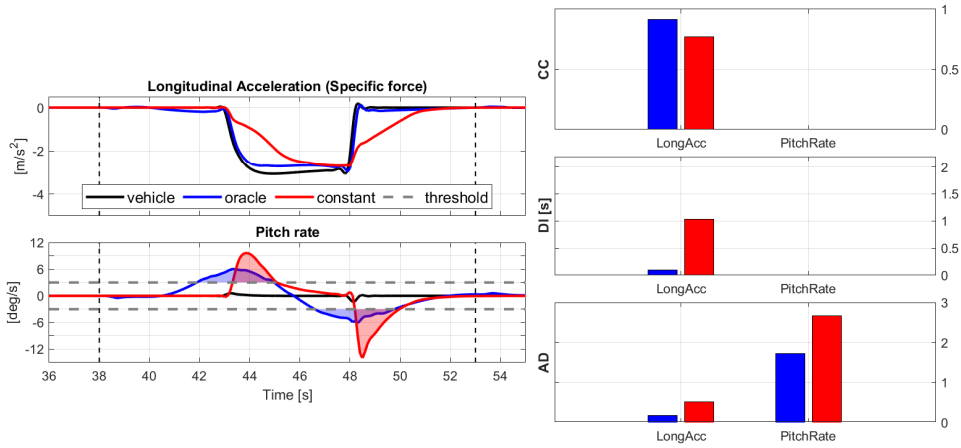


Figure 3.2: Resulting motion, and corresponding motion quality indicators, for the braking maneuver B. The results are shown compared to the vehicle motion. Also the rotational velocity perception threshold of 3 deg/s is represented for reference.

strategy results in a delayed acceleration cue. The analysis of the motion signals finds correspondence in the indicators results, where the main difference between indicators for the lateral acceleration is obtained for the DI, which is 0.05 seconds for the *oracle* and 0.87 seconds for the *constant*. The results for the correlation and absolute difference indicators do not show major differences between the prediction strategies, with

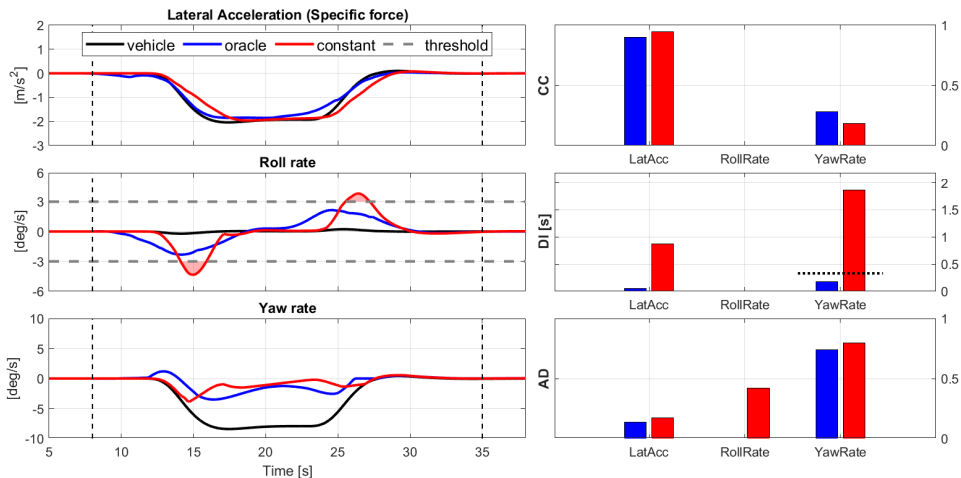


Figure 3.3: Resulting motion, and corresponding motion quality indicators, for the constant turn maneuver CT. The results are shown compared to the vehicle motion. Also the rotational velocity perception threshold of 3 deg/s is represented for reference.

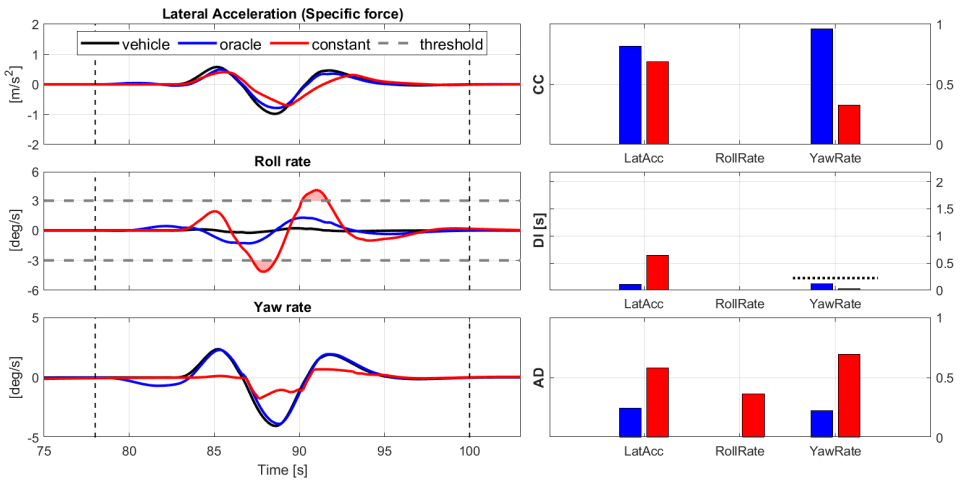


Figure 3.4: Resulting motion, and corresponding motion quality indicators, for the double lane change maneuver DLC. The results are shown compared to the vehicle motion. Also the rotational velocity perception threshold of 3 deg/s is represented for reference.

CC values of 0.90 and 0.95, and AD of 0.13 and 0.17 for the *oracle* and the *constant* strategy respectively. For the roll rate, the motion signal obtained with the *oracle* strategy is always below the perception threshold, consequently the AD is zero. Oppositely, the roll rate resulting from the *constant* strategy exceeds the perception threshold, with an AD value of 0.42. Regarding the yaw rate, both *oracle* and *constant* strategies fail to reproduce the amplitude of the reference motion signal, resulting both in low values of CC and high values of AD. On the other hand, the shape of the signal can still be compared with the reference. The yaw rate obtained with the *oracle* strategy starts by going in the opposite direction but overall it has a shape very similar to the reference with only a small delay. The yaw rate resulting from the *constant* strategy is initially better than the one of the *oracle*, but at 15 seconds, changes direction and the signal goes almost to zero. This is reflected in the CC and DI indicators, where the CC is 0.28 for the *oracle* and 0.18 for the *constant* strategy, and the signal delay is 0.17 seconds for the *oracle* and 1.86 seconds for the *constant*. Together with the results of DI, also the delay threshold at 0.33 seconds is plotted, this value represents the maximum delay that cannot be perceived given the 22 deg of phase error threshold and the frequency content of the reference signal.

The results for the double lane change maneuver are shown in Figure 3.4. The lateral acceleration signal obtained with the *oracle* strategy is very similar to the reference, with only a small reduction in signal amplitude. The acceleration signal obtained with the *constant* strategy has a different shape than the reference, with reduced amplitude and a delay that increases during the maneuver. Also in this case, the results of the indicators reflect the outcome of the analysis. The CC is 0.82 for the *oracle* and 0.69 for the *constant* strategy, the DI is 0.11 seconds for the *oracle* and 0.64 seconds for the *constant* strategy and finally the AD is 0.25 for the *oracle* against 0.58 for the *constant* strategy. For the roll rate, the signal computed with the *oracle* strategy is always below the perception

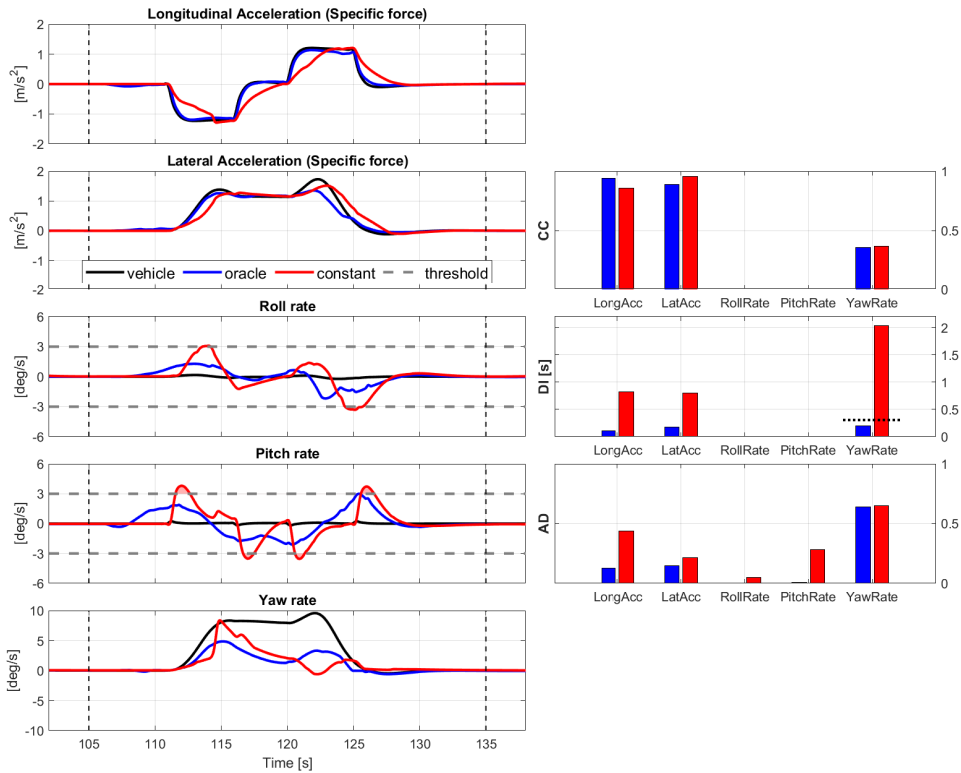


Figure 3.5: Resulting motion, and corresponding motion quality indicators, for the combined dynamic maneuver BCTA. The results are shown compared to the vehicle motion. Also the rotational velocity perception threshold of 3 deg/s is represented for reference.

threshold with a consequent AD value of zero, while the *constant* strategy passes the perception threshold with an AD value of 0.36. Looking at the yaw rate, the results obtained with the *oracle* is very similar to the reference motion, with a small deviation before the beginning of the maneuver and a slight delay. On the contrary, the *constant* strategy fails to reproduce the reference motion, providing a yaw rate signal which only partially reproduces the original motion. The indicators computed for the *oracle* strategy reflect the analysis of the motion, with a CC of 0.96 and a DI of 0.12 seconds. The computed DI is also below the delay threshold of 0.22 seconds. The resulting DI value for the *constant* strategy is equal to 0.03 which is even lower than the DI obtained with the *oracle*, this is most likely due to the very different signal shape which invalidates the result. The AD obtained is equal to 0.23 for the *oracle* and 0.70 for the *constant* strategy.

LONGITUDINAL/LATERAL DYNAMICS

For the analysis of the indicators of the combined dynamic maneuver, the motion channels for both longitudinal and lateral dynamics are considered.

The results obtained for the combined dynamic maneuver are shown in Figure 3.5.

The longitudinal acceleration obtained with the *oracle* strategy is again very similar to the reference motion, the signal shape corresponds, with a short delay and a small difference in amplitude. The corresponding indicator values reflect the analysis with CC of 0.94, DI of 0.11 seconds and AD of 0.13. On the contrary, the longitudinal acceleration resulting from the *constant* strategy differs from the reference motion. The signal shape is distorted, with alternating missing and false cues and an overall delayed signal. The results given by the indicators are representative of these differences, with CC of 0.86, a DI of 0.82 seconds and AD of 0.44. For the lateral acceleration the differences between the motion obtained by the two prediction strategies is less evident but still present. Regarding the shape of the signals, the best result is obtained with the *constant* strategy, which contrary to the *oracle*, is able to reproduce also the peak of acceleration between 120 and 125 seconds. The CC obtained with the *constant* strategy is 0.95, while for the *oracle* is 0.89. On the other hand, the lateral acceleration motion obtained with the *constant* is delayed with respect to the reference, resulting in a DI of 0.80 seconds. In comparison, the DI computed for the *oracle* is 0.18 seconds. The absolute difference for the lateral acceleration motion is comparable for the two prediction strategies, with a value of AD of 0.15 for the *oracle* and 0.22 for the *constant* strategy. For the pitch and roll rate, the motion obtained with the *oracle* strategy is mostly smooth and always below the perception threshold and consequently the AD is in both cases equal to zero. In contrast with the *oracle*, the motion signals obtained with the *constant* strategy is less smooth and passes the perception threshold for both roll and pitch rate, with AD of 0.05 for the roll rate and 0.28 for the pitch rate. For the yaw rate, the resulting motion signals are both different from the reference motion in terms of shape and amplitude, but the signal obtained with the *oracle* strategy is better synchronized with the reference. The indicator results for correlation and absolute difference are very similar for both strategies, with CC of 0.36 and 0.37 and AD of 0.64 and 0.65 for *oracle* and *constant* strategy respectively. The only clear difference in the indicator results is obtained for the DI, which is 0.20 seconds for the *oracle* and 2.04 seconds for the *constant* strategy. Also in this case the delay threshold is computed, the result is 0.31 seconds, which is higher than the DI obtained with the *oracle* strategy.

3.3.2. MOTION CUEING MECHANISMS

Tilt coordination is used in all maneuvers by both prediction strategies. In Figure 3.6, both effects of tilt coordination and velocity buffering can be seen. The usage of tilt coordination from both prediction strategies is evident from the analysis of the components of the longitudinal acceleration. In fact, only the linear component of the acceleration would not be sufficient to reproduce the sustained acceleration, therefore the gravitational component is used, tilting the motion system to use a component of the gravitational acceleration.

Also the effect of velocity buffering can be seen in Figure 3.6, in particular between 40 and 45 seconds and between 55 and 60 seconds. The *oracle* strategy starts accelerating the platform in the opposite direction, while compensating with tilt coordination. The *constant* does not make use of velocity buffering as it starts to tilt the motion platform only when the acceleration begins.

An example of prepositioning can be seen in Figure 3.7, where the lateral displace-

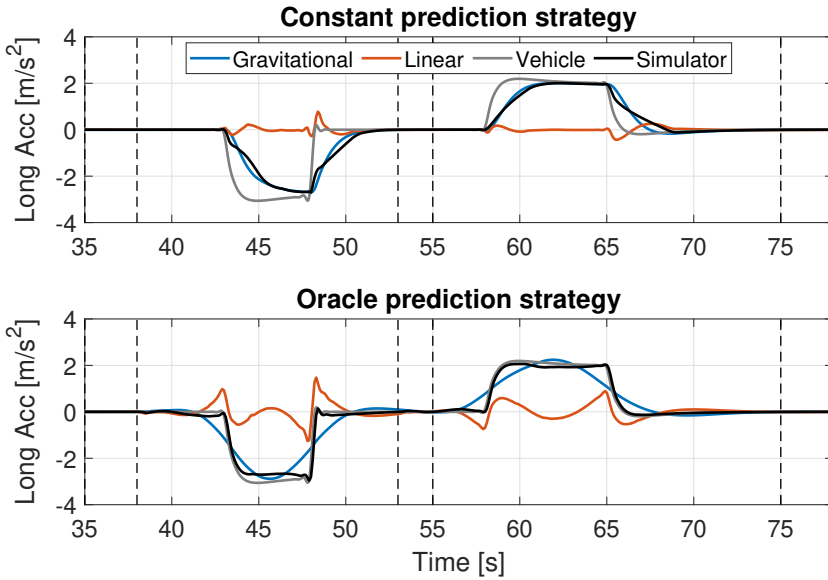


Figure 3.6: Different contributions to linear acceleration reproduction for *oracle* and *constant* prediction strategy in longitudinal dynamic maneuvers.

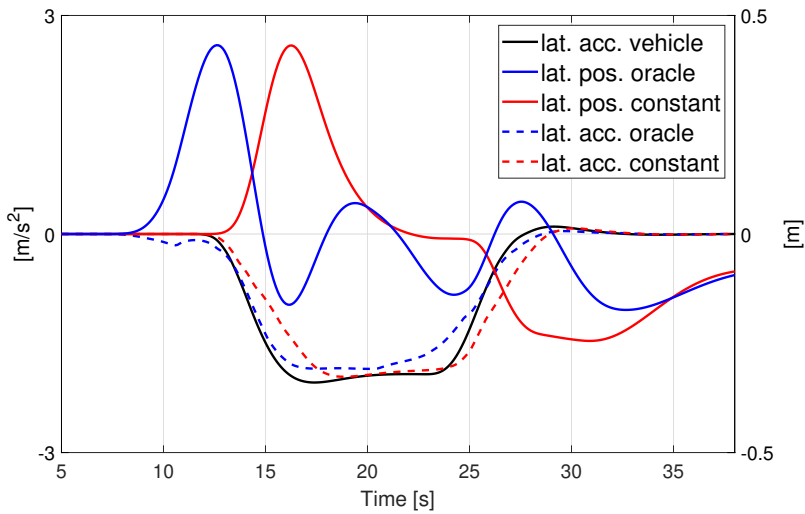


Figure 3.7: Comparison of simulator lateral displacement and perceived lateral acceleration during the constant turn maneuver for *oracle* and *constant* prediction strategy.

ment of the motion system is shown together with the resulting lateral acceleration for each prediction strategy. A few seconds before the maneuver, the *oracle* strategy moves

on one extreme of the available workspace, making possible the use of a longer excursion to reproduce the lateral acceleration. The *constant* strategy does not show similar behavior, by starting the simulator motion at the start of the maneuver.

3.3.3. WORKSPACE USAGE

The actuators' length is computed for the entire sequence of maneuvers and for the two prediction strategies. The length of each actuator is then normalized between 0 and 1 and the interquartile range is computed. The results are shown in Figure 3.8, where it can be seen that the interquartile range is always larger for the *oracle* strategy compared to the *constant* strategy and therefore it can be inferred that the *oracle* makes more use of the actuators' length.

Regarding the usage of the motion platform position workspace, the results are shown in Figure 3.9 for translations and Figure 3.10 for rotations, where the motion envelope for the reproduction of the entire sequence of maneuvers is shown for both prediction strategies. For translations, the volume of the convex hull of the motion envelope used by the *constant* is 0.0451 m^3 and the volume used by the *oracle* is 0.0642 m^3 , which is 42.4% larger. In addition to this, it can be noticed that the *oracle* uses the workspace also in proximity of the physical system's limitation. From the top view of Figure 3.9 it can be noticed that the maximum longitudinal position reached by the *oracle* is very close to the position workspace limit. This point is reached during the braking maneuver, where a large longitudinal displacement is needed to reproduce the reference acceleration. Similarly, the results obtained for the orientation workspace are shown in Figure 3.10. The volume of the convex hull of the motion envelope used by the *constant* is $5.54\text{e}6 \text{ deg}^3$ and the volume used by the *oracle* is $6.17\text{e}6 \text{ deg}^3$, which is 11.4% larger.

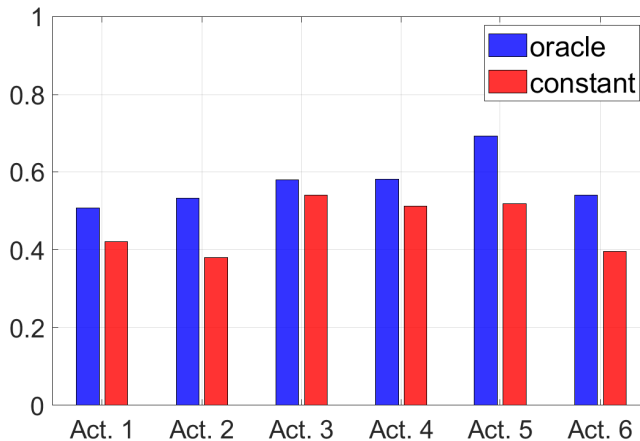


Figure 3.8: Interquartile range of the normalized actuators' length for all the maneuvers. Comparison between the adopted prediction strategies.

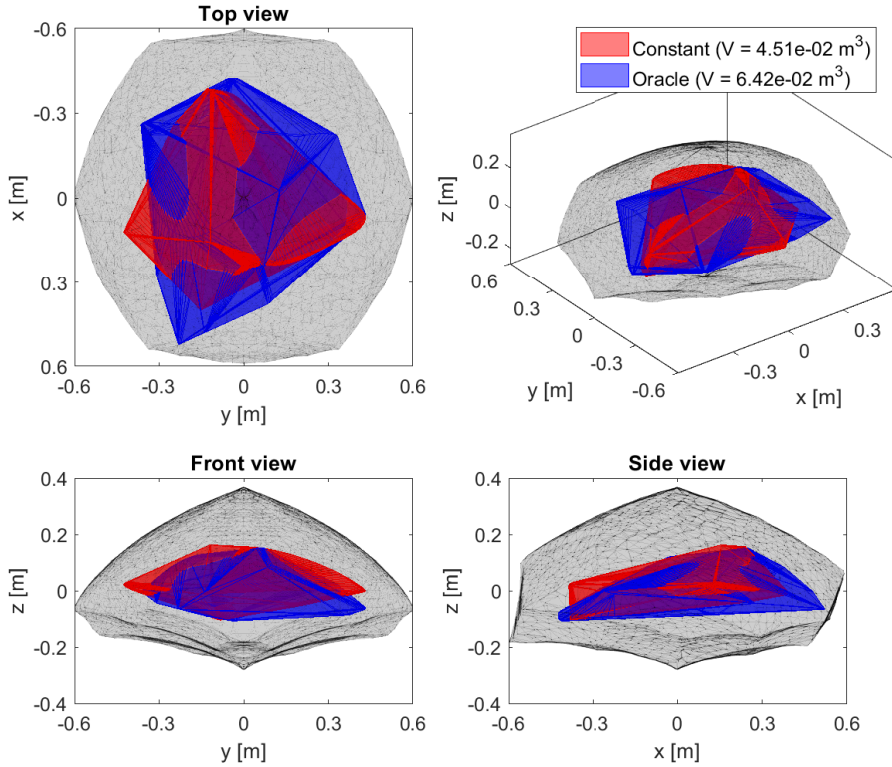


Figure 3.9: Simulator position workspace comparison between *oracle* and *constant* prediction strategy. The motion envelope is computed considering X-Y-Z coordinates. The bigger area represented in light grey is the complete motion platform position workspace considering all reachable orientation.

3.4. DISCUSSION

THE inspection of actual response curves and the corresponding motion quality indicators shows that the indicators are able to qualify and quantify the differences between the reference motion and the motion obtained with the considered prediction strategies. From the results it emerges that several indicators are useful to understand one particular difference between the signals - i.e. shape difference, delay or absolute difference - but only the combined analysis of the indicators provides a complete understanding of the motion resulting from a particular prediction strategy.

The *oracle* strategy achieves higher motion cueing quality than the *constant* by starting the simulator motion before the beginning of the maneuvers, allowing the use of prepositioning and velocity buffering, in addition to tilt coordination, which is the only motion cueing mechanism adopted by the *constant* strategy. The combined use of multiple motion cueing mechanisms adopted by the *oracle* leads to a larger interquartile range for the actuators and therefore to a better use of the simulator workspace, espe-

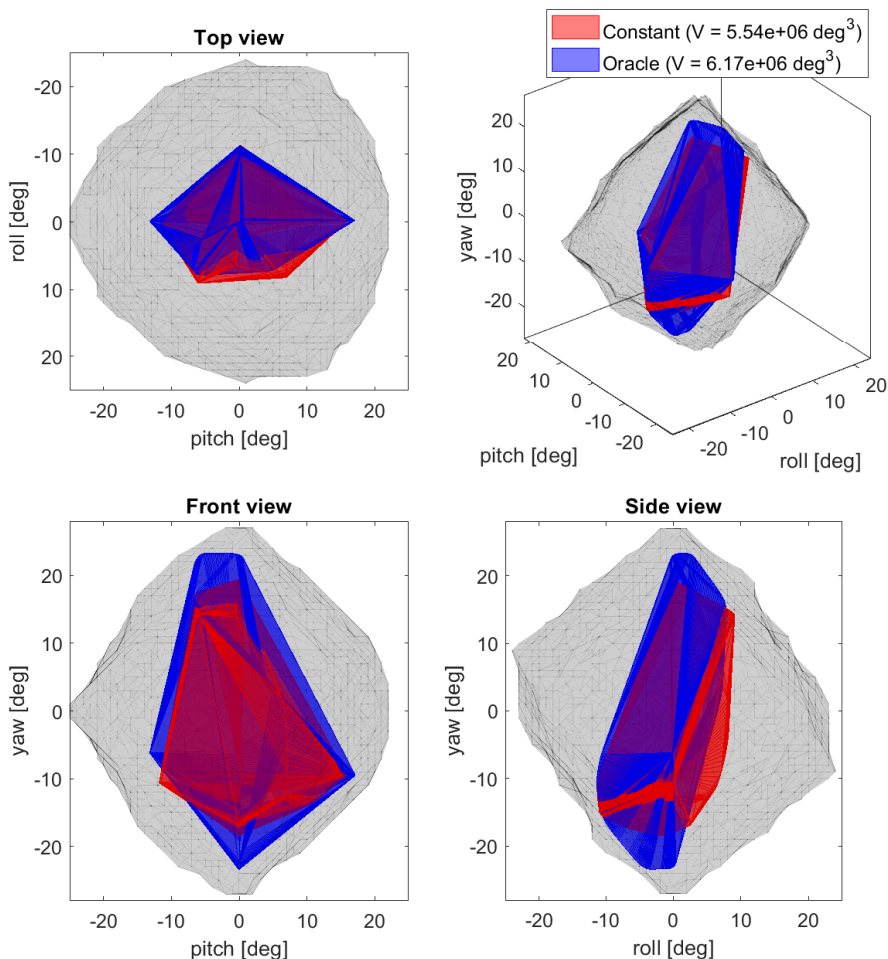


Figure 3.10: Simulator orientation workspace comparison between *oracle* and *constant* prediction strategy. The motion envelope is computed considering Roll-Pitch-Yaw coordinates. The bigger area represented in light grey is the complete motion platform orientation workspace considering all reachable position.

cially when most needed. For example, in the braking maneuver, when the longitudinal acceleration reaches its maximum, the *oracle* strategy results in a simulator motion very close to the maximum longitudinal displacement of the hexapod. It is important to notice that the motion cueing mechanisms are not direct functionalities of the predictive MCA but rather the results of the optimization and they provide better results when the future prediction is perfectly accurate. When the future prediction is incorrect, the quality of the motion cueing could be reduced by a misuse of the motion cueing mechanisms resulting from the attempt of the predictive MCA to reproduce an incorrect reference.

From the results obtained for the workspace usage, it can also be inferred that to

achieve the same motion cueing quality performances, the *oracle* requires a smaller motion system workspace than the *constant*. Or, that the *constant* strategy requires a larger workspace to achieve the same motion cueing quality that can be obtained with the *oracle* strategy.

Moreover, from the analysis of the simulator motion, it can be noticed that the *constant* strategy results are less smooth, with higher linear jerk and angular acceleration values. Previous studies [58, 142] found that this can reduce the quality of perceived motion, which is another aspect that underlines the lower performances of the *constant* with respect to the *oracle* strategy.

The analysis of the maneuvers divided in longitudinal, lateral and combined dynamics shows that the differences in motion cueing quality between *oracle* and *constant* are more evident especially for longitudinal and combined dynamic maneuvers. In particular for longitudinal dynamic maneuvers, the analysis shows large improvement with a more accurate prediction strategy knowing future motion. Nevertheless, the *oracle* strategy cannot be used for DIL simulations, while the *constant* strategy, with its sub-optimal results, can be used for simulating active driving. The results indicate that it is worthwhile to invest in a better prediction than the *constant* and this could be done by using information about the road and traffic, such as traffic signs/lights and/or velocity of leading vehicles. The information could be used to predict if the driver will accelerate or brake the vehicle. Similarly, for the lateral dynamics, information about the future road profile can be used to foresee turning maneuvers. These approaches could be combined with a simplified vehicle model to predict longitudinal and lateral accelerations. Such a prediction strategy would result in improved motion cueing quality performances and still be usable in DIL simulations.

Finally, the objective evaluation carried out in this study is based on objective metrics that have been shown to highly correlate with subjective evaluation and therefore, the results of objective and subjective evaluations are expected to correspond. Nevertheless, it is useful to conduct a human-in-the-loop experiment to identify which indicator weighs most for the overall perceived motion quality and what is the difference between indicator values which is large enough for humans to detect the quality difference. A suitable method to adopt here could be the Continuous Rating method [25], where the subjects of a passive driving experiment continuously provide a feedback of the mismatch between visual and motion.

3.5. CONCLUSIONS

IN this study, the effects of two prediction strategies on optimization-based MCA have been analyzed. The first strategy, *oracle*, assumes perfect knowledge of future vehicle motion, it cannot be used for DIL simulations and it is considered as a reference to evaluate the best motion cueing quality that can be achieved. The second strategy, *constant*, ignores changes in the future reference and assumes a constant reference equal to last vehicle status. The objective analysis carried out aimed to qualify and quantify the effects of the prediction strategies by means of dedicated metrics. Motion cueing quality indicators have been defined to quantify correlation, delay and absolute difference of the simulator motion with respect to the reference vehicle motion. An analysis of the adopted motion cueing mechanisms has been performed together with a study

on the usage of the motion system workspace. As expected, the *oracle* outperforms the *constant* strategy, being able to coordinate the usage of multiple motion cueing mechanisms and manage the use of the limited workspace to obtain better motion cueing quality performances. The combined analysis of multiple indicators confirms the differences in performance and provides the metrics to quantify these differences. From the indicator results, the larger performance difference is obtained for longitudinal dynamic maneuvers, providing an indication of what should be improved in the future design of advanced prediction strategies for optimization-based MCA.

3.6. ACKNOWLEDGEMENT

THE research leading to these results has received funding from the People Programme (Marie Curie Actions) of the European Union's Seventh Framework Programme FP7 2007-2013 under REA grant agreement n. 608092, "MOTORIST". The authors acknowledge the Max Planck Institute for Biological Cybernetics, the researchers and the technicians who were involved in this study. In particular Maria Lächele, Joachim Tesch and Daniel Diers are kindly acknowledged for their technical support. Mikhail Katliar and Ksander de Winkel are also acknowledged for the helpful discussions and suggestions.

II

MOTORCYCLE SIMULATOR EVALUATION: BEHAVIORAL FIDELITY AND PERCEIVED REALISM

4

EMERGENCY BRAKING AT INTERSECTIONS: A MOTION-BASE MOTORCYCLE SIMULATOR STUDY

Powered two-wheeler riders are frequently involved in crashes at intersections because an approaching car driver fails to give right of way. This simulator study aimed to investigate how riders perform an emergency braking maneuver in response to an oncoming car and, second, whether longitudinal motion cues provided by a motion platform influence riders' braking performance. Twelve riders approached a four-way intersection at the same time as an oncoming car. We manipulated the car's direction of travel, speed profile, and its indicator light. The results showed that the more dangerous the situation (safe, near-miss, impending-crash), the more likely riders were to initiate braking. Although riders braked in the majority of trials when the car crossed their path, they were often unsuccessful in avoiding a collision with the car. No statistically significant differences were found in riders' initiation of braking and braking style between the motion and no-motion simulator configurations.

This chapter has been published as:

Natália Kováčsová, Marco Grottolì, Francesco Celiberti, Yves Lemmens, Riender Happee, Marjan P. Hagenzieker, and Joost C. F. de Winter. "Emergency braking at intersections: A motion-base motorcycle simulator study". In: *Applied Ergonomics* 82 (Jan. 2020), p. 102970. DOI: [10.1016/j.apergo.2019.102970](https://doi.org/10.1016/j.apergo.2019.102970).

4.1. INTRODUCTION

BECAUSE of their ability to maneuver on congested roads, Powered Two Wheelers (PTWs) are an efficient mode of transport, especially in dense urban areas. Accident analyzes have shown that a common type of collision involving a PTW in an urban environment is a situation where a car drives into the path of the PTW rider at an intersection [23, 104]. Although it is the car driver who violates the formal rules [118], the PTW rider may have been able to prevent the crash by performing an appropriate evasive maneuver. As pointed out by [35], the majority of studies on these right-of-way crashes have been concerned with the behavior of car drivers, and little empirical evidence exists concerning the behavior of riders.

An in-depth study of human errors in PTW-car crashes showed that riders often fail to perceive and anticipate the car driver's intentions and also fail to perform a satisfactory braking maneuver [119]. Various photo- or video-based studies have been performed to study road users' ability to predict the intentions of car drivers, motorcyclists, and cyclists [44, 98, 152, 153, 157]. For example, [98] found that participants were more accurate in judging turning maneuvers when a vehicle was indicating the turn compared to a condition when the vehicle's indicator was off. Furthermore, it was found that participants viewing video clips were able to judge whether the vehicle would turn even when an invalid turn signal was provided.

Previous studies on PTW rider's braking performance have relied on test-track experiments in which riders had to brake in response to discrete or artificial stimuli such as lights, road markings, or barricades [39, 40, 46, 47, 148]. These studies showed that the average braking distance to an unexpected object (i.e., a barricade) when traveling at a speed of 60 km h^{-1} was approximately 52 m [39], and that response times ranged between 0.55 and 2.55 s [40]. Similarly, a literature review about car driver's brake response times showed that the majority of studies used simple acoustic or visual stimuli rather than more naturally evolving traffic situations [62].

Several researchers have experimentally evaluated how riders respond to right-of-way violations of car drivers. [82] investigated riders' braking behavior in response to an approaching car at a mock three-way intersection. The results showed large individual differences in mean deceleration during emergency braking (between 3.5 ms^{-2} and 7.6 ms^{-2}), and an effect of the car's turn indicator, where deceleration values were lower when the indicator was on compared to when it was off, possibly because braking started earlier. [35] used a motorcycle simulator in a no-motion configuration to investigate how riders of different experience levels approached a three-way intersection when a car pulled out from a side road. The riders who had participated in an advanced riding training showed safer performance in terms of anticipatory slowing down before the intersection compared to regular and novice riders.

Simulators have proved to be a valuable instrument for measuring hazard anticipation skills in ethically challenging emergency events [147]. However, achieving realistic braking performance in simulators remains a challenge [5, 6, 86]. Furthermore, it is technologically challenging to implement independently working front and rear brakes on PTW simulators [143] as well as to simulate realistic motorcycle behavior at low speeds at which the motorcycle is unstable. Despite these technological challenges, simulators are attractive tools for studying rider behavior, as simulators offer the possibility of safely

exposing participants to critical situations [14, 42].

The purpose of this study was twofold: (1) to understand how PTW riders brake at an intersection when encountering a car that might violate the formal right-of-way traffic rule, and (2) to compare how no-motion and motion configurations of the simulator affect rider's braking performance. This study addressed the following two research question:

1. How do riders brake in impending-crash, near-miss, and safe intersection situations?

A rider can use the car's speed, distance to the intersection, and additional cues such as the car's indicator and car's heading to anticipate the intention of the car driver [98, 158]. In line with [82] and [98], we expected that the turn indicator light would contribute to earlier braking as compared to when the car does not use its indicator light. Further, we expected that PTW riders would initiate braking earlier when the car is approaching from the right because this car can be seen to be on a collision course with the rider. If the car is approaching an intersection from the opposite direction, the PTW rider would typically not brake unless the car initiates a left turn and starts to cross the rider's path.

2. Do longitudinal motion cues provided by a motion platform influence riders' braking performance?

We expected that there would be no significant differences in the timing of emergency braking action between no-motion and motion because no motion cues are provided to the rider when riding straight at a constant speed in the motion configuration. Based on previous research in driving simulators [141], we expected that riders would adopt a lower deceleration (i.e., less braking) in the motion configuration than in the no-motion configuration.

4.2. METHOD

4.2.1. PARTICIPANTS

Nine motorcycle riders (license A) and four moped riders (license AM) were recruited from the employees of Siemens PLM Software, Belgium. One motorcycle rider withdrew from the experiment during the practice session due to simulator sickness. Three other participants partially completed the experiment due to simulator sickness (see Section 4.3). The mean age of the remaining 12 participants (10 males, 2 females) was 32.9 years (SD = 6.1). Participants had held their PTW license on average for 10.9 years (SD = 5.8) and their driving license on average for 13.1 years (SD = 5.6), see Table 4.1 for an overview of participants' riding experience. The study was approved by the TU Delft Ethics Committee (Ethics application no. 176, 2017).

4.2.2. APPARATUS

MOTORIST RIDING SIMULATOR

The experiment was conducted on the "MOTORIST" motion-base riding simulator. The simulator consisted of a motorcycle mock-up, type Piaggio Beverly 350 cc, mounted on

Table 4.1: Riding experience in the last 12 months.

Riding frequency	Never	< 1/month	1/month to 1/week	1-3 days/week	4-6 days /week
Nr. participants	2	4	2	2	2
Yearly kilometers	0	1-500	501-1000	1001-5000	10001-20000
Nr. participants	2	4	3	2	1



Figure 4.1: The MOTORIST simulator with a rider wearing an Oculus Rift and safety equipment.

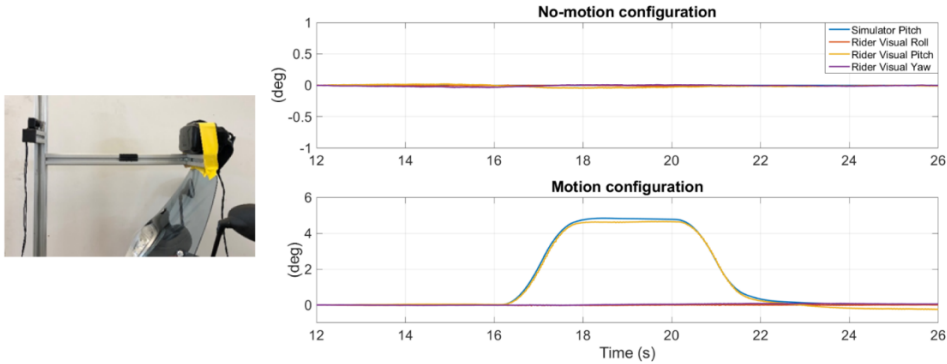


Figure 4.2: Left: Support used to fix the Oculus with respect to the tracking camera. Right: The visual orientation computed with the Oculus Rift SDK remains constant during a no-motion configuration, whereas the visual orientation is affected by the simulator motion. The introduced pitch angle in the visualization follows the angle of the motion system as if the rider would be looking downward/upward during braking/accelerating maneuvers.

a MOOG motion platform (Figure 4.1). The rider could interact with the motorcycle using the throttle handle and two brake levers. The front and rear brake levers worked independently from each other. The rider's braking action was measured by reading the brake lever angles using an encoder. The brake lever angle was sent to a model of the hydraulic braking system, which computed the virtual braking torque applied to the wheels to slow down the simulated vehicle. The rider's steering input did not affect the virtual motorcycle in this experiment. An overview of the simulator is provided by [19]. For safety reasons, participants had to wear a helmet and a protective jacket while riding the simulator. The helmet and jacket were also used to enhance the fidelity regarding the feeling of riding a motorcycle. Furthermore, a full-body safety harness was used to secure the participant to the motorcycle's frame.

HEAD-MOUNTED DISPLAY

The virtual environment was shown to participants using a head-mounted display "Oculus Rift Developer Kit 2" (SDK 0.4) at a rate of 30 frames per second. The binocular setting of Oculus providing stereo vision was used with an inter-pupillary distance of 64 mm. The urban virtual environment was modeled using the PreScan simulation software. A speedometer was presented at the bottom of the displayed image.

The head-mounted display was mounted on a helmet, and the external camera was mounted on a pole attached to the platform in front of the motorcycle mock-up (Figure 4.1). This external camera tracked the headset position and was used in conjunction with an inertial measurement unit in the headset to create a visual field that takes head motion into account [116]. Ideally, the visual image is not affected by the motion of the platform, and the visual orientation remains the same in both the no-motion and motion simulator configurations. The Oculus Rift uses sensor fusion to combine the data measured by the tracking camera and the inertial unit embedded in the Oculus. Even though

the camera was fixed with respect to the motion system of the simulator, the measurement of the inertial unit affected the orientation of the rider view. This effect has been measured by fixing the Oculus with respect to the camera while moving the simulator as in the real experiment (Figure 4.2 left). The results (Figure 4.2 right) showed that, in the motion configuration, the visual orientation computed with the sensor fusion algorithm of the Oculus Rift is following the simulator's physical angle, introducing a visual pitch as if the rider would be looking downward/upward during braking/accelerating maneuvers. This effect does not occur for the no-motion configuration.

RIDING CONFIGURATIONS

In the motion configuration, the motorcycle model provided feedback to the motion base. A traditional washout motion filter was applied using pitch (forward rotation) to simulate sustained acceleration (see Supplementary material for the motion filter parameters). The motion reference point (also called "center of rotation") was located approximately at the position of the rider's head. In the no-motion configuration, no motion cues were provided by the motion platform. Head rotation was possible around three axes in both simulator configurations.

4

4.2.3. STIMULI

The simulated urban environment consisted of a two-lane straight road, where after approximately 295 m, the rider arrived at a four-way intersection at which a car was always encountered. The speed limit was 50 km h^{-1} , and a priority sign was placed before the intersection. The lane width was 3.5 m, and 3 m wide sidewalks were present on both sides of the road. Small visual obstructions were present in the form of trees before the intersection. The same urban virtual environment was used for the practice and experimental sessions, see Figure 4.3 for a top view of the intersection.

Three independent variables were manipulated to create nine different intersection situations:

1. Car's direction of travel. The car could approach the intersection:
 - (a) from the opposite direction on the main road ("From opposite"), or
 - (b) from the right side road ("From right").
2. Car's motion. The speed profile of the car and car's heading were programmed to create three intersection encounters (see Figure 4.4 left). This variable was crossed with the car's direction of travel variable, resulting in six intersection situations.
 - (a) The car continues straight ("Straight"). The car was triggered at a speed of 40 km/h, and it did not decelerate. This was a safe situation if the car approached from the opposite direction, and an impending-crash situation if the car approached from the right. A crash would occur unless the participant braked considerably.
 - (b) The car begins a left turn and stops ("Stops"). The car was triggered at a speed of 40 km/h, and it decelerated to 0 km/h. This was a near-miss for both directions of travel of the car, as the car came to a stop just before making the turn.

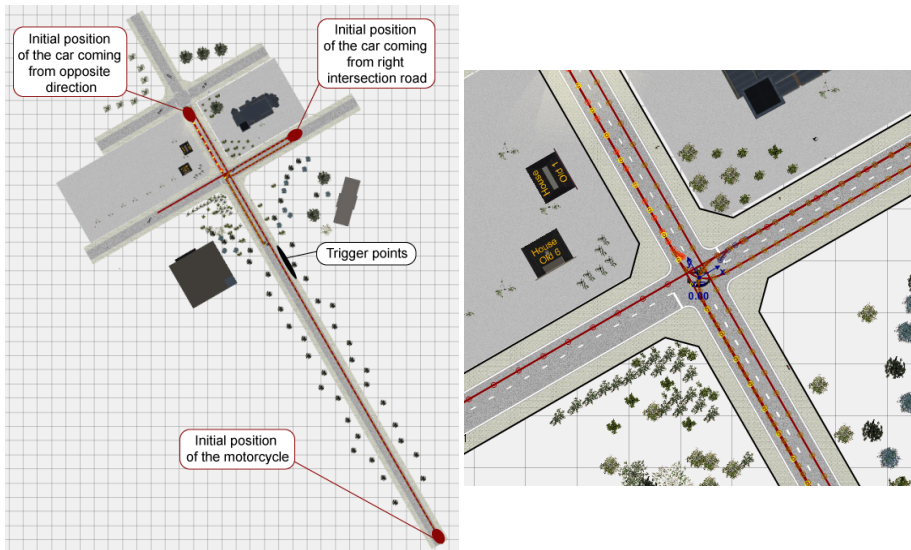


Figure 4.3: Left: Top view of the simulated world. The trajectories of the car and motorcycle are depicted as red lines on the road. Right: Zoomed-in view. The differently colored circular markers (yellow, red, light brown, dark brown) distinguish the different trajectories of the car. The motorcycle approached from the south and always drove in the center of the right lane.

- (c) The car turns left (“Turns”). The car was triggered at a speed of 40 km/h, and it decelerated to 20 km/h before making the turn. This was an impending-crash situation for both directions of travel of the car. In case the car came from the opposite direction of the main road, a crash would occur unless the participant braked considerably.
3. Car’s indicator. Due to low visibility of the actual indicator light in the virtual world, the left headlight was used as an indicator only in the three “car from the opposite direction” situations creating three additional intersection situations (see Figure 4.4 right, situation “From opposite, Stops (I)”). The indicator was either:
- (a) on (abbreviated I), or
 - (b) off.

The cars were triggered when the rider was at a certain distance from the intersection (see Figure 4.4 left for trigger points). The car behaved in a pre-programmed manner and did not adjust its behavior to the participant’s motorcycle in any way. If a participant collided with the car, the simulation continued, and the participant did not receive any collision feedback. The simulation of each intersection situation stopped either approximately 50 m after the intersection or when a participant came to a stop. At the end of each intersection situation, the rider was placed back in the initial position.

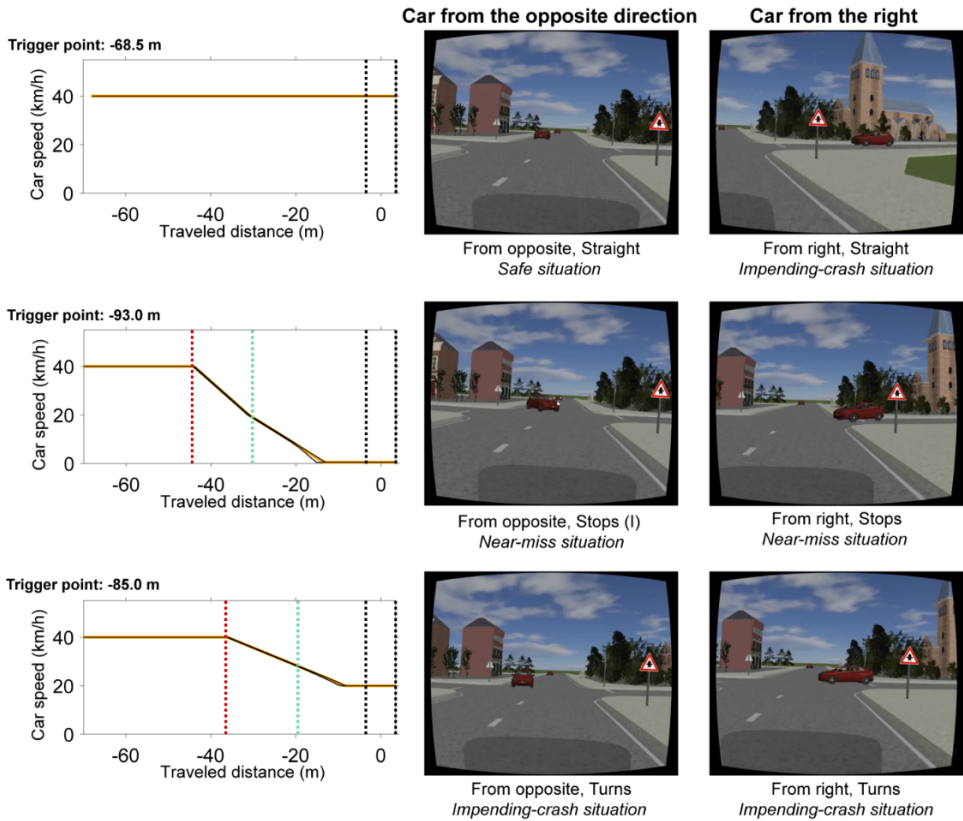


Figure 4.4: Left: Car speed profiles and trigger points (distance between the motorcycle and the center of the intersection when the car was spawned). The black vertical lines indicate the start and end of the intersection, the red vertical line indicates the moment the approaching car started to decelerate, and the green vertical line indicates the moment when the heading of the approaching car started to change. Right: Screenshots of six intersection situations as observed by the participant. The speedometer (which was presented at the bottom of the displayed images) is not included in these screenshots.

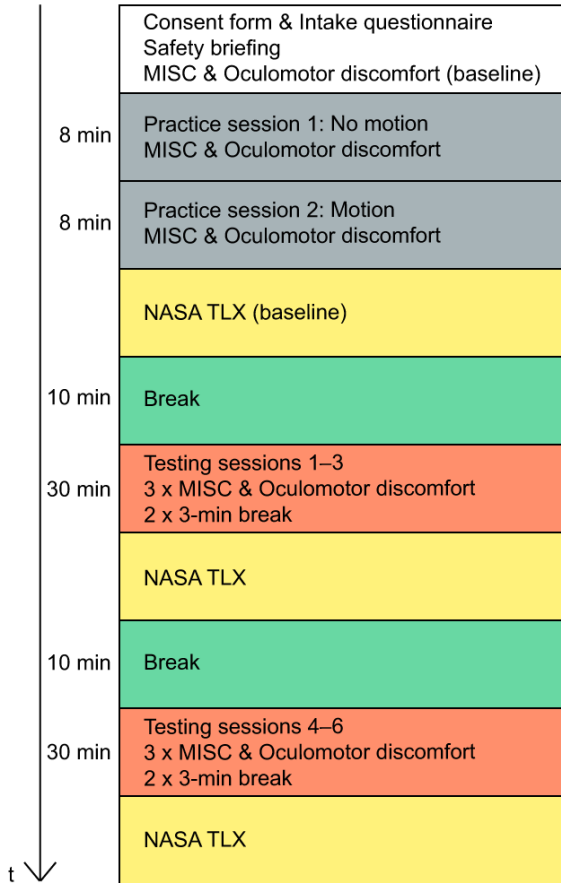


Figure 4.5: The experimental timeline. The orange blocks consisted of either three no-motion or three motion configuration sessions and were counterbalanced across participants.

4.2.4. PROCEDURE

The experiment was conducted at the Siemens PLM Software facilities, Belgium. Before the simulator sessions, a consent form was signed, and the participants completed an intake questionnaire. The intake questionnaire consisted of items on demographic characteristics, riding and driving experience, and a baseline questionnaire on simulator sickness. See Figure 4.5 for the experimental timeline.

Participants conducted two practice sessions to familiarize themselves with the simulator controls, visual stimuli (e.g., triggered cars), and the emergency braking task. Riders were informed about the nine intersection situations in the consent form, and they experienced them during the practice sessions. Each practice session consisted of nine different intersection situations presented in random order. The first practice session was conducted in the no-motion configuration and the second practice session in the motion configuration.

Following the two practice sessions, a participant completed 54 different repetitions of the intersection situations (9 intersection situations x 3 repetitions x 2 simulator configurations), divided into six sessions. Similar to the practice sessions, each testing session consisted of nine different intersection situations presented in random order and lasted approximately 8 min. Two blocks of three no-motion and three motion configuration sessions were created and counterbalanced across participants.

At the beginning of each trial, the participant was asked to hold the throttle to indicate that the simulation could start. The motorcycle automatically accelerated to 50 km/h, and this speed was maintained using cruise control until the rider started to brake. The throttle position did not influence the simulation when the motorcycle was already moving. When the rider started to brake and did not come to a full stop, the PTW automatically accelerated back to 50 km/h if the brake was fully released. Participants' task was: "You will be riding 50 km/h, try to keep this speed as long as you can and brake only when needed to avoid a crash".

After each session, simulator sickness was measured using the Misery Scale (MISC) [7] and by the item on experienced oculomotor discomfort from the Simulator Sickness Questionnaire [92]. The NASA Task Load Index (NASA TLX) [78] was administered three times during the experiment; once after the practice sessions, and twice after the no-motion and motion blocks. The entire experiment took approximately 2 hours per participant.

4.2.5. MEASURES

RIDING PERFORMANCE MEASURES

The braking signal was averaged across the front and rear brake levers, in order to obtain an index of total braking input, where 100% represents the maximum value possible (occurring when braking 100% at the front and at the rear). A threshold of 3% of the average brake signal was used to distinguish braking from non-braking. The following measures were calculated as an average across available trials per intersection situation per person.

Brake initiation moment (m). This measure describes the moment of braking, expressed as the participant's distance to the center of the intersection at the moment the participant pressed the brakes. We used distance (m) instead of elapsed time (s) for the sake of interpretability regarding situational events such as trigger points of the car. However, it is noted that distance can readily be converted to time because the participant's motorcycle had a constant approach speed of 50 km/h. This measure was calculated for a traveled distance between 70 m before the intersection and the entrance to the intersection located 3.5 m before the center of the intersection.

Minimum riding speed (km/h). This measure describes the minimum riding speed while approaching the intersection (i.e., before a potential collision with the car). This measure was calculated for the same travel distance as the previous measure. Speed data were logged until approximately 2 km/h, after which a trial ended.

Maximum brake position (%). The maximum brake position was used as an index of how hard riders decelerated. This measure is the maximum percentage of the rider's braking. This measure was calculated for a distance between -70 m and -3.5 m before the center of the intersection.

Brake rise distance (m). This measure represents the rider's braking style. It describes the traveled distance between the initiation of braking (threshold at 3%, as above) to the maximum brake position before the rider entered an intersection.

Percentage of trials with a stop (%). This measure indicates whether the rider came to a stop before entering the intersection. This measure was calculated for each of the four impending-crash intersection situations separately. We used a threshold of 5 km/h to distinguish stopping from not stopping.

Percentage of trials with a crash (%). The crash percentage was calculated using the distance between the centers of two vehicles in the virtual world. If this distance was below 2.4 m, a crash was recorded. The percentage of crashes was calculated for the four impending-crash intersection situations.

SELF-REPORTS

Simulator sickness (010). The 11-point MISC [7] and an item on oculomotor discomfort "I experience oculomotor discomfort at the moment (eyestrain, difficulty focusing, blurred vision or headache)." [92] were provided to participants to monitor the development of simulator sickness during the experiment. The MISC ranges from no problems (0) to vomiting (10). The experienced oculomotor discomfort was rated on a scale from not at all (0) to very much (10). If the participant reported a score of 6 or higher on one of these items, the experiment was interrupted, and either a longer break was taken by the participant or the participant withdrew from the experiment.

NASA TLX (121). The six-item NASA TLX questionnaire was used to assess riders' workload. The questionnaire contained items on mental demand, physical demand, temporal demand, performance, effort, and frustration [78]. Items were rated on the 21-point scale ranging from very low (1) to very high (21) and failure (1) to perfect (21) for the performance item.

4.3. RESULTS

ONE female and one male participant withdrew from the motion test sessions because of experiencing severe nausea and medium oculomotor discomfort during the first motion test session. The female participant had completed two no-motion sessions, and the male participant had completed all three no-motion sessions without experiencing severe discomfort. Therefore, these two participants were included in the analysis for the no-motion configuration only. Another female participant experienced severe nausea and severe oculomotor discomfort during the last motion test session. This participant was included in the analysis for both the no-motion and motion conditions; only data from the last (sixth) session were excluded. Further, a data quality check revealed that there was a data logging error in the last no-motion session for one participant and in one motion trial for another participant. Results reported below are based on 306 trials completed in the no-motion configuration and 260 trials completed in the motion configuration.

4.3.1. SIMULATOR SICKNESS AND EXPERIENCED WORKLOAD

There were no significant differences in experienced motion sickness and oculomotor discomfort between the two simulator configurations among ten participants who com-

Table 4.2: Minima, maxima, means, standard deviations, and results of paired sample t-tests for self-reported simulator sickness and NASA TLX per simulator configuration for the 10 participants who completed both simulator motion configurations.

	No Motion			Motion			No Motion vs. Motion	
	Min	Max	Mean (SD)	Min	Max	Mean (SD)	t (df)	p
Sickness (0–10) ^a	0	4.33	1.00 (1.40)	0	4.67	1.47 (7.90)	-1.26 (9)	0.240
Oculomotor discomfort (0–10) ^a	0	5.00	1.50 (1.86)	0	5.00	1.77 (1.87)	-1.10 (9)	0.299
NASA TLX: Mental demand (1–21) ^b	3	7	4.40 (1.43)	3	11	5.90 (2.96)	-2.29 (9)	0.048
NASA TLX: Physical demand (1–21) ^b	1	12	4.90 (3.03)	3	20	8.50 (5.84)	-2.66 (9)	0.026
NASA TLX: Temporal demand (1–21) ^b	3	12	5.30 (2.71)	3	14	6.30 (3.62)	-2.24 (9)	0.052
NASA TLX: Performance (1–21) ^b	5	17	10.80 (4.21)	6	17	11.60 (3.89)	-1.31 (9)	0.223
NASA TLX: Effort (1–21) ^b	3	15	8.20 (3.99)	3	16	9.90 (5.04)	-2.85 (9)	0.019
NASA TLX: Frustration (1–21) ^b	1	14	5.10 (4.33)	1	16	4.80 (4.66)	0.90 (9)	0.394

Notes. *p* values < 0.05 are in boldface.

^a asked after each session, ^b asked after each block, i.e., three sessions.

pleted trials for both configurations (Table 4.2). The self-reported mental demand, physical demand, and effort were significantly higher for the motion condition as compared to the no-motion condition.

4.3.2. EFFECT OF VISUAL STIMULI ON RIDERS' SPEED AND BRAKING PERFORMANCE

Riders initiated braking in 16.7% of the 126 safe situation trials in which the car from the opposite direction drove straight ahead, in 50.5% out of 188 near-miss trials where the car performed an emergency stop, and in 98.0% out of 252 impending-crash trials in which the car drove into the path of the rider. Figure 4.6 shows that the riders did not brake immediately after the car approaching from the opposite direction started to decelerate (top and middle rows). Instead, the riders started to initiate braking right after the car started to change its heading. On average, riders initiated braking further from the intersection in “car stops” situations as compared to the “car turns” situations (Table 4.3).

Table 4.3: Means and standard deviations of the brake initiation moment, maximum brake position, and brake rise distance for nine intersection situations.

	Brake initiation moment (m)				Minimum riding speed (km/h)				Maximum braking position (%)				Brake rise distance (m)			
	No Motion		Motion		No Motion		Motion		No Motion		Motion		No Motion		Motion	
	Mean(SD)	n	Mean(SD)	n	Mean(SD)	n	Mean(SD)	n	Mean(SD)	n	Mean(SD)	n	Mean(SD)	n	Mean(SD)	n
From opposite, Stops ^{nm}	-25.19 (1.98)	9	-25.75 (3.45)	8	34.48 (17.06)	12	33.71 (20.34)	10	36.91 (28.50)	12	33.82 (32.72)	10	6.97 (2.67)	9	4.49 (2.55)	8
From opposite, Turns ^{ic}	-17.80 (5.28)	12	-17.94 (4.31)	10	24.31 (10.01)	12	25.27 (7.83)	10	78.91 (15.26)	12	77.39 (16.00)	10	9.26 (5.37)	12	9.33 (5.86)	10
From opposite, Straight ^s	-18.87 (7.32)	2	-23.95 (3.89)	2	50.02 (0.97)	12	50.23 (0.50)	10	1.61 (3.83)	12	0.73 (1.32)	10	6.45 (1.48)	2	4.50 (1.13)	2
From opposite, Stops (I) ^{nm}	-30.24 (11.24)	9	-28.58 (10.31)	7	34.47 (18.69)	12	33.05 (19.66)	10	31.89 (30.20)	12	30.47 (33.23)	10	9.37 (6.59)	9	7.44 (5.70)	7
From opposite, Turns (I) ^{ic}	-18.45 (5.59)	12	-21.59 (10.70)	10	23.81 (12.03)	12	21.57 (10.01)	10	78.07 (15.99)	12	75.61 (16.26)	10	8.81 (4.92)	12	11.44 (8.31)	10
From opposite, Straight (I) ^s	-29.83 (6.56)	4	-24.44 (11.08)	4	45.50 (13.22)	12	48.10 (4.54)	10	8.00 (16.98)	12	7.15 (11.19)	10	8.84 (7.42)	4	6.58 (6.50)	4
From right, Stops ^{nm}	-33.51 (6.90)	5	-39.50 (4.28)	4	46.20 (9.71)	12	43.55 (12.44)	10	8.32 (17.36)	12	10.39 (18.90)	10	6.26 (3.17)	5	12.90 (8.26)	4
From right, Turns ^{ic}	-26.83 (5.65)	11	-27.60 (7.07)	10	17.23 (14.02)	12	10.92 (8.50)	10	61.00 (25.59)	12	70.19 (21.26)	10	12.22 (5.85)	11	12.57 (9.54)	10
From right, Straight ^{ic}	-19.37 (7.31)	12	-20.15 (9.99)	10	20.39 (14.08)	12	22.89 (17.00)	10	77.14 (16.95)	12	73.98 (19.99)	10	10.19 (4.82)	12	10.66 (6.20)	10

Notes. (I), the car was indicating a turn. ^s, safe situation; ^{nm}, near-miss situation; ^{ic}, impelling crash situation.

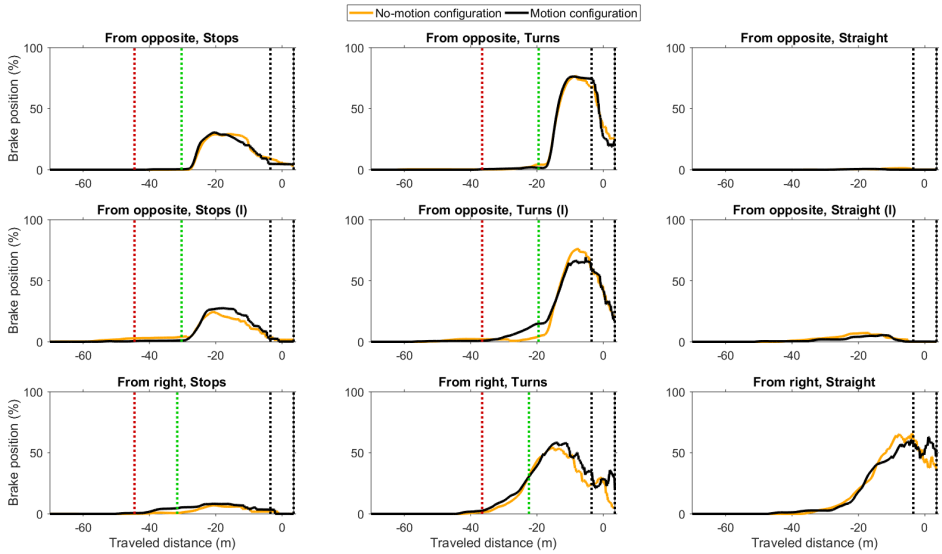


Figure 4.6: Mean brake position (front and rear brake averaged) during the nine intersection situations per simulator motion configuration. In case a participant came to a stop, data are not shown further. The black vertical lines indicate the start and end of the intersection, the red vertical line indicates the moment when the approaching car started to decelerate, and the green vertical line indicates the moment when the heading of the approaching car started to change.

CAR'S INDICATOR

Riders initiated braking on average 3.94 m (in “Stops” situations) and 2.15 m (in “Turns” situations) earlier when the car from the opposite direction indicated the turn as compared to when the car did not (Table 4.3). The average riding speed while approaching the intersection was similar for both indicator conditions (Figure 4.7). The effect of the indicator on the brake initiation moment was not statistically significant for the “car turns” situations ($t(11) = 0.50$, $p = 0.627$ and $t(9) = 1.50$, $p = 0.169$ for the no-motion and motion configurations, respectively). The effect of the indicator on the minimum riding speed in the “car turns” situations was not significant either ($t(11) = 0.27$, $p = 0.791$ and $t(9) = 0.93$, $p = 0.377$ for the no-motion and motion configurations, respectively). The t -tests were not conducted for the “car stops” situations due to the low number of braking events. Although riders braked in the “car turns” situations, they still often crashed into the car (Table 4.4). The percentage of crash involvement was slightly lower in situations when the car indicated a turn compared to situations when the car did not indicate the turn.

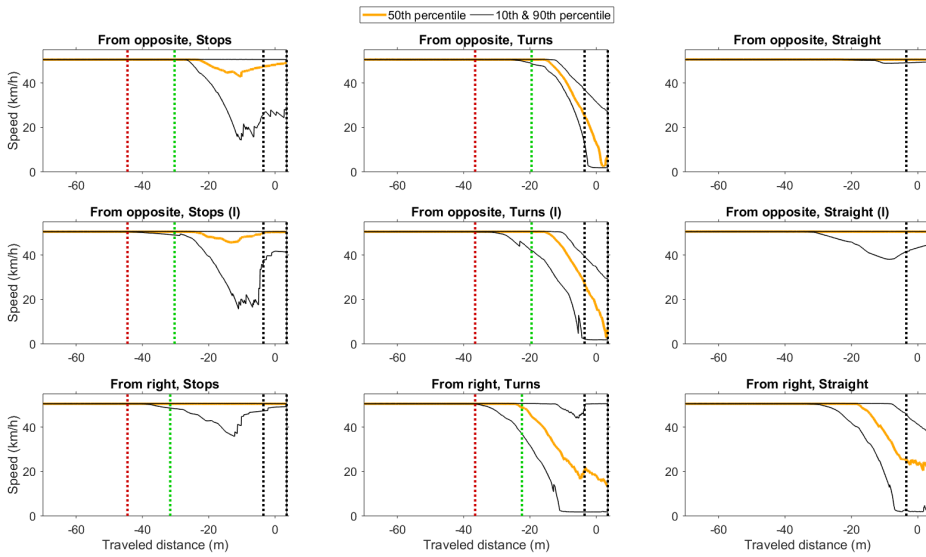


Figure 4.7: Median, 10th percentile, and 90th percentile of speed across trials per intersection situation. In case a participant came to a stop, data are not shown further. The black vertical lines indicate the start and end of the intersection, the red vertical line indicates the moment when the approaching car started to decelerate, and the green vertical line indicates the moment when the heading of the approaching car started to change.

Table 4.4: Percentage of trials when riders came to a stop (threshold at 5 km/h) before entering the intersection and percentage of trials in which riders were involved in a collision for the four impending-crash situations.

	From opposite Turns		From opposite Turns (I)		From right Turns		From Right Straight	
	Stop	Crash	Stop	Crash	Stop	Crash	Stop	Crash
No Motion	8.82%	76.47%	17.65%	73.53%	50.00%	0.00%	32.35%	8.82%
Motion	0.00%	79.31%	24.14%	65.52%	62.07%	0.00%	31.03%	20.69%

Notes. (I) - The car was indicating a turn.

Crash in the “From right, Turns” situation could not happen because this car was triggered at the same time as the cars in “From opposite, Turns” situations as a result of which the potential collision point was located further down the road.

CAR’S DIRECTION OF TRAVEL

When the car approached the intersection from the right and turned (“From right, turns”), riders on average braked 9.34 m earlier compared to the situation where the car approached from the opposite direction and turned (“From opposite, turns”). This effect, which can be seen in Figure 4.6 (bottom middle vs. top middle), was significant ($t(10) = 4.79, p < 0.001$ and $t(9) = 5.61, p < 0.001$ for the no-motion and motion configurations, respectively). As can be seen in Table 4.4, riders were less likely to come to a stop before entering an intersection when the car approached from the opposite direction as compared to situations when the car approached from the right intersecting road.

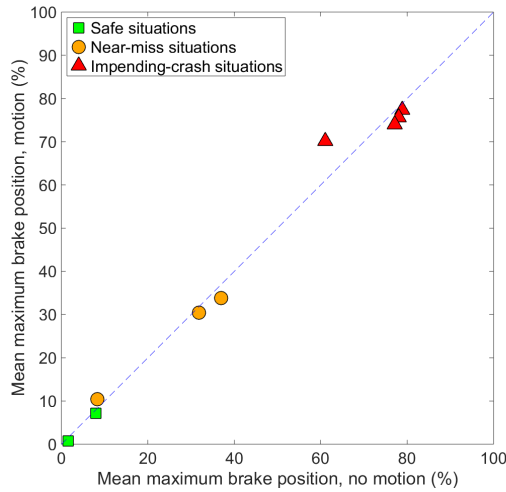


Figure 4.8: Mean maximum brake position for the nine scenarios shown in Table 4.3, for the no-motion configuration and the motion configuration. The diagonal dashed line is the line of unity.

4.3.3. COMPARISON OF BRAKING PERFORMANCE BETWEEN THE MOTION AND NO-MOTION CONFIGURATIONS

Figure 4.6 shows the mean brake position and Table 4.3 shows the means and standard deviations of the brake initiation moment, maximum brake position, and the distance from initiating of braking to the point of maximum braking (i.e., brake rise distance) for the two motion configurations. The results of paired sample t-tests did not show a significant effect of simulator motion on the maximum brake position ($p > 0.215$ for each of the nine situations) nor on brake rise distance ($p > 0.131$ for each of the nine situations). Lastly, no substantial differences were observed in the initiation of the braking maneuver between the motion and no-motion configurations ($p > 0.022$ for each of the nine situations).

Further illustration for the lack of effect of motion is provided in Figures 4.8 and 4.9. Figure 4.8 shows the maximum brake position for the nine intersection situations. It can be seen that the effect of situation is stronger than the effect of motion; the correlation between the values for the two configurations was close to unity ($r = 0.99$, $n = 9$). Figure 4.9 shows a bimodal distribution of the maximum brake position; participants either braked hard or did not brake, with relatively few instances of mild braking (5–40%).

4.4. DISCUSSION

ACCIDENT statistics show that a frequent crash scenario involving a PTW rider is a crash with a car at an intersection [23, 104]. An in-depth investigation of PTW-car accidents showed that car drivers often failed to perceive the oncoming motorcycle, whereas the PTW riders failed not only in perception but also in executing an avoidance maneuver, such as too weak braking [119]. To study this issue from the perspective of the PTW rider, we performed a simulator study that compared riders' braking performance

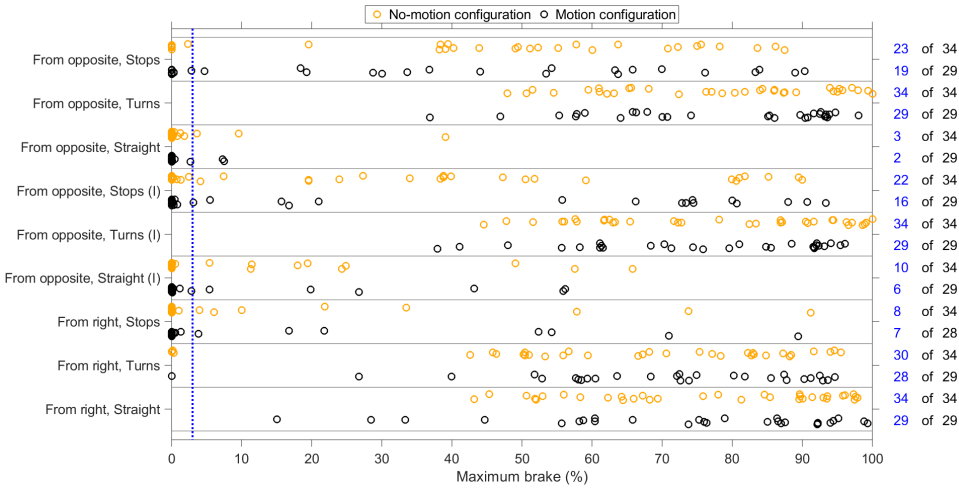


Figure 4.9: The maximum brake position prior to entering the intersection. Each marker represents a single trial. Blue numbers represent the number of trials in which participants pressed the brakes (threshold at 3% brake input).

for impending-crash, near-miss, and safe intersection situations.

The results showed that riders initiated braking right after the car from the opposite direction made a heading change that could signal an imminent threat. The riders initiated braking later (i.e., when they were closer to the intersection) in impending-crash situations compared to near-miss situations. This finding can be explained by the fact that riders appeared to brake immediately after a change in the car’s heading, which occurred earlier in near-miss situations than in the impending-crash situations.

Results further indicate that, in situations where a car driver suddenly initiates a left turn, riders are often unable to avoid a collision. It should be noted, however, that the approach speed was fixed at 50 km/h and riders were instructed to try to keep this speed as long as they could and brake only to avoid an upcoming crash. A previous study [35], showed that expert riders tend to slow down when approaching an intersection, indicating that not only “bottom-up” visual cues but also “top-down” expectancies guide riders’ behavior. A similar account is provided by another study [145], which illustrated the interaction of top-down factors and bottom-up factors leading up to cyclist-driver crashes. The results from our study suggest that such precautionary strategies are essential for safety, as a purely detective/reactive behavior of the rider is not enough to avoid a collision.

In line with the findings from previous studies on the importance of the car’s indicator [81, 98], riders initiated their braking maneuver slightly earlier when the car was indicating the turn as compared to when the indicator was off. However, the motion of the car and change of heading had stronger effects on the initiation of braking than the indicator signal, as inferred from the fact that riders were unlikely to brake in safe situations even if the turn signal was on. According to the instructions that we provided, participants should not brake when the car continued straight or stopped. In other words,

the indicator had to be ignored in these two situations. The effect of the indicator could be smaller in our study as compared to on-road riding because, in reality, the cars' indicator would guide the rider's expectancies and thereby cause the rider to slow down. Furthermore, we note that in real-life cases, riders may be able to anticipate what other road users will do, not only based on the turn indicator but also with the help of other types of precursors or foreshadowing elements [147, 151]. Examples of such precursors, which were not simulated in our study, include the pre-positioning of the lateral position of the car, additional conflicting vehicles, road markings, head orientation, and eye contact. Future research could employ a more varied visual environment in which multiple road features (e.g., signs, lights, multiple road users) are present, thereby placing high demands on anticipation skills.

Riders initiated their braking maneuver in crash situations earlier when the car was approaching from the right compared to situations when the car approached the intersection from the opposite direction. This effect corresponds to the relatively high percentage of stops before the intersection in the "car from right" situations. One plausible explanation is that the car from the right is on a collision course with the rider, whereas the car coming from the opposite direction is on a collision course only when it turns to its left. Accordingly, in the car-from opposite situations, the riders started to brake only when visual information such as the car's indicator or heading in combination with high speed could be observed.

The second aim of this research was to compare riders' braking performance when longitudinal motion cues are provided by a motion platform compared to a no-motion simulator configuration. Our results did not show detectable effects of motion on the riders' braking behavior. This result appears to contradict literature that indicates that drivers brake more smoothly when motion cues are enabled as compared to when they are disabled [63, 141] as well as more general studies showing that simulator motion can have strong effects on driving behavior [4, 140].

Apart from statistical power, three possible explanations for the discrepancy between our results and the literature can be thought of. First, because the riders approached the intersection using cruise control and steering input did not affect the virtual motorcycle, motion cues were unavailable before the rider started to brake in both the no-motion and motion conditions. This means that the effects of motion on the riders' risk perception and subjective presence in the virtual environment may have been limited; only after the rider started to brake, he/she could feel the motion. Second, we showed that the riders' decisions were rather binary: short-lasting hard braking or no braking (Figure 4.9). This observation ties into theories about open-loop versus closed-loop manual control [83]. In particular, if riders "slam on the brakes to avoid a collision" [83], no association between braking control and motion feedback ought to be expected. A third explanation for the lack of observable motion effects concerns the motion cueing algorithm itself. It is possible that our adaptive filter-based algorithm as detailed in the Supplementary material yielded a too sluggish response for the highly dynamic braking maneuver under investigation. Thus, the lack of effect by no means implies that motion would not have effects for other types of riding/driving tasks and other types of motion drive laws. It remains to be investigated whether motion affects closed loop braking behavior. This research question could be studied in non-emergency tasks such as ap-

proaching an intersection where a rider does not have the right of way or before entering a turn.

Several limitations should be considered when interpreting the present results. First, only 12 people participated, raising questions about statistical power (i.e., 1 minus the false-negative rate), false positives [12], and generalizability. The small sample size is a concern for the results for the turn indicator, where significant effects may plausibly be expected if larger samples were used. On the other hand, some of the other observed effects presented in this paper are very strong and may not require larger samples. Specifically, the effects concerning the car's direction of travel on the participant's behavior were strong and significant ($p < 0.001$), suggesting high replicability. Also, the finding that motion increases self-reported physical demands and effort is interpretable from a biomechanics viewpoint and thus expected to be replicable. Also, the fact that participants in near-miss scenarios braked harder as compared to safe scenarios, but less hard as compared to impending-crash scenarios, is interpretable and strong, with little overlap of distributions (see also Figure 4.7). In summary, we argue that the present sample size is a limitation for some of our findings (e.g., effect of the indicator), but still sufficient for our primary research purposes. It should be reminded that our type of research involves ethical and safety challenges regarding motion sickness after-effects [9, 45]. Hence, we would advise other researchers not to test more participants than needed if they were to conduct this type of research. The current results show a learning curve where participants grew accustomed to the fact that they did not have to brake in the safe situations, and gradually braked less hard in the near-miss and impending-crash situations (supplementary material [94]). It would be interesting to examine how these trends develop in an even larger number of trials.

A second limitation is that our study aimed to investigate whether riders are capable of avoiding a potential collision based on “bottom up” visual cues in situations where a crash could be expected. In reality, situations in which a car driver does not give right of way are encountered only rarely. Instead, on the road, riders may show a later initiation of braking in case the situation is not expected by the rider [62, 117] as well as anticipatory braking before the relevant visual cues are available. More research should be conducted to understand to what extent a precautionary approaching strategy could significantly reduce the number of crashes.

Third, the realism of the simulator deserves further consideration. Future research could employ a more realistic PTW dynamics model, allowing for the in-depth examination of brake modulation of the front and rear brakes and motorcycle stability in emergency braking conditions (for models see [28, 101]). The virtual environment built in PreScan and projected in the Oculus Rift DK2 resulted in a limited screen resolution. For this reason, the car's headlight had to be used instead of the car's indicator light. This limitation is relatively easily countered in future research, as the resolution and refresh rate of the head-mounted display is rapidly increasing [150]. Future research could also use richer virtual environments in order to examine the effect of the aforementioned hazard precursors, although it remains to be seen whether higher visual fidelity would improve the validity of research data [97].

4.5. CONCLUSIONS AND RECOMMENDATIONS

IN conclusion, riders' braking patterns differed between impending-crash, near-miss, and safe situations: the more dangerous the situation, the more likely riders were to brake and the harder they braked. Riders appear to brake in response to a deviation in the approaching car's heading. Additionally, we showed that riders were often unable to avoid a collision with the car in impending-crash conditions.

Possible remedies to PTW-car crashes could be adjustments in road design (e.g., the presence of a left-turn lane), automated emergency braking for PTWs [134], and vehicle-to-vehicle communication technologies for providing warnings in advance [80]. Furthermore, we see an opportunity for our results to be used in risk awareness training programs [121]. That is, it would be valuable for PTW riders to be taught, using a PC-based animation, in which cases crashes are unavoidable, and why it is important to slow down before intersections.

Although we did not observe a significant effect on rider's emergency braking performance between the two simulator configurations, it may be that this study concerned a particular task for which motion is not needed, or it may be due to the specific parameter settings of the motion cueing algorithm (supplementary material [94]). It remains to be investigated how motion cues provided by a hexapod would affect riding performance in tasks such as continuous braking or turning, where closed-loop control is to be expected.

4.6. SUPPLEMENTARY MATERIAL

SUPPLEMENTARY materials (motion cueing algorithm, learning curves), characteristics of the virtual world, an illustrative video of the experiment, and other supplementary files are available in an [online repository](#).

5

MOTORCYCLE SIMULATOR SUBJECTIVE AND OBJECTIVE VALIDATION FOR LOW SPEED MANEUVERING

The use of driving simulators for training and for development of new vehicles is widely spread in the automotive industry. In the last decade, a few motorcycle riding simulators have been developed for similar purposes, with focus on maneuvering at high speed. This chapter presents the subjective and objective evaluation of a motorcycle riding simulator specifically for low speed longitudinal and lateral maneuvering, between 0 and 10 meters per second. An experiment was conducted with 3 maneuvers, acceleration from standstill, braking to standstill and turning at constant speed, both without and with platform motion. Participants briefly evaluated the fidelity of the simulator after each maneuver and more extensively after each motion condition. Behavioral fidelity was evaluated using experimental data measured on an instrumented motorcycle. Overall, the results show that the participants could reproduce the selected maneuvers without falling or losing balance, reporting a sufficient level of simulator realism. In terms of subjective fidelity, motion had a positive effect on simulator presence, significantly increasing the feeling of being involved in the virtual environment. In terms of behavioral fidelity, the comparison between the simulator and experimental results shows good agreement, with a limited positive influence of motion for the braking maneuver, which indicates that for this maneuver the use of motion is beneficial to reproduce the real-life experience and performance.

This chapter is planned to be submitted for a journal publication.

5.1. INTRODUCTION

DRIVING simulators are widely used in the automotive industries, with applications ranging from driver training and testing of active safety systems, to the analysis of vehicle design modifications and subjective vehicle performance assessment. Applications are generally limited to cars and this technology is rarely used for motorcycles. Due to the complex dynamics of two-wheeled vehicles, the use of a motorcycle riding simulator would be beneficial to train riders to cope with vehicle instabilities, and simulators could also be used to evaluate design changes and the impact of active safety systems. However, the complex dynamics of motorcycles also pose unique challenges for the design of realistic, high fidelity, simulators.

The fidelity of a simulator partly depends on the quality of the vehicle dynamics model, as this is the basis for rendering the visual stimuli as well as haptic and motion cueing [1, 120]. This topic was addressed in Chapter 2, where a high fidelity model of a motorcycle was developed based on multibody dynamics theory, together with models for motorcycle sub-systems, such as: engine, CVT, brakes and tires. The presented model was validated for a selection of longitudinal and lateral dynamic maneuvers with experimental results in the speed range currently of interest, namely between 0 and 10 m s^{-1} . Despite its complexity, the model can be simulated in real-time and in Chapter 4 it was integrated in a riding simulator for a study on braking at intersection. In that study, the motorcycle model was simplified for the use in longitudinal direction only and further investigation is required to validate the use of the motorcycle model for combined longitudinal and lateral dynamics.

The output of the motorcycle model simulation provides the reference motion that needs to be rendered to the simulator rider as realistically as possible. This introduces challenges for the reproduction of motion, visual and haptic cues. In previous studies, different methods have been adopted to render motion. In all these studies, a combination of physical and visual stimuli is used to create perception of roll motion. In [88], a gain was tuned on both physical motion and visual roll, to find the optimal subjective compromise during an experiment with 4 participants. The results showed that participants preferred a larger physical roll (250% of the vehicle roll) rather than visual roll (119% of the vehicle roll). In another motorcycle simulator study [34], the opposite approach was used, where a larger visual roll was presented to the simulator riders and only a small part of the vehicle roll was rendered using the physical tilting of the mock-up. In [75], a 50:50 split between visual and physical roll provided the most realistic perception of roll motion. More recently [156], the physical roll motion was scaled to 25%, while the visual roll was not scaled (i.e., 100%) with positive results in terms of simulator realism and presence. In [137] the participants of a motorcycle simulator experiment were asked to tune the visual and physical roll, resulting in visual roll close to 100% with a physical roll between 40% and 85% of the motorcycle roll, depending on vehicle velocity and turning radius. In the present study an approach based on motion perception was adopted, where the physical roll motion was used to render specific forces at the rider's head, while visual roll was not modified (i.e., visual gain of 100%).

Another challenge in the rendering of vehicle motion in a riding simulator is the reproduction of visual cues. In many existing riding simulators a large screen [32, 143, 106, 76] or a multiple screen [133] setup was used, while in other cases a Head Mounted

Display (HMD) was adopted [22, 156]. In this study a HMD with stereo vision and head tracking system was adopted, as it was also used in the study presented in Chapter 4 with positive results.

Regarding the simulator control loading, different approaches have been used to render the exchange of forces between the vehicle steer and the rider of a motorcycle simulator. In a low-cost motorcycle simulator a torsional spring was used to provide a torque proportional to the steering angle [133]. In [156] an admittance control was implemented, where the torque applied by the rider was fed to the model and the resulting steering angle was used to control the position of the steering motor while limiting its torque. In the current study, an impedance control was adopted. The rider imposes a steering angle which is passed to a lateral dynamics controller (Section 2.2.3) to control the vehicle model. The motorcycle model then returns a steering torque that is applied using the steering motor.

Previous studies have considered the development and evaluation of riding simulators, but so far all of them focused on motorcycle maneuvering at high speed (i.e., above 10 m s^{-1}), where the motorcycle vehicle dynamics become stable [138]. In contrast, this study focused on the subjective evaluation of a motorcycle riding simulator specifically for low speed maneuvering (i.e., between 0 and 10 m s^{-1}).

The main research question of this study is whether the developed motorcycle simulator provides an adequate reproduction of a real vehicle, both in terms of perceived realism and behavioral fidelity in low speed maneuvers, including cornering. Perceived realism is evaluated both after and during simulator trials, by means of questionnaires and a continuous evaluation of realism [26]. Behavioral fidelity is evaluated by comparing the performance of the subjects of this study performing a set of maneuvers, with the performance of a test rider on a real instrumented motorcycle performing the same maneuvers. Additionally, the influence of simulator motion is evaluated on both perceived realism and behavioral fidelity.

5.2. METHOD

5.2.1. RIDING SCENARIO

The riding scenario presented to the experiment subjects is very similar to the scenario used for the experimental validation of the motorcycle model used in Chapter 2, where the test data acquired on a real motorcycle were used to validate simulation results. The maneuvers used for model validation were selected to be reproduced here:

- A30: accelerating from standstill to 30 km h^{-1} (8.3 m s^{-1}),
- U25: constant turn with 10.5 m radius performed at 25 km h^{-1} (6.9 m s^{-1}), and
- B12: braking from 30 km h^{-1} (8.3 m s^{-1}) to standstill in 12 m.

In the experiment these maneuvers resulted in accelerations up to 3 m s^{-2} (A30), 4 m s^{-2} (U25) and 3 m s^{-2} (B12). When the experiment started, the participants could see themselves sitting on a standstill motorcycle in a virtual environment. The road on which they were driving was divided in three lanes, 2 m wide each, with the vehicle starting in the middle one. The middle lane also included a green center line which indicated

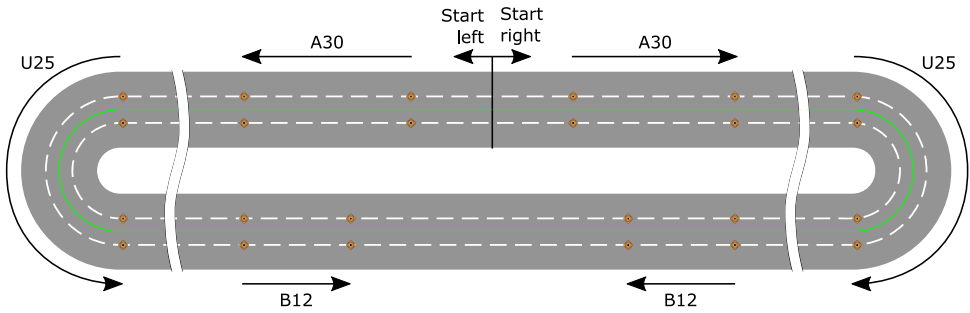


Figure 5.1: Road track used for the experiment. The motorcycle always started in the middle of the top road, heading left or right depending on the initial direction of the turn. The straight parts have been shortened for representation.

5

the ideal trajectory that they had to follow. A schematic of the road track created for the experiment is shown in Figure 5.1.

The first maneuver that they had to reproduce was the acceleration maneuver, which started a few meters ahead of their starting position in the virtual environment. The beginning and the end of the maneuver was indicated with traffic cones on the virtual road. The second maneuver was the constant turn (left or right alternatively) indicated also by traffic cones at the beginning and at the end. The third maneuver was the braking to standstill. The target beginning and the stopping locations were indicated using cones.

In-between maneuvers, a 200 m long straight road was placed to allow the participants to align on the center of the lane and get to the correct speed. The execution of these three maneuvers in series was defined as a run. After the final maneuver (braking) the motorcycle was automatically repositioned to start a new run. The run could start with a right or a left turn, alternating after each run. The execution of three consecutive runs was defined as a trial.

5.2.2. MOTION CUEING

In this study, an approach based on motion perception was adopted to render the roll motion to the riders of the motorcycle simulator. It is possible to analyze both physical and inertial forces acting on the motorcycle in steady state cornering, assuming that the rider body does not move with respect to the vehicle and that the rider is in line with the motorcycle.

A scheme of a motorcycle performing a right turn seen from behind is shown in Figure 5.2, where the masses of the rider and the vehicle are lumped as one. The motorcycle lean angle is noted as ϕ , m is the sum of the mass of the motorcycle and the mass of the rider and g is the gravitational acceleration. The sum of front and rear tires' lateral and vertical forces are noted as F_y and F_z , respectively.

From the equilibrium of the forces it is possible to compute the lateral (a_y) and ver-

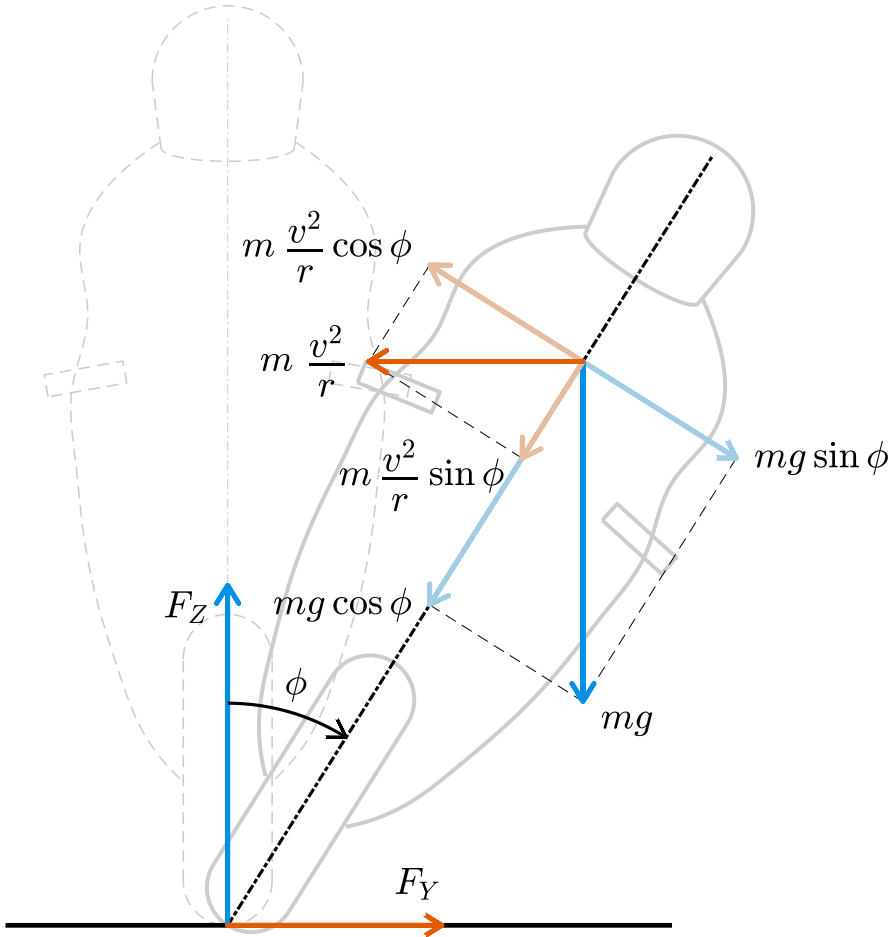


Figure 5.2: Physical and inertial forces acting on the motorcycle and the rider while leaning in a right turn in steady state conditions (rear view).

tical (a_z) accelerations acting on the rider:

$$a_y = g \sin \phi - \frac{v^2}{r} \cos \phi = 0, \quad (5.1a)$$

$$a_z = g \cos \phi + \frac{v^2}{r} \sin \phi. \quad (5.1b)$$

The lateral acceleration in a steady state turn depends on the leaning angle, the vehicle velocity v and the turn radius r . In the reference frame of the rider and in steady state conditions, if it is assumed that the rider is not moving with respect to the motorcycle, the total lateral acceleration will be zero. In the same reference frame, but in vertical direction, both centrifugal and gravitational accelerations are oriented downwards and their resultant pushes the rider on the seat of the motorcycle. The accelerations computed using Equations 5.1a and 5.1b, together with longitudinal acceleration and angular velocities obtained from the solution of the motorcycle model are used as input for the MCA that computes the platform motion.

The MCA adopted in this study is an algorithm by MOOG, provided together with their motion system. It is based on a classical motion cueing algorithm with adaptive washout [21]. The MCA parameters were tuned to reproduce the accelerations perceived by the rider. The intent was to optimize the motion cueing for the ideal maneuvers, this way, when the participants were improving their performance, they would obtain the most realistic motion experience possible with the adopted motion system and cueing algorithm. More details about the MCA and the parameters used can be found in Appendix B. To evaluate the effects of motion, two different conditions were tested:

- M: motion computed using a filter-based MCA, and
- NM: no motion.

In both conditions, speed-dependent road rumble was added.

5.2.3. DEPENDENT MEASURES

In order to answer the research question of this study, four classes of metrics were defined. The first class involved metrics of riding performance that can be directly compared with the data acquired on a real vehicle performing the same maneuvers. These objective metrics were complemented with 3 classes of subjective evaluation metrics. The second class is a continuous measure of realism given by the subjects of the experiment. The third class measured simulator presence based on a questionnaire after the experiment. The fourth class measured simulator sickness.

PERFORMANCE METRICS

The rider performance metrics computed for this study are based on lateral position and longitudinal velocity of the vehicle. Lateral deviation of the vehicle with respect to the prescribed path was considered as an error and its sum was computed during the execution of each maneuver. The velocity of the simulated vehicle during acceleration and braking was directly compared with the experimental data acquired on a real instrumented motorcycle, where a test rider performed the same maneuvers as in this experiment [66]. For the turning maneuver the ideal speed was considered to be constant. The

deviation from this ideal speed was computed as error and integrated over the execution of the maneuvers.

Position and velocity errors for each maneuver were computed using:

Acceleration performance:

$$\left\{ \begin{array}{l} err_{pos} = \sum_{i=1}^N |(y_i - \hat{y}_{A30})(x_i - x_{i-1})| \\ err_{vel} = \sum_{i=1}^N \frac{|v_i - \hat{v}_{A30,i}|}{|x_i - x_{i-1}|} \end{array} \right. \quad (5.2a)$$

$$\left\{ \begin{array}{l} err_{pos} = \sum_{i=1}^N |(y_i - \hat{y}_{B12})(x_i - x_{i-1})| \\ err_{vel} = \sum_{i=1}^N \frac{|v_i - \hat{v}_{B12,i}|}{|x_i - x_{i-1}|} \end{array} \right. \quad (5.2b)$$

Braking performance:

$$\left\{ \begin{array}{l} err_{pos} = \sum_{i=1}^N |(y_i - \hat{y}_{B12})(x_i - x_{i-1})| \\ err_{vel} = \sum_{i=1}^N \frac{|v_i - \hat{v}_{B12,i}|}{|x_i - x_{i-1}|} \end{array} \right. \quad (5.3a)$$

$$\left\{ \begin{array}{l} err_{pos} = \sum_{i=1}^N |(y_i - \hat{y}_{B12})(x_i - x_{i-1})| \\ err_{vel} = \sum_{i=1}^N \frac{|v_i - \hat{v}_{B12,i}|}{|x_i - x_{i-1}|} \end{array} \right. \quad (5.3b)$$

Turning performance:

$$\left\{ \begin{array}{l} err_{pos} = \sum_{i=1}^N |r_i - \hat{r}_{U25}| r_i (\psi_i - \psi_{i-1}) \\ err_{vel} = \frac{\sum_{i=1}^N |v_i - \hat{v}_{U25}| r_i (\psi_i - \psi_{i-1})}{\sum_{i=1}^N r_i (\psi_i - \psi_{i-1})} \end{array} \right. \quad (5.4a)$$

$$\left\{ \begin{array}{l} err_{pos} = \sum_{i=1}^N |r_i - \hat{r}_{U25}| r_i (\psi_i - \psi_{i-1}) \\ err_{vel} = \frac{\sum_{i=1}^N |v_i - \hat{v}_{U25}| r_i (\psi_i - \psi_{i-1})}{\sum_{i=1}^N r_i (\psi_i - \psi_{i-1})} \end{array} \right. \quad (5.4b)$$

In these equations, x and y are the longitudinal and lateral displacement of the motorcycle with respect to x_0 and y_0 , which are the motorcycle planar coordinates at the beginning of each maneuver. The motorcycle velocity during the maneuver is indicated with v_i while the reference velocity for each maneuver is indicated with \hat{v} , with the specific maneuver indicated in the subscripts. For the turning maneuver, the instantaneous turning radius r_i and the angle with respect to the center of the turn ψ are computed using the motorcycle coordinates. The reference constant lateral displacement for maneuvers A30 and B12 are indicated with \hat{y}_{A30} and \hat{y}_{B12} , respectively. The reference turning radius for the maneuver U25 is indicated with \hat{r}_{U25} . All the sums end at the index N , which represents the last point in which the motorcycle coordinates are within the predefined space of each maneuver.

The computed error for both position and velocity was presented to the subjects of the experiment at the end of each run. Participants were instructed to pursue a high score and therefore tended towards the ideal riding scenario, minimizing the dispersion of the data. In order to provide a number that can be quickly interpreted by the participants, the errors computed during the simulation have been normalized within a range from 0% to 100%, where a score close to 100% is representative of good performance. The normalization was done using a hyperbolic tangent function where also a normal-

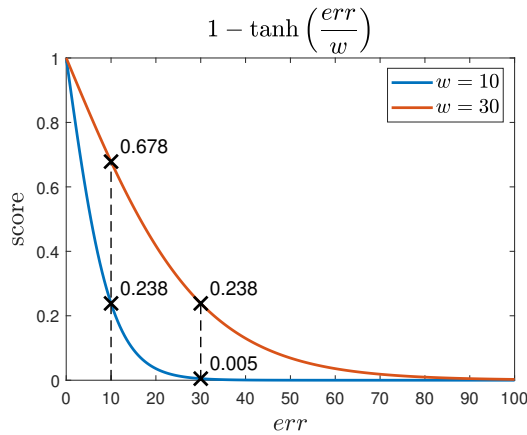


Figure 5.3: Variation of the score when using two different normalization factors. The value of the score remains between 0% and 100%, but as the normalization factor increases, a higher score is associated with the same error value. As an example in the figure, the scores associated with an error of 10 and 30 are shown for the two normalization factors.

5

ization factor was used to change the sensitivity of the score to the error variation:

$$\text{score}_{pos} = 1 - \tanh\left(\frac{err_{pos}}{w_{pos}}\right) \quad (5.5a)$$

$$\text{score}_{vel} = 1 - \tanh\left(\frac{err_{vel}}{w_{vel}}\right) \quad (5.5b)$$

The normalization factor used was related to physical quantities of the experiment. For the position error for acceleration and braking maneuvers a factor of 10 was used, which is in the order of magnitude of the road width (6 m), while for the position error of the turning maneuver the factor used was 30, which is related to the length of the semi-circular trajectory with a radius 10.5 m (33.0 m). For the velocity scores, the normalization factor used was 30 for all the maneuvers and it was related to the target vehicle velocity of 30 km h⁻¹ during the experiment.

Examples of position error calculation for the acceleration maneuver A30 are shown in Figure 5.4a. In the figure, two motorcycle trajectories that are parallel to the ideal trajectory but at a certain distance from it are shown. The areas between the trajectories and the ideal trajectory represents the position error. The area colored in green represents a linear trajectory parallel to the ideal one and at a distance of 0.1 m from it. The position error is computed as the area between the motorcycle trajectory and the ideal trajectory (3 m²), which results in a position score of 70.9%. The area colored in red represents the position error relative to a motorcycle trajectory parallel to the ideal trajectory and at a distance of 0.8 m (position error of 24 m²) with a relative position score of 1.6%. For the braking maneuver B12, the calculation of position error, and relative position score, was done in the same way.

Similarly, examples of position error calculations for the turning maneuver U25 are

shown in Figure 5.4b. Also in this case the position error is computed as the area between the trajectory of the motorcycle and the ideal trajectory. The examples shown in the figure would result in position errors of 6.6 m² and 39.6 m², and position scores of 78.4% and 13.3% for the green and red area, respectively.

After the execution of the experiment, the performance of the participants was divided in three categories:

- Desired performance: the participant performed the maneuver keeping the motorcycle in the middle lane, maximum lateral deviation from the target path below 1 m on either side,
- Adequate performance: the participant performed the maneuver driving the motorcycle also deviating to the lateral lanes of the road, maximum lateral deviation from the target path below 3 m on either side, and
- Inadequate performance: the participant drove the motorcycle off road while performing the maneuver, lateral deviation from the target path greater than 3 m.

In case of inadequate performance, the position and velocity scores calculated were neglected. The number of times that a participant was not able to obtain desired or adequate performance was analyzed as a measure of difficulty for performing the maneuver. For desired and adequate performances the scores of each participants was averaged per maneuver and per motion condition where addition of simulator motion is expected to be beneficial to the riding performance.

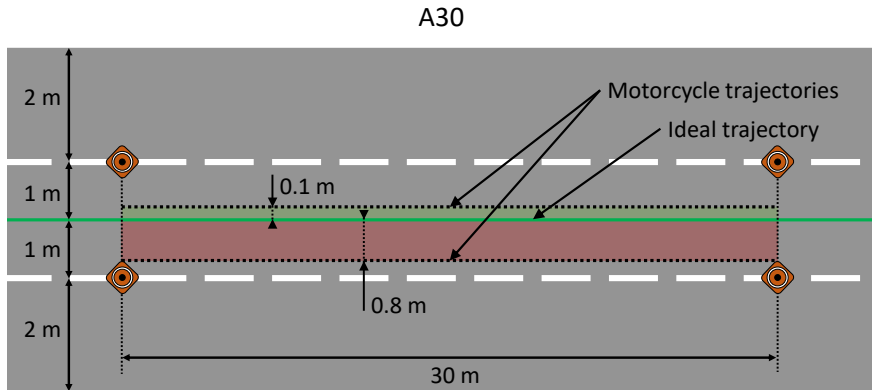
REALISM

In order to rate the perceived realism the participants were asked to provide a realism score using a Likert-like scale [100] in the range between 0 and 10, where 0 meant “far from reality” and 10 meant “close to reality”. The participants provided this score by comparing the simulator with their real life experience. They had to provide this score verbally after each maneuver for the entire duration of the experiment. In order to practice with the realism score rating, a training session was performed after the familiarization and before the start of the experiment trials.

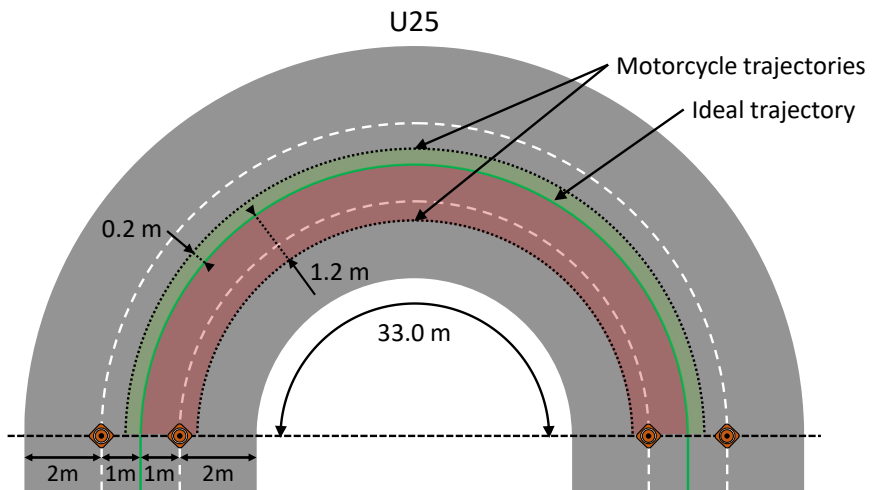
The realism scores provided by each participant were averaged per motion condition and per maneuver. The average results over all participants was then computed using the averages of each participant. Although the scale used for the realism score provides ordinal data, in this study it is assumed that the interval between values is the same and therefore the calculation of mean and standard deviation is allowed [85, 115]. A higher realism score is expected to be found for the simulator condition with motion, irrespectively of the considered maneuver.

SIMULATOR PRESENCE

In order to evaluate the simulator presence experienced by the participants during the experiment, a questionnaire was prepared with eight questions selected from a previous study [161]. These questions are meant to measure the major contributing factors to a sense of presence: Control Factors (CF), Sensory Factors (SF), Distraction Factors (DF) and Realism Factors (RF). The participants were asked to provide an answer between 1



(a) Position error examples for maneuver A30.



(b) Position error examples for maneuver U25.

Figure 5.4: Motorcycle trajectories and relative position errors for the calculation of position scores for acceleration and turning maneuver.

(very low) and 21 (very high/very much) to the questions reported in Table 5.1. Each participant had to respond to all the questions twice, once for each motion condition. The scale provides ordinal data, but with the assumption of equally spaced intervals, the calculation of mean and standard deviation is allowed [85, 115]. The answer of each question per motion condition was averaged for all the participants to analyze the influence of simulator motion on the different factors contributing to simulator presence. A higher mean value is expected when simulator motion is active.

Table 5.1: Questionnaire evaluating simulator presence for each motion condition.

Nr	Question	Factors
1	To what extent did you feel consciously aware of being in the real world while being on the simulator?	DF
2	To what extent did you feel that you were interacting with the simulation environment?	CF
3	How natural did your interaction with the environment seem?	CF
4	How much did the visual aspects of the environment involve you?	SF
5	How much did the motion aspects of the environment involve you?	SF
6	How well could you concentrate on the assigned tasks or required activities rather than on the mechanisms used to perform those tasks or activities?	DF
7	How much did your experience in the virtual environment seem consistent with your real-world experience?	RF, CF
8	How compelling was your sense of moving around inside the virtual environment?	SF

Notes. Factor categories: CF = Control Factors, SF = Sensory Factors, DF = Distraction Factors, RF = Realism Factors.

SIMULATOR SICKNESS

Simulator sickness was measured during the experiment using the MISC rating [7]. The rating ranges from no symptoms (0) to vomiting (10) and the participants were asked to report their rate in the introduction phase before the beginning of the experiment, after familiarization and training and after each trial. If at any moment during the experiment the MISC rating would reach a value of 6 or higher, the experiment was interrupted and the ongoing scenario was not considered in the analysis.

5.2.4. PARTICIPANTS

The 12 participants involved in the experiment were recruited from the employees of Siemens Industry Software in Leuven (Belgium), where the motorcycle simulator is located. All participants were male with average age of 35.8 years (SD 8.7), and all have a motorcycle driving license (AM, A1 or A). In the 12 months previous to the experiment, half of them reported to have never driven a motorcycle, the other half reported to have driven between once a month and a few times per week.

5.2.5. RIDING SIMULATOR

The experiment was conducted on the “MOTORIST” motorcycle riding simulator. The simulator consist of a Piaggio Beverly 350 cc motorcycle mock-up mounted on top of a 6 DOF MOOG motion system [95]. A HMD integrated in a motorcycle helmet was

used to provide stereo vision with visual roll and an infrared camera position in front of the rider was used to track the head motion of the rider. The setup is shown in Figure 5.5 (left), where the tracking camera was attached to the vertical pole mounted in front of the motorcycle. The motorcycle was instrumented with sensors to measure the rider inputs of steering, throttle and independent front and rear braking. The steering column was instrumented with an electric motor to provide torque feedback at the handlebar and a rotary encoder to measure the steering angle. The throttle was measured using an encoder mounted on the throttle body of the motorcycle. The braking action was measured independently for front and rear brakes by means of encoders measuring the braking lever's angle. Throttle and braking signals were sent to a combined powertrain and braking system model to compute the traction and braking torques to apply to the motorcycle model's wheels. The steering angle was sent to a lateral controller algorithm responsible for calculating the steering torque that was applied to the motorcycle model. A detailed description of these models can be found in Chapter 2.

5.2.6. PROCEDURE

Before the beginning of the experiment, each participant was asked to fill out an intake questionnaire and was given a document with a description of the experiment, including a set of instructions for the correct execution of the experiment. After reading the experiment description, the experimenter would answer all their questions and then briefly summarize the instructions using the same vocabulary as in the written document and using the same explanation for each subject. Subsequently the participants had to sign a consent form and provide a preliminary MISC rating.

The participants were then escorted to the riding simulator and helped to wear the protective equipment (safety harness, protective vest and helmet). Participants started with a familiarization trial to get acquainted with the system. During the familiarization they could drive along the predefined path and attempt to perform the maneuvers, but their performance was not evaluated and they did not have to provide any realism score.

Following the familiarization, they had a training trial. During the training they performed the predefined maneuver and they were also asked to provide a realism score after each maneuver. This score was not considered in the results and was only used to let the participant get used to provide this score at the right time. Both familiarization and training trials were performed with the no motion (NM) condition for all the participants.

After the training, three identical trials with one motion condition were performed. After each trial, the participants were asked to provide a rating on the motion sickness, measured using the MISC rating, and at the end of the third trial, the participants were asked to step out of the simulator and fill in a presence questionnaire to evaluate the first motion condition. After a 10 minutes break, the participants performed the remaining three trials of the experiment with the other motion condition. Also in this case, a MISC rating was requested after each trial, and at the end of the last trial, the participant filled in a final presence questionnaire on the second motion condition. Each participant performed a total of 18 repetitions of each maneuver, 9 for each motion condition. The order in which the motion conditions were presented was selected to have half of the participants starting with motion and the other half without. The overall duration of

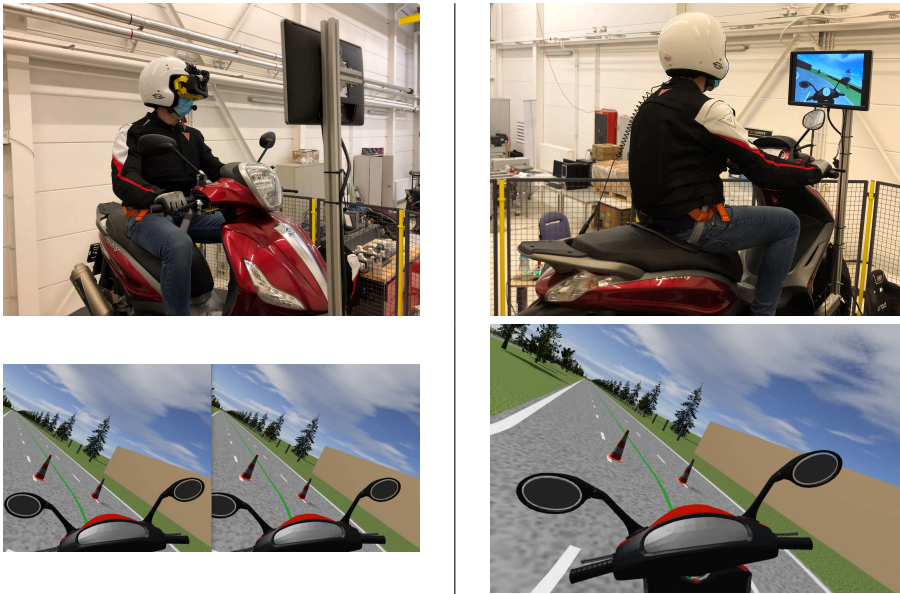


Figure 5.5: The motorcycle simulator using Head Mounted Display (left) and screen (right) to present the driving environment. The lower images represent a screen shot from the turning maneuver.

the experiment was approximately 90 minutes per participant according to the timeline reported in Table 5.2.

The study was approved by the TU Delft Ethics Committee (Ethics application no. 515, 2018).

5.3. RESULTS

5.3.1. REPLACING THE HMD WITH A SCREEN

The first 10 participants of the experiment used the HMD as visualization device. Only three of these 10 participants managed to complete the experiment, the other seven were interrupted due to inability to drive the motorcycle or motion sickness. These riders were mostly controlling the handlebar too aggressively, resulting in the impossibility to drive in a straight line or control the heading direction. From the feedback collected during post-experiment debriefing, they reported issues with the steering control.

The steering angle that was visualized in the HMD was different from the physical steering angle imposed by the driver. At very low speeds (below 0.5 ms^{-1}), the physical steering angle was shown, while at higher speeds (above 3 ms^{-1}) the steering angle of the motorcycle model was visualized. In between, a speed dependent gain coefficient was used to smoothly fade between these behaviors, resulting in inaccurate visual reproduction of the handlebar angle. Curiously, none of the participants mentioned this in their feedback.

To proceed with the experiment, the HMD was replaced by a screen mounted in front

Table 5.2: Experiment timeline.

Introduction Intake questionnaire Experiment description Consent form MISC rating	20 min
Familiarization NM motion condition MISC rating	10 min
Training NM motion condition realism score practice MISC rating	5 min
3 Trials one motion condition realism score measurement MISC rating after each trial Presence questionnaire	20 min
Break	10 min
3 Trials other motion condition realism score measurement MISC rating after each trial Presence questionnaire	20 min
Conclusion	5 min
Total	90 min

of the motorcycle that was moving together with the motion platform. The adapted setup is shown in Figure 5.5 (right). With the modified setup, 12 participants were invited to the experiment and all of them were able to complete the study. Three of these participants had started the familiarization with the HMD but interrupted it within few minutes. Therefore, learning from the previous test was considered minimal.

5.3.2. TIME HISTORIES COMPARISON WITH REAL MEASUREMENTS

The average motorcycle velocity profile for all participants and for each motion condition was computed and compared with the reference maneuvers in Figure 5.6. The averaged velocity profile for the acceleration maneuver does not start from zero. This is due to the fact that during the trial the motorcycle was re-positioned a few meters before the beginning of the maneuver and the participants had to drive to the beginning and stop before the start. In some cases, the participants started accelerating before the correct start position and in some other cases, the participants started after this position, resulting in an initial averaged velocity higher than zero. This effect can be seen in the velocity profiles of a representative participant for which all the velocity profiles are plotted in Figure 5.6 (top). The final velocity during the acceleration maneuver is close to 30 km h^{-1} for both motion conditions. The reference velocity profile that was measured in experimental conditions does not reach the target speed of 30 km h^{-1} , although the instructions provided to both test rider and participants of the simulator experiment were identical. This indicates that it is easier to reach the ideal final velocity on the simulator rather than on the real vehicle.

For the braking maneuver, the averaged velocity of the motorcycle started to drop before the beginning of the maneuver, resulting in a motorcycle velocity starting below the reference. The shape of the averaged velocity profile is also distorted and it differs from the reference. This is due to the averaging in the last part of the maneuver, where for some of the trials the velocity was already at zero (see the velocity profiles for a representative participant in Figure 5.6 (middle)). For this maneuver it can be seen that with motion, the velocity profile is closer to the reference.

The velocity profile for the turning maneuver was always below the reference value of 25 km h^{-1} , with a somewhat higher average value for the condition with simulator motion, as shown in Figure 5.6 (bottom). This result is in opposition with the results obtained for the acceleration maneuver, where the velocity of the vehicle was always above the reference. This suggests that the ideal reproduction of the turning maneuver was difficult to achieve on the simulator.

5.3.3. RIDING PERFORMANCE METRICS AND REALISM

Simulator realism was positively evaluated with an average score of 6.2, and was higher with motion (6.8 with standard deviation of 1.5 for M and 5.6 with standard deviation of 1.7 for NM condition). However this effect was not significant ($t(11) = 1.61$, $p = 0.123$, in a paired sample t-test). The results of realism and performance evaluation were first averaged per participant and per motion condition and then represented graphically in box plots in Figure 5.7. In order to evaluate significance of the effect of motion, a paired t-test was performed and the results are reported in Table 5.3.

For the acceleration maneuver A30, the results are reported in Figure 5.7 (top). The

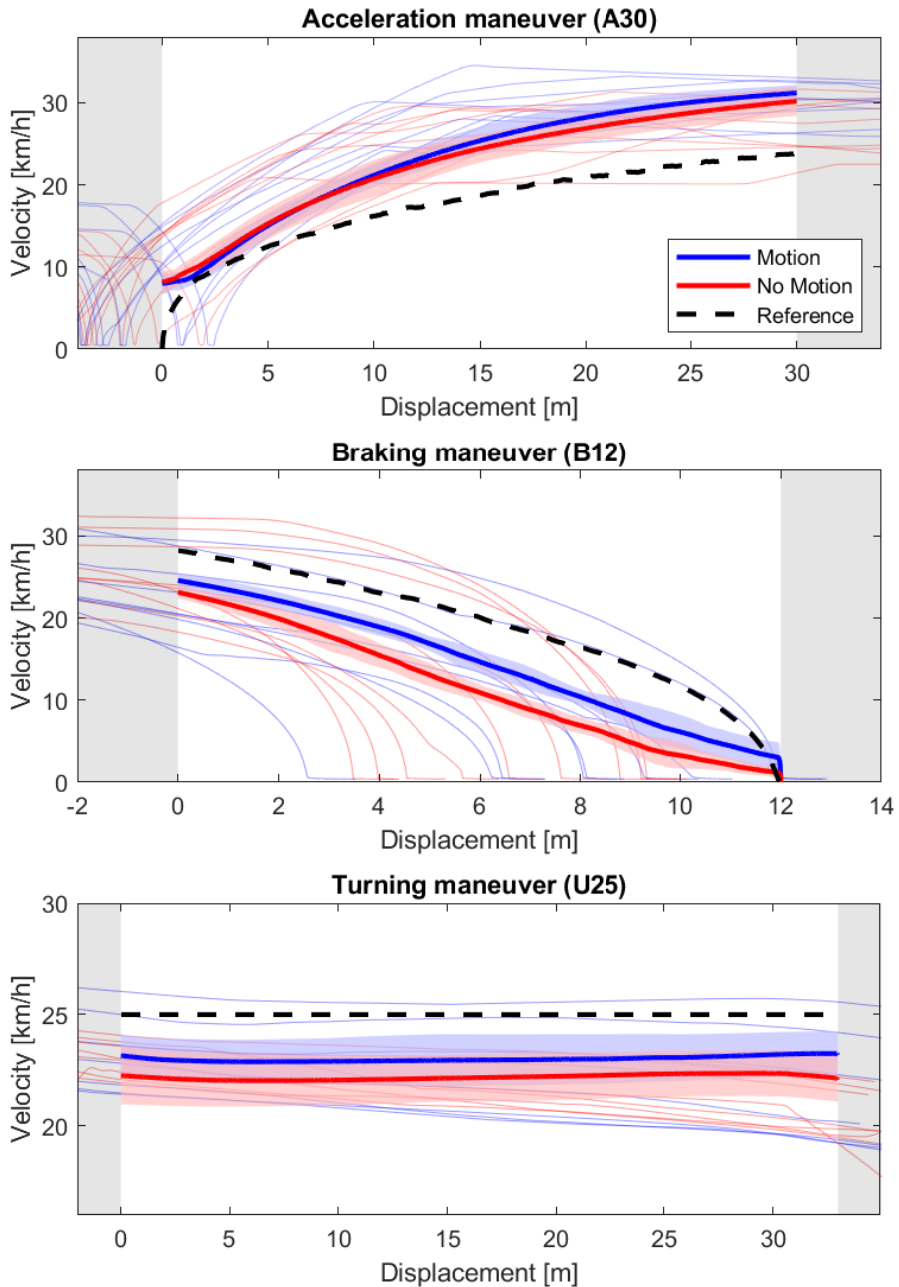


Figure 5.6: Velocity over distance for the experiment maneuvers. The black dashed line indicates the reference profile, blue and red lines the averaged velocity profile for all the participants and shaded areas the interquartile range for motion and no motion condition. Thin lines are velocity profiles of a representative participant.

Table 5.3: Minima, maxima, means, standard deviations and results of paired sample t-tests for realism and riding performance metrics. p values < 0.05 are reported in boldface.

	M			NM			t (df)	p
	Min	Max	Mean (SD)	Min	Max	Mean (SD)		
Acceleration (A30)								
Realism	4.0	10.0	6.87 (1.61)	0.0	8.0	5.62 (1.96)	1.8 (11)	0.092
Pos. score	0.0	93.0	20.89 (24.19)	0.0	95.7	27.75 (28.21)	-1.3 (11)	0.214
Vel. score	26.7	84.6	51.06 (13.05)	26.9	83.4	54.21 (13.96)	-0.7 (11)	0.491
Braking (B12)								
Realism	2.0	10.0	6.71 (1.88)	1.0	8.0	5.19 (2.17)	1.9 (11)	0.068
Pos. score	7.2	97.2	63.43 (23.24)	6.6	98.7	74.61 (20.78)	-2.5 (11)	0.021
Vel. score	0.0	94.0	37.98 (27.03)	0.0	91.9	28.56 (26.57)	2.5 (11)	0.019
Turning (U25)								
Realism	1.0	10.0	6.74 (1.70)	2.0	9.0	6.13 (1.69)	0.9 (11)	0.365
Pos. score	2.9	83.8	33.46 (22.41)	5.0	92.1	37.84 (21.88)	-0.9 (11)	0.382
Vel. score	93.2	100.0	97.51 (1.68)	92.8	99.9	97.55 (1.65)	-0.3 (11)	0.763

effects of motion were not significant for this maneuver, with a minor influence on realism, for which the mean value is slightly higher with motion. The position scores obtained are quite low, with an average value around 20%, which represents an error value of 11.0 m², 0.37 m for 30 m of acceleration. Results for the braking maneuver B12 are reported in Figure 5.7 (middle). For this maneuver the effect of motion is significant for both position and velocity score. In particular, the position score is significantly higher for the NM condition (10.5%), while the velocity score is significantly higher for the M condition (8.8%).

For the turning maneuver U25, the results are reported in Figure 5.7 (bottom). The average velocity score for all the participants was always between 95.0% and 99.5%, with a corresponding error between 1.5 km h⁻¹ and 0.15 km h⁻¹. The small range of these results is explained by the small amplitude of the error value and the normalization factor used for the calculation of this score. In this case, as for the other velocity scores, a normalization factor of 30 was used. As shown in Figure 5.3, a smaller factor would result in an increased score range for a small error in magnitude. These results were re-scaled using a normalization factor of 1, resulting in a score range between 9.5% and 85.1% and a similar statistic result ($t(11) = -0.25$, $p = 0.802$) for the difference between motion and no motion condition. Although the updated normalization factor provides a better use of the score range, the number presented in Figure 5.7 were presented to the participants of the experiment during the execution and they were used to adjust their performance. Since the normalization factor does not influence the outcome of the analysis, the results with the pre-selected factor are shown.

For the calculation of the performance scores reported above, only the maneuvers where the participant achieved desired or adequate performances were considered. For inadequate performances, the scores were excluded from the analysis. The total numbers of inadequate performances for each maneuver, and the percentage of the total number of repetitions, are reported in Table 5.4, for both screen and HMD visuals. Overall, no falls or loss of balance were reported during the execution of the experiment, and the participants were able to successfully reproduce acceleration from standstill and

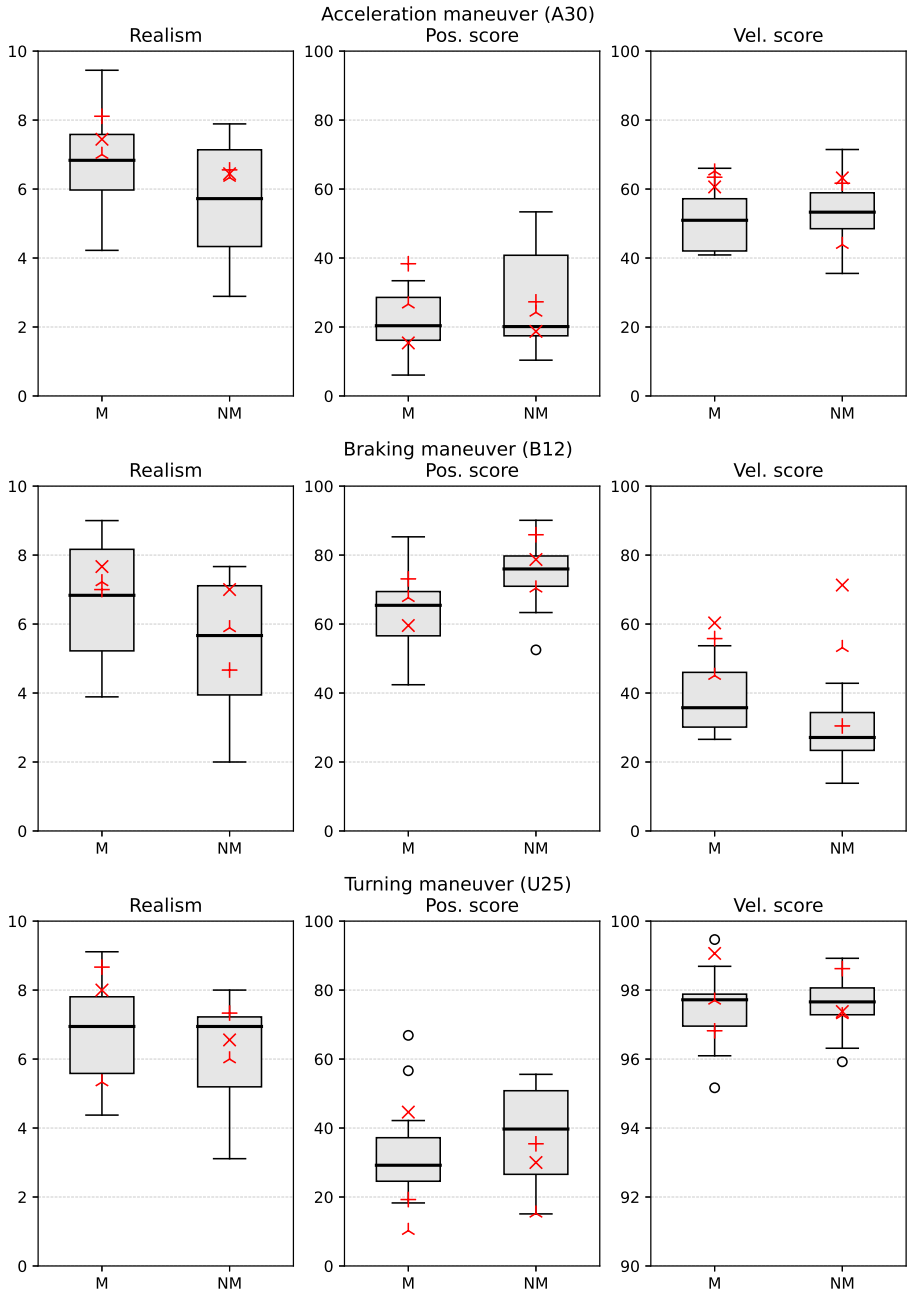


Figure 5.7: Box plot of realism scores, position scores and velocity scores for the acceleration maneuver (top), braking maneuver (middle) and turning maneuver (bottom) grouped by motion condition (M: motion, NM: no motion). p values for effects of motion result from a paired sample t-test. Boxes show results with screen. The red markers represent the 3 participants that completed the experiment using the Head Mounted Display.

Table 5.4: Number of inadequate performances (failures) for each maneuver per motion condition and percentage of the total number of repetition.

	Screen (12 participants)				HMD (3 participants)			
	M		NM		M		NM	
	Failed	%	Failed	%	Failed	%	Failed	%
Acceleration (A30)	7	6.5	7	6.5	1	3.7	2	7.4
Turning (U25)	33	30.6	33	30.6	11	40.7	8	29.6
Braking (B12)	1	0.9	3	2.8	1	3.7	1	3.7

Table 5.5: Minima, maxima, means, standard deviations and results of paired sample t-tests for presence questionnaire. p values < 0.05 are reported in boldface.

	M			NM			t (df)	p
	Min	Max	Mean (SD)	Min	Max	Mean (SD)		
Q1	2	17	9.92 (5.62)	0	15	8.92 (5.38)	0.41 (11)	0.683
Q2	7	20	13.08 (4.25)	5	20	11.83 (4.63)	0.69 (11)	0.498
Q3	3	17	11.42 (4.60)	2	15	9.50 (4.50)	1.03 (11)	0.314
Q4	2	19	9.83 (5.87)	2	20	10.33 (6.31)	-0.20 (11)	0.844
Q5	5	20	14.25 (4.94)	1	15	9.08 (4.48)	2.68 (11)	0.014
Q6	10	18	13.00 (2.76)	5	20	14.17 (4.17)	-0.81 (11)	0.428
Q7	4	18	11.75 (4.11)	2	15	8.67 (4.54)	1.74 (11)	0.095
Q8	3	17	11.67 (4.56)	2	13	8.50 (3.42)	1.92 (11)	0.067

braking to standstill with the help of the balancing control. In terms of deviation from the desired path, participants failed to achieve adequate performances for the acceleration maneuver 7 times for each motion condition. For the braking the number of inadequate performances was 1 for motion and 3 for no motion condition. For the turning maneuver, the inadequate performances were 33 for each motion condition.

5.3.4. SIMULATOR PRESENCE

The results from the simulator presence questionnaire are presented graphically in Figure 5.8. The results of a paired t-test are reported in Table 5.5. Only for question 5 ("How much did the motion aspects of the environment involve you?") a significant effect was found, with participants feeling more present in the virtual environment with simulator motion. The results show that the value is generally higher with motion, except for question 6 ("How well could you concentrate on the assigned tasks or required activities rather than on the mechanism used to perform those tasks or activities?"), where simulator motion results in lower presence.

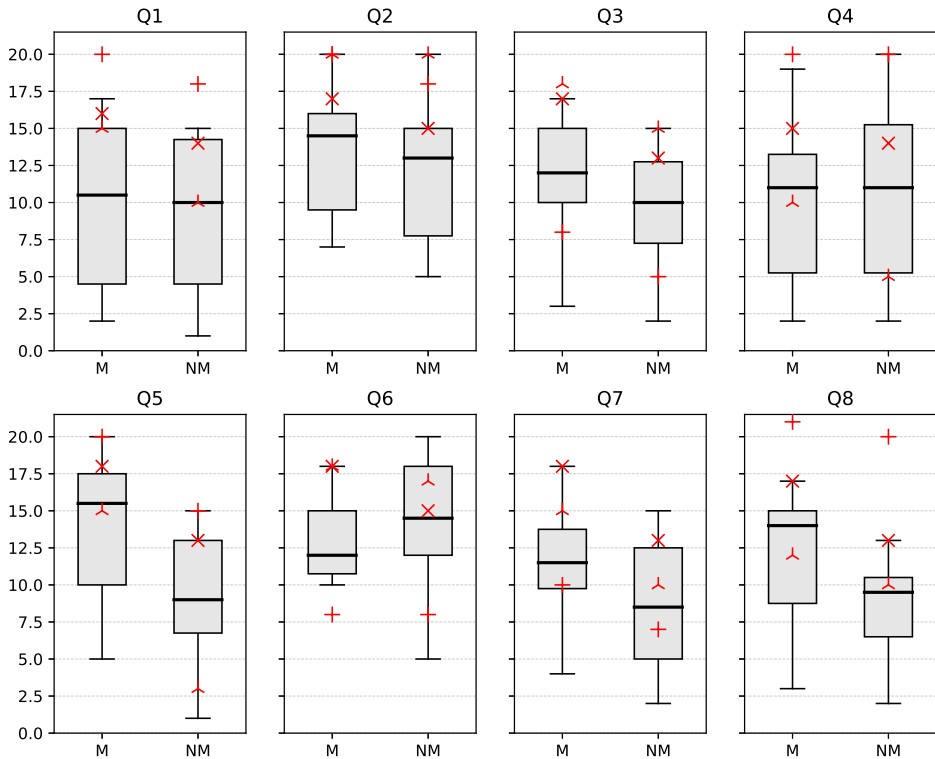


Figure 5.8: Presence questionnaire results grouped by motion condition (M: motion, NM: no motion). p values from effects of motion result from a paired sample t-test. The markers represent the 3 participants that completed the experiment using the Head Mounted Display.

5.3.5. SIMULATOR SICKNESS

The results of the self-reported simulator sickness for the experiment using the screen are reported in Table 5.6, with a comparison between the motion and no motion conditions. The maximum MISC rating value during trials was 2 and it was reported during a trial without motion. The average MISC rating during trials was 0.25 and 0.22 with motion and without motion, respectively. The highest average MISC rating was reported in the introduction phase of the experiment with a value of 0.33.

Table 5.6: Self-reported simulator sickness for the 12 participants with screen and the 3 participants with HMD.

	Screen (12 participants)			HMD (3 participants)		
	Min	Max	Mean (SD)	Min	Max	Mean (SD)
Introduction	0	1	0.33 (0.49)	0	1	0.33 (0.58)
Familiarization	0	1	0.17 (0.39)	0	2	1.00 (1.00)
Training	0	1	0.08 (0.29)	0	2	1.00 (1.00)
Trials M	0	1	0.25 (0.44)	0	2	0.33 (0.71)
Trials NM	0	2	0.22 (0.48)	0	3	1.00 (1.00)

5.4. DISCUSSION

IN order to make use of a motorcycle riding simulator for training purposes at low speed, validation is needed in representative driving conditions. In this study, simulator realism and behavioral fidelity of a motorcycle simulator are evaluated for acceleration, cornering and braking maneuvers at low speed. The participants of the experiment performed these maneuvers while controlling the vehicle using throttle, brake and steering. At the end of each maneuver, they provided measures of realism while their performances were used to evaluate behavioral fidelity.

5.4.1. SIMULATOR EVALUATION

Overall, the simulator can be used to reproduce the targeted maneuvers at low speed. This is based on the analysis of the results obtained in the conducted experiment with screen visualization, results obtained with HMD are discussed in Section 5.4.3 below.

From the performance analysis it can be seen that all the participants were able to perform the maneuvers, with the turning maneuver resulting to be slightly more difficult, with 30.6% inadequate performances exceeding the intended path with more than 3 m.

As shown in Figure 5.6 (top and bottom), the targeted beginning of the acceleration and braking maneuvers was not easily identified by the participants, as the reference point was placed in the center of gravity of the motorcycle and the only visual reference available to them were the cones placed on the road, which were not clearly visible once passed with the front wheel. This resulted in a somewhat scattered distribution of the initial point of the acceleration and braking maneuvers.

From the analysis of the velocity profiles for the acceleration maneuver, it can be seen that the participants were able to accelerate to exactly 30 km h^{-1} , while in the real vehicle

experiments, giving the same instructions to the rider, the velocity reached at the end of the maneuver was lower (see Figure 5.6). One of the possible explanations for this could be the fact that the speedometer in the riding simulator was placed close to the center of the field of view, allowing for a better speed control than on a real motorcycle, where the speedometer is placed in a lower position. Another possible explanation is related to the limited field of view of the visualization screen used during the experiment. A previous study [122] has found a correlation between the field of view and the perception of speed. In this study, the limited field of view could have influenced the participants to drive faster during the acceleration maneuver, although this did not occur in the other two maneuvers performed during the experiment.

5.4.2. EFFECT OF SIMULATOR MOTION

The analysis of riding performance shows limited influences of motion only for the braking maneuver, with a positive effects on velocity score and a negative effect on position score. Minor influence of motion was found in the presence questionnaire, where the results for the question related to the motion aspects of the simulation were found to be significantly higher when physical motion was present. Similar results were found also in a previous experiment on the same simulator (Chapter 4) in longitudinal only scenarios and on another simulator [156] in high speed longitudinal and lateral scenarios.

Given the multiple number of t-tests performed in the analysis of the results shown in Figures 5.7 and 5.8, the chance of type I errors is increased. This would mean that the tests that resulted in a significant difference might be false positives, where the null hypothesis was wrongly rejected. A Bonferroni correction [27] could be applied to take this effect into account. These correction adjusts the critical p-value to take into account the number of repeated t-tests, lowering the threshold from 5% to 0.3% (5% / 17 t-tests). This correction would make the rejection of the null hypothesis invalid for all the tests performed, and consequently indicate no significant difference between motion and no motion condition.

Another study analyzed the effect of motion on a riding simulator at higher speed [160]. They found that the addition of motion was beneficial to achieve higher simulator behavioral fidelity and presence. But when the participants were asked to rank which sensory cue was mostly influencing their performance, the majority indicated that motion was the least contributing cue of all presented. Investigations on the effect of motion can be found in literature studies on driving simulators. In the reproduction of highly dynamic lateral maneuvers, the effect of motion was found to be significant in terms of both behavioral fidelity and presence in different studies [29, 130]. Another study investigates the effects of motion while turning on a car driving simulator [38], showing that differences in driving performance are not significant with respect to the adopted motion cueing strategy, although motion cueing had an impact on perceived realism. Similarly, in this study it was found that the motion has a small impact on performance (with the exception of the braking maneuver) but a significant impact on the motion element of perceived simulator realism. We conclude that, depending on the task assigned to the participant of the simulator study, the influence of motion cueing is not a key factor to achieve a sufficient level of behavioral fidelity, while it still has an impact on the realism perceived on the simulator.

5.4.3. CONSIDERATIONS ON VISUALIZATION TECHNOLOGIES

Regarding the adopted simulator visuals, the original simulator configuration adopted a HMD as used in Chapter 4 with positive results for the reproduction of longitudinal maneuvers. In this experiment, also lateral maneuvering was added, and the HMD was found to be quickly unusable for 7 out of 10 participants due to induced motion sickness or simply due to inability to drive. The results obtained by the 3 participants who completed the study using the HMD are reported for completeness with the other results as red markers in Figures 5.7 and 5.8 and in Table 5.4. However, given the limited sample, no further conclusions can be drawn from these results.

The modification of the simulator to adopt a screen with static background resulted in the elimination of motion sickness occurrence. This can be explained with the rest frame theory found in literature [124, 123], which states that creating a static visual background consistent with the absence of inertial motion information reduces motion sickness induced by visual stimulation. This result is in contrast with a previous study [156], however, where a HMD was used in a motorcycle simulator to reproduce high speed maneuvers without inducing motion sickness. The occurrence of motion sickness when using the HMD can be therefore explained by the rest frame theory. However, it cannot be excluded that HMD can be successfully adopted in a motorcycle simulator at low speeds. Improvements may be found using more advanced HMD in combination with improved control technique for both visual and visual/motion combinations.

5.5. CONCLUSIONS

AN experiment was performed to validate a motorcycle riding simulator in the speed range between 0 and 10 ms⁻¹. Participants were asked to reproduce a set of maneuvers which were previously performed on a real motorcycle. From the analysis of the results it can be concluded that the selected maneuvers can be reproduced on the motorcycle riding simulator, and the overall level of realism measured during the experiment is sufficient (6.2 overall on a scale from 1 to 10, 6.8 with motion and 5.6 without motion).

In terms of behavioral fidelity, the comparison between the simulator and experimental results shows good agreement, with a limited, positive, influence of the simulator motion. Only for the braking maneuver this effect was significant, which indicates that for this maneuver the use of motion is beneficial to reproduce the real-life experience and performance. Motion also had a positive effect on simulator presence, significantly increasing the feeling of being involved in the virtual environment.

5.6. ACKNOWLEDGMENT

THIS work has been funded by the European Union's Seventh Framework Programme through the international consortium MOTORIST (Motorcycle Rider Integrated Safety) agreement No. 608092.

6

DISCUSSION AND CONCLUSIONS

IN the last decades, several motorcycle riding simulators have been developed. The use of these simulators can be beneficial to develop new vehicles in combination with active safety control systems and to train riders to cope with the complex dynamics of motorcycles. These applications are very relevant, but so far, most of the riding simulators have focused on reproducing maneuvers at high speeds, where the intrinsic motorcycle instability is not of concern. The accuracy of the adopted motorcycle model is not always verified, where low model fidelity undermines the quality of the overall simulator through its different cueing systems. Mechanical motion systems have been widely adopted, with different MCAs based on washout filters or on empirical approaches. Literature studies showed the relevance of physical and visual motion cueing, particularly for the rendering of roll motion, but the adopted MCAs are not based on understanding of human motion perception. In order for riding simulators to be accepted as valid tools for their application, a subjective and objective validation should be performed. This process is not always performed/reported for simulators found in literature, but it remains crucial for the simulators adoption and understanding of the influence of cueing systems. These aspects have been divided in development and evaluation and have been treated, respectively, in Part I and II of this thesis. Next, the main findings of each part are presented, followed by an overall discussion. Finally the conclusions of this thesis are presented, together with recommendations for future work.

6

6.1. MAIN FINDINGS

6.1.1. PART I: MOTORCYCLE SIMULATOR DEVELOPMENT

In Chapter 2, a motorcycle multibody model, in combination with engine and transmission, has been developed and validated together with control strategies for low-speed stability and lateral dynamics to facilitate the task of steering and balancing the motorcycle. From the combined analysis of acceleration and braking maneuvers, it is possible to conclude that the results of the motorcycle model correlate well with experimental data measured on an instrumented motorcycle in the speed range between 0 and 10 ms^{-1} , with longitudinal accelerations up to 5 ms^{-2} in acceleration and 8 ms^{-2} in braking. For the lateral dynamics, the model results have a lag in lateral acceleration due to the lateral controller. Nevertheless, the value of lateral acceleration in steady turning is matched up to 4 ms^{-2} .

Main findings of Chapter 2

- The high fidelity motorcycle model can be used to realistically reproduce longitudinal and lateral maneuvers at low speeds.
- The lateral dynamics controller applied on the steering allows the reproduction of cornering maneuvers, but introduces a lag.
- The model can be integrated in a riding simulator for human-in-the-loop simulations.

Chapter 3 investigates the usability of optimization-based MCAs for the reproduction of longitudinal and lateral maneuvers at low speed. The investigation was carried

out for four-wheeled vehicles for practical reasons, including avoiding to deal with motorcycle low speed instability. The discussion in Section 6.2.2 below includes considerations related to the application of these algorithms to two-wheeled vehicles. Two different prediction strategies were evaluated. The first strategy, *oracle*, assumes perfect knowledge of future vehicle motion, it cannot be used for Driver-In-the-Loop (DIL) simulations and it is considered as a reference to evaluate the best motion cueing quality that can be achieved. The second strategy, *constant*, ignores changes in the future reference and assumes a constant reference equal to last vehicle status. The objective analysis carried out aimed to qualify and quantify the effects of the prediction strategies by means of dedicated metrics. Motion cueing quality metrics have been defined to quantify correlation, delay and absolute difference of the simulator motion with respect to the reference vehicle motion. An analysis of the adopted motion cueing mechanisms has been performed together with a study on the usage of the motion system workspace. As expected, the *oracle* outperforms the *constant* strategy, being able to coordinate the usage of multiple motion cueing mechanisms and manage the use of the limited workspace to obtain better motion cueing quality performances. The combined analysis of multiple indicators confirms the differences in performance and provides the metrics to quantify these differences. From the indicator results, a larger performance difference is obtained for longitudinal dynamic maneuvers, providing an indication of what should be improved in the future design of advanced prediction strategies for optimization-based MCAs.

Main findings of Chapter 3

- The performance of a predictive MCA varies depending on the adopted strategy to predict future reference motion.
- With an ideal prediction, optimization-based MCAs provide better usage of limited workspace to achieve superior motion cueing quality.

6.1.2. PART II: MOTORCYCLE SIMULATOR EVALUATION

The evaluation of the riding simulator specifically developed for this thesis was carried out in Chapters 4 and 5. In Chapter 4 only longitudinal maneuvers were performed. The simulator evaluation, and the effect of added physical motion, was carried out by analyzing rider's behavior and their assessment of simulator presence during an experiment with 12 participants. Participants were able to accelerate from 0 to 13.9 ms^{-1} and brake to standstill at an intersection depending on the different situation that they were presented. The effect of simulator motion on rider's braking performance was found to be not significant for the task investigated, while it had a significant positive influence on simulator presence.

In Chapter 5, another experiment with 12 participants was performed to validate the riding simulator for both longitudinal and lateral dynamics in the speed range between 0 and 10 ms^{-1} . Participants were asked to reproduce a set of maneuvers which were previously performed on a real motorcycle and used in Chapter 2 for validating the motorcycle model integrated in the simulator. The analysis of the results shows that the

participants could reproduce the selected maneuvers without falling or losing balance, with the turning maneuver resulting often in a large path deviation. The overall level of realism measured during the experiment is sufficient (6.2 overall on a scale from 1 to 10, 6.8 with motion and 5.6 without motion). In terms of behavioral fidelity, the comparison between the simulator and experimental results shows good agreement, with a limited, positive, influence of the simulator motion for the braking maneuver, which indicates that for this maneuver the use of motion is beneficial to reproduce the real-life experience and performance. In terms of subjective fidelity, motion had a positive effect on simulator presence, significantly increasing the feeling of being involved in the virtual environment.

Main findings of Chapters 4 and 5

- The developed riding simulator can be used to reproduce longitudinal and lateral dynamics maneuvers at low speeds (between 0 and 13.8 ms^{-1}).
- No falls or loss of balance were reported, with participants able to reproduce acceleration from standstill and braking to standstill without using their feet.
- Participants were able to reproduce the turning maneuver without falls, but often with a large deviation from the path.
- Simulator motion had limited positive influence on riding performance in longitudinal dynamics and simulator presence.

6.2. DISCUSSION

6.2.1. USABILITY OF THE HIGH FIDELITY MOTORCYCLE MODEL

The first objective of this thesis was to analyze the usability of a high fidelity motorcycle model in the reproduction of low speed maneuvers. The vehicle model adopted in a simulator has a crucial role as it has to accurately reproduce the vehicle dynamics to be rendered [54]. The results from the solution of the vehicle's equation of motions are used as input for the cueing systems of the simulator and therefore, the model needs to be accurate in reproducing the target maneuvers to be reproduced on the simulator.

In a riding simulator, when the objective is to reproduce maneuvers at low speeds, it is crucial to adopt a motorcycle model that accurately captures the vehicle behavior, including model instabilities which are intrinsic of single-track vehicles. In addition, the vehicle model shall create a realistic steering feel through physics based steering torque calculation. Chapter 2 focused on the development and experimental validation of a high fidelity motorcycle model to be integrated in a riding simulator, and therefore addressed the first objective of this thesis. As reported in the findings of Chapter 2 in Section 6.1.1, the developed model accurately reproduces the behavior of a real motorcycle for both longitudinal and lateral maneuvers at low speed, and it was integrated in a riding simulator for Human-in-the-Loop (HuiL) simulations.

The possibility to adopt a high fidelity model in a riding simulator implies that the inputs provided to the cueing system are more accurate and therefore the overall simula-

tor fidelity is improved. High fidelity models, however, also have their disadvantages. To accurately model the dynamics of the vehicle, its powertrain, braking system and tires, numerous parameters are necessary. Some of these parameters can be found in literature for specific vehicles models, when the parameters cannot be found elsewhere they need to be estimated either with simulation or with physical testing, and consequent additional investment of time and resources.

Additionally, high fidelity models are generally more complex and often include non-linear dynamics. Real-time integration of multibody models in a riding simulator requires the adoption of efficient algorithms to formulate and numerical integrate the equation of motions [84, 36], resulting again in additional effort required. In order to identify the specific benefits of using a high fidelity model a comparison study could be carried out to underline what are the differences in simulator fidelity when simplified vehicle dynamics are adopted [73]. This was not one of the objectives of this thesis, but it is fair to assume that a more accurate model leads to higher simulator fidelity.

6.2.2. EVALUATION OF OPTIMIZATION-BASED MOTION CUEING

Once the vehicle model has been developed and integrated in the riding simulator, the results of its simulation can be used to provide cues to the simulator rider. Given the peculiar dynamics of motorcycles, particularly in relation to physical roll motion, it is crucial to understand how to correctly reproduce roll motion on a riding simulator. Approaches found in literature show the relevance of combining physical and visual motion cueing specifically for roll [137, 75, 156]. However the applied motion cueing methods are not based on understanding of human motion perception. Additionally, optimization-based MCAs have been recently found to be very suitable for the motion cueing in driving simulators, as they offer an optimal trade off between motion quality and limited motion system workspace [24].

In Chapter 3 of this thesis, an optimization-based MCA has been developed and its performance has been evaluated for a driving simulator. The objective of this chapter was to investigate the usability of such algorithms and the influence of the adopted prediction strategy used to define the future motion reference required by these algorithms. The prediction strategies that were analyzed are opposed to each other, as one of them (*oracle*) is ideal, resulting in better motion cueing quality and workspace usage but not suitable for DIL simulations; and the other one (*constant*) too simplistic, feasible for DIL simulations but with sub optimal performances.

Results show the importance of the prediction strategy in optimization-based MCAs and the potential advantages associated with the adoption of an accurate prediction strategy. However, these algorithms are based on optimization, where the dynamics of the motion system and its constraints are modeled and integrated in a MPC together with an optimization function aiming at minimizing motion cueing errors. Generally, MPC problems are computationally more expensive than typical washout algorithms and their real-time implementation is often based on advanced techniques such as the real-time iteration (RTI) scheme [43]. To avoid these complications, studies found in literature decouple the solution of the 6 DOF spatial MPC problem in smaller (simpler) problems associated to a single direction of motion (e.g., surge/pitch, sway/roll, heave, yaw) [10]. Such simplification results in better computational performances but it does

not consider the coupling between different motion channels and therefore results in lower motion cueing quality.

Independently from the approach taken, the need for an accurate prediction strategy remains a challenging task, where in some applications assumptions can be made which simplify the prediction of future vehicle motion given the objective of the simulations. As an example, in racing applications it might be relatively easier to estimate future vehicle motion as, especially expert racing drivers are very consistent among different laps.

An additional challenge is given by the time available to compute the prediction, in fact the MPC problem requires a complete prediction at each time step, where typical prediction lengths vary between 0.5 and 8 seconds [90] while the time step for the MPC problem is typically two orders of magnitude smaller. The requirements for an accurate prediction can be partially relaxed in relation to the estimation of vehicle motion in 6 DOF, as the most important motion channels, requiring the largest motion system displacement, are typically longitudinal and lateral accelerations and yaw rate. Therefore, an accurate prediction of only these channels should already provide significant improvements to motion cueing quality. The considerations made here are certainly valid for driving simulators, but they can be applied to riding simulators as well.

The approach adopted has the objective to optimize the motion perceived by the subject on the simulator, independently from what the motion is. Therefore, by replacing the reference with the motion of a motorcycle, the same algorithm can be also used for motion cueing in a riding simulator, with similar considerations regarding the adopted prediction strategy. Similar criteria to optimize motion cueing quality can also be adopted, based on the metrics introduced in Chapter 3. Washout MCAs are further adopted and evaluated in this thesis for practical reasons, including implementation simplicity and computational efficiency for human-in-the-loop simulations.

6.2.3. HUMAN-IN-THE-LOOP EVALUATION OF THE RIDING SIMULATOR

In the second part of this thesis, the last research objective addressed is the evaluation of riding simulator realism when reproducing longitudinal and lateral dynamics maneuvers at low speed. In order to deal with this objective, a complete riding simulator was developed integrating the motorcycle model presented in Chapter 2.

The simulator was evaluated in two different studies, first for only longitudinal (Chapter 4) and then for combined longitudinal and lateral (Chapter 5) dynamic maneuvers. In both studies the effects of motion cueing on rider behavior/performance and perceived realism was evaluated. The results of the conducted experiments show that the riders were able to reproduce the maneuvers on the riding simulator with a sufficient level of realism. The reproduction of longitudinal dynamics maneuvers was positively judged in terms of realism, and participants were able to performed the assigned maneuvers most of the times.

Lateral dynamics maneuvers were somewhat more difficult to reproduce, given the amount of times that the riders were not able to complete the cornering maneuver without going outside of the allowed boundaries. Simulator motion had a small positive influence on riding performance limited to longitudinal maneuvers, in particular on braking performance, and on perceived realism. As expected, results show that the sensory aspects of simulator presence associated to the sense of moving within the virtually sim-

ulated environment were significantly higher when simulator motion was present. Minor differences were also noticeable in results associated with distraction factors, indicating that simulator riders might be less focused on their tasks due to the presence of simulator motion.

Overall, the addition of motion to the riding simulator, brought to minor, but positive results. Adding a motion system does bring additional technological and scientific challenges, such as: the choice of a MCA and its tuning, the potential occurrence of motion sickness and the ethical challenges associated with operating heavy machinery with human subjects.

Together with motion systems, also other cueing devices contribute to the creation of an immersive riding simulator, including visual, acoustic and actuated steering. Considering them separately, we can use objective metrics to identify whether these cueing are accurate, as done in Chapter 3, and use these metrics to improve their realism before integrating them in the simulator. However, it cannot be concluded that the individually tuned cueing systems will improve the overall realism of the riding simulator. Of course, it can be expected that improving the quality of each cueing will have a positive effect on the realism of the simulator, but this can only be concluded after an accurate objective and subjective evaluation. It is also possible that the addition of a particular cueing might result in a reduction/modification of simulator realism. One example of this effect is the physical rendering of vehicle acceleration in a simulator, causing the motion of the human body on the simulator and therefore influencing the input on the control action device. This effect is known as biodynamic feedthrough and it requires mitigation control techniques to be adopted on input control devices to remove its detrimental effects [149].

6.3. CONCLUSIONS

WITH respect to the first objective it can be concluded that the adopted high fidelity motorcycle model well reproduced low speed maneuvers. The model presented in Chapter 2 not only reproduces vehicle accelerations at low speeds, but it also reproduces the behavior of the motorcycle powertrain (engine and transmission) and braking system. The validation was conducted by comparing model simulation results with data acquired on an instrumented motorcycle with more than satisfactory results for both longitudinal and lateral dynamics maneuvers. The adoption of a high fidelity model, although requiring additional effort, has the potential to improve the overall simulator fidelity as the results of model simulation generates the reference for all the cueing systems used in the simulator.

Based on the results presented in Chapter 3, it can be concluded that optimization-based MCAs offer the potential to improve motion cueing quality in a variety of simulation scenarios, and in particular for low speeds maneuvers. The full potential of these algorithms is fully unleashed when an accurate reference of future vehicle motion is known a priori. A simplified, yet feasible, prediction strategy was evaluate against the ideal prediction, but provided only sub optimal results both in terms of motion cueing quality and workspace utilization. With respect to the second research objective of this thesis, predictive MCAs are computationally expensive but with an accurate prediction they provide optimal results based on the trade off between the motion perceived on the

simulator and the available motion system workspace.

Finally, with respect to the third and last research objective of this thesis it can be concluded that the developed riding simulator provides sufficient level of realism for the reproduction of longitudinal and lateral maneuvers at low speeds. In Chapter 4 only longitudinal dynamics were evaluated, while in Chapter 5 also lateral dynamics maneuvering was included. The addition of motion cueing had a small positive effect on riding performance in longitudinal maneuvers and improved sensory factors of simulator presence, with a possible negative influence due to participant distraction from their task. The evaluation of additional/modified cueing systems needs to be evaluated individually on the overall simulator realism, as their influence does not only depend on their single effect, but also on the potential (unwanted) combination with other cues.

6.4. RECOMMENDATIONS

GOING beyond the scope of this thesis, a few recommendations for future work are identified based on the outcome of this thesis.

Regarding vehicle modeling specifically for riding simulators, but for all simulators in general, the adoption of high fidelity models is recommended. Although they require an additional effort for their implementation and validation, they represent the single most effective simulator component that can greatly improve the overall simulator fidelity, as the results of their numerical integration provides the input for all the cueing systems. Additionally, the adoption of high fidelity models (sometimes referred as Digital Twins) offers the opportunity to evaluate model modifications on the riding/driving experience, allowing to subjectively evaluate a design concept before the physical prototype is available. This approach can be used to improve vehicle ride and handling performances as well as comfort associated with vertical dynamics. Additionally it can be used for validation and verification of control techniques used in support of the rider/driver of the vehicle, including, but not limited to, advanced Anti-lock Braking Systems (ABS) to support the riders to brake as quickly as possible without dramatically changing direction and different Advanced Driver-Assistance Systems (ADAS) to support driving functions like adaptive cruise control, intersection crossing assistant and automatic valet parking.

With respect to MCAs and their usage for human-in-the-loop simulations, this thesis underlines the capabilities of predictive algorithms based on optimization. To benefit of the full potential of these algorithms, a strategy capable of accurately predict future vehicle motion is necessary, at least for the motion channels which require the largest workspace (surge, sway and yaw). One possibility to obtain a potential strategy is the embedding of a simplified vehicle-driver model with a reference trajectory which can be solved to obtain a quick approximation of future vehicle motion. Such prediction strategy would provide information to the predictive MCA regarding large motion that are about to occur, giving the possibility to the algorithm to adopt motion cueing strategies like pre-positioning on velocity buffering, as well as the coordination of the two.

Another possible strategy to formulate an accurate prediction strategy can be achieved by analyzing data measured on real vehicles. With the technological advances of the last years, commercial vehicles are equipped with more and more sensors and communicate with base station collecting extremely large amount of data. By using vehicle accelerations information measured with an Inertial Measurement Unit (IMU), and combining

these information with images from a front viewing camera, a neural network can be trained to predict what the future vehicle motion will look like for the next few seconds. These technologies are already being developed to accelerate the rise of automated vehicles and could be applied also here to improve motion cueing in simulators.

Additionally, given the general formalism of MPCs which is at the base of predictive MCAs, the model used within the optimization could also be extended to include a perception model, which would compute the motion that a human would perceive when subjected to the vehicle accelerations computed by the vehicle dynamic model. The main human organ responsible for motion perception is the vestibular system. Different linear models have been developed and can be found in literature, but given the complexity and the subjectivity of the matter, the adoption of these model is somewhat controversial for applications like riding or driving simulators. Future work should focus on further understanding the human process of motion perception and the interaction with other sensory systems in order to provide additional insight for the development of even more advanced MCAs.

On riding simulator evaluation, a recommendation for future work is to focus on the effects of other cues and their interaction with each other. In this thesis, motion cueing was specifically investigated, while a single technique was adopted for proprioceptive cueing to render the forces exchanged between the rider and the motorcycle handlebar. The technique adopted in this thesis could be further improved by refining the tuning parameters of the lateral dynamics controller acting on the motorcycle handlebar to improve the performances in cornering maneuvers. Future works should focus on investigating different techniques for proprioceptive cueing on simulator realism, based on experimental measurement of steering torque on an actual motorcycle.

Additionally, other rider/vehicle interactions that have not been considered in this study should be investigated. Riders do not only control their vehicle by means of the handlebar, but they also interact by moving their body, shifting they weight on the vehicle and applying forces on the footrests. On the usability of HMD on motion riding simulator, the results presented in this thesis were partially unsuccessful. However, it cannot be excluded that future HMD technology might improve their usage by providing faster algorithms for head tracking and computer graphic rendering combined with higher screen resolutions.

A

MOTORCYCLE MULTIBODY MODEL

A.1. INTRODUCTION

SOME details of the motorcycle model introduced in Chapter 2 are reported in this appendix. The model is based on multibody dynamics theory where each body of the motorcycle is modeled separately as well as the connections between bodies. These connections can be ideal, only allowing a very specific relative motion, depending on the type of connection, or they could have some compliance, modeled with an elastic and a viscous force depending on the relative displacement and velocity between the bodies. Other elements adopted in the model are lumped springs and dampers to reproduce forces and torques exchanged within the model, as well as other forces and torques elements such as tires.

A.2. REFERENCE FRAMES

A fixed global reference frame is used to determine the position and orientation of each body in space. An additional reference frame system, which is defined as Non-Centroidal Body Fixed (NCBF) frame, is used to define the inertial properties of the bodies. The center of gravity of the body is then defined with respect to its NCBF frame. The position in the global reference frame of the NCBF frame of each body is defined by the three-point method, which are used for locating and orienting a reference frame in space.

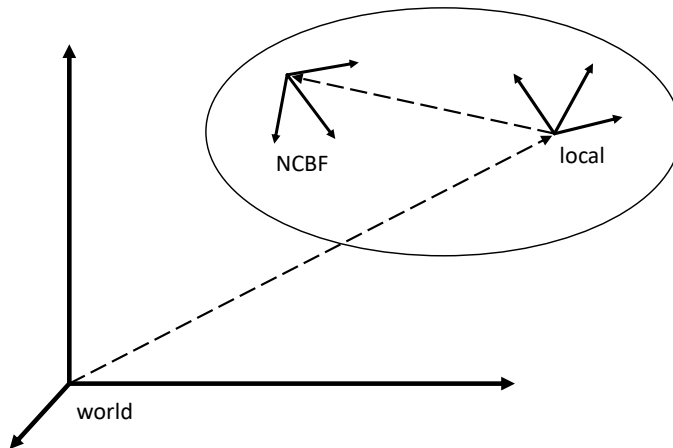


Figure A.1: Frames used to define position, orientation and inertial properties of each body of the motorcycle model.

A.3. THREE-POINT (PQR) METHOD

THE three-point method of locating and orienting a reference frame relative to a parent reference frame involves defining the Cartesian coordinates of three points:

- the origin of the reference frame (called point P),

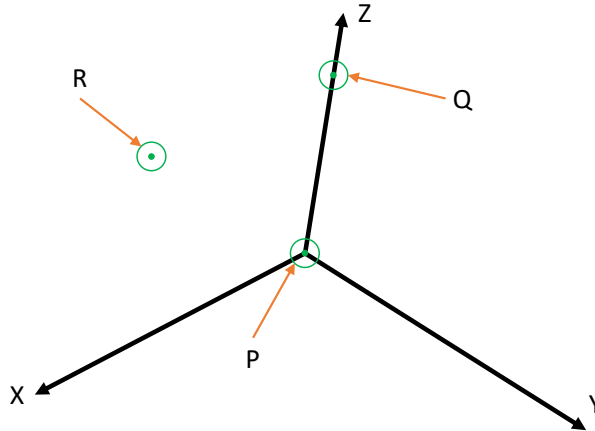


Figure A.2: Graphical representation of the three-point (PQR) method.

- a point on the reference frame's positive Z axis (called point Q), and
- a point in the reference frame's positive X-Z plane (called point R).

These three points must not be collinear, otherwise the reference frame will not be well defined.

A.4. BODIES PROPERTIES

USING the three-point (PQR) method, the position of the NCBF frame for each body of the motorcycle can be defined. The position of the center of gravity of each body is defined in Cartesian coordinates with respect to the NCBF frame. The coordinates of the P, Q and R points in the global reference frame for each body, as well as the position of their center of gravity and the inertial properties of the bodies are property of the vehicle manufacturer and cannot be disclosed in this thesis.

A.5. MODEL TOPOLOGY

THE bodies presented in the previous section are connected to each other by means of joints. The joints used for the motorcycle model, with the relative constrained bodies are reported in Table A.1. Each joint allows only a specific movement between the bodies, depending on the type, and constrains the other degrees of freedom. The joint types used on the motorcycle model are:

- Revolute joint (REV): allows the relative rotation around a defined axis and provides 5 degrees of constraint,
- Translational joint (TRA): allows the relative translation along a defined axis and provides 5 degrees of constraint,

- Spherical joint (SPH): allows the relative rotations and provides 3 degrees of constraint,
- Universal joint (UNI): allows the rotation around two defined perpendicular axis and provides 4 degrees of constraint, and
- Bracket joint (BRA): does not allow any relative motion and provides 6 degrees of constraint.

The model comprises of 16 bodies, each body has 6 degrees of freedom in space and therefore the total number of degrees of freedom of the model without joints is 96. The total number of degrees that are constrained by the joints can be calculated by adding the degrees of constraint of all joints. The joints provide a total of 83 degrees of constraint, computed as follows:

- 6 revolute joints for 5 degrees of constraint: 30, plus
- 3 translational joints for 5 degrees of constraint: 15, plus
- 2 spherical joint for 3 degrees of constraint: 6, plus
- 2 universal joints for 4 degrees of constraint: 8, plus
- 4 bracket joints for 6 degrees of constraint: 24.

The remaining number of degrees of freedom of the motorcycle model is 13, computed by subtracting the total number of degrees of constraint from the total number of degrees of freedom ($96 - 83 = 13$). A scheme of the motorcycle model topology is shown in Figure A.3.

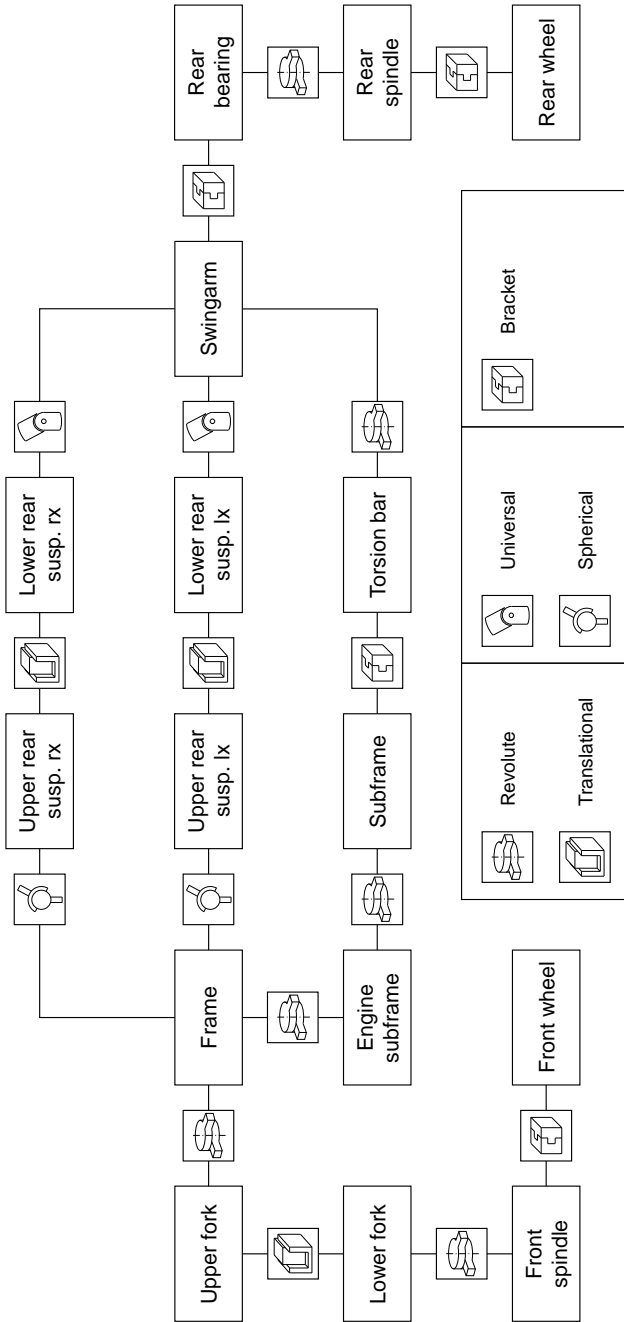


Figure A.3: Topology of the motorcycle multibody model.

Table A.1: List of joints used in the motorcycle model.

Joint type	Body 1	Body 2
REV	Frame	Upper fork
REV	Frame	Engine subframe
REV	Lower fork	Front spindle
REV	Engine subframe	Subframe
REV	Torsion bar	Swingarm
REV	Rear bearing	Rear spindle
TRA	Upper fork	Lower fork
TRA	Upper rear susp. rx	Lower rear susp. rx
TRA	Upper rear susp. lx	Lower rear susp. lx
SPH	Frame	Upper rear susp. rx
SPH	Frame	Upper rear susp. lx
UNI	Lower rear susp. rx	Swingarm
UNI	Lower rear susp. lx	Swingarm
BRA	Subframe	Torsion bar
BRA	Swingarm	Rear bearing
BRA	Rear spindle	Rear wheel
BRA	Front spindle	Front wheel

Notes: Joint types: REV = Revolute, TRA = Translational, SPH = Spherical, UNI = Universal, BRA = Bracket.

B

ADAPTIVE FILTER-BASED MOTION CUEING ALGORITHM

B.1. INTRODUCTION

THE Motion Cueing Algorithm (MCA) adopted in Chapters 4 and 5 is described here. This algorithm is an adaptive version of a filter-based MCA typically adopted in the automotive and aerospace domains, commonly known as “washout”, for its effect of removing (washing out) the sustained accelerations. A scheme of the adopted MCA is represented in Figure B.1 and it differs from a standard washout filter due to the adoption of the adaptive block.

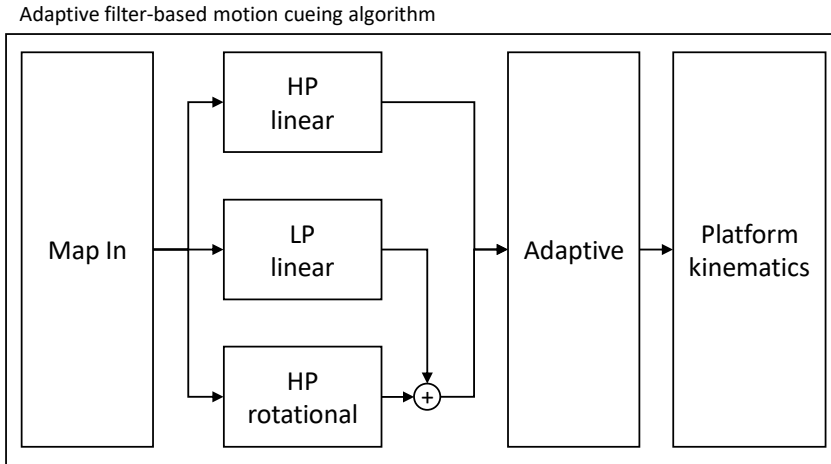
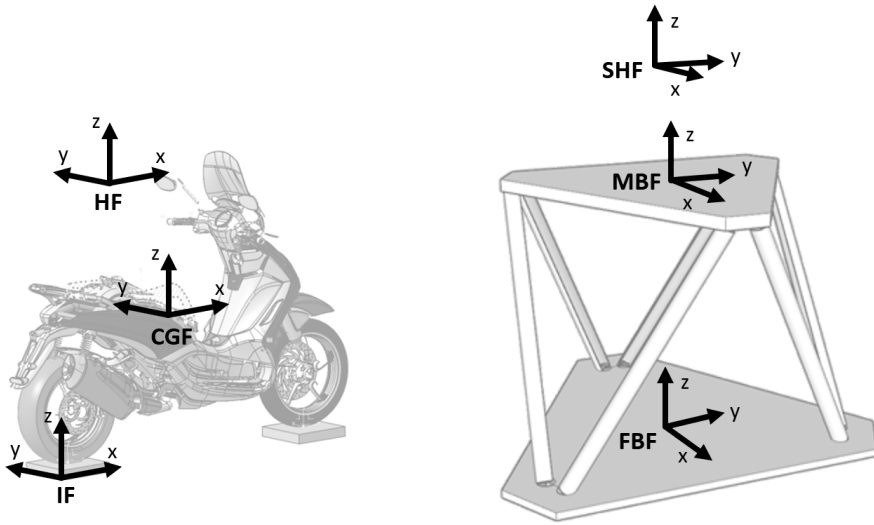


Figure B.1: Scheme of the adaptive filter-based motion cueing algorithm.

B.2. REFERENCE FRAMES

THE input for the MCA are the specific forces and angular velocities to be reproduced on the motion system. Typically these quantities are computed by the time integration of a vehicle model. The vehicle model has three main reference systems (see Figure B.2a): the inertial reference frame (IF), the reference frame placed in the center of gravity of the vehicle (CGF) and the reference frame of the riders head (HF). The vehicle accelerations and angular velocities are typically computed in the CGF reference frame, but the targets for the motion cueing are the specific forces and angular velocities in the HF frame. By knowing the position of HF with respect to CGF, a kinematic transformation can be performed which translates the input in the HF frame. This kinematic transformation is performed in the Map In block of the MCA, where the relative position of the HF with respect to the CGF is reported in Table B.1.

Similarly, three reference frames are defined for the simulator (as shown in Figure B.2b): the fixed base frame (FBF), the moving base frame (MBF) and the frame of the rider’s head on the simulator (SHF). The MBF is typically positioned in the center of the moving base, but the objective of the MCA is to reproduce the motion translated in SHF. In order to perform the change of reference the position of the SHF with respect to the



(a) Motorcycle model reference frames: inertial frame (IF), center of gravity frame (CGF) and rider's head frame (HF).

(b) Simulator reference frames: fixed base frame (FBF), moving base frame (MBF) and simulator head frame (SHF).

Figure B.2: Reference frames used by the motion cueing algorithm.

MBF must be specified. This operation is performed in the Platform kinematics block of the MCA and the relative position of the SHF with respect to the MBF are reported in Table B.1.

Table B.1: Relative coordinates of the HF and SHF with respect to CGF and MBF, respectively.

Parameter	Value	Unit
Position of HF with respect to CGF: x	0	m
Position of HF with respect to CGF: y	0	m
Position of HF with respect to CGF: z	0.9	m
Position of SHF with respect to MBF: x	0	m
Position of SHF with respect to MBF: y	0	m
Position of SHF with respect to MBF: z	1.9	m

B.3. MAP IN

THE Map In block also has two additional functions. First, it includes a first order low-pass filtering of the input signals, this allows to remove the high frequency content that cannot be reproduced on the motion system as well as signal noise. Second, it implements a rate limiting function on linear accelerations and rotational velocities. The cut-off frequency of the low-pass filter and the rate limiting values are reported in Table B.2.

Table B.2: Parameters of the Map In block of the motion cueing algorithm.

Parameter	Value	Unit
Low-pass filter cut-off frequency	120	rads^{-1}
Rate limit for linear accelerations	100	ms^{-3}
Rate limit for angular velocities	100	rads^{-2}

B.4. HIGH-PASS LINEAR

The linear accelerations in longitudinal direction (surge), lateral direction (sway) and vertical direction (heave) are passed to the High-Pass (HP) linear block, which is responsible for scaling them and removing the low-frequency content of the signals by means of a first order high-pass filter. The transfer function of the high-pass filter in the Laplace domain can be written as follows:

$$\frac{s}{s + \omega}, \quad (\text{B.1})$$

where ω is the the cut-off angular frequency of the filter. Besides filtering the input signals, the HP linear block also limits the output accelerations to ensure that they never exceeds the maximum value. The parameters used for HP linear block in the experiments described in the Chapters 4 and 5 are reported in Table B.3.

Table B.3: Parameters of the HP linear block of the motion cueing algorithm.

Parameter	Value (Ch.4)	Value (Ch.5)	Unit
HP filter Surge cut-off freq.	3	1.5	rads^{-1}
HP filter Surge gain	0.25	0.5	-
HP filter Sway cut-off freq.	-	1.5	rads^{-1}
HP filter Sway gain	-	0.5	-
HP filter Heave cut-off freq.	-	1.5	rads^{-1}
HP filter Heave gain	-	0.5	-
Limit value of output accelerations	3	3	ms^{-2}

B.5. LOW-PASS LINEAR

LONGITUDINAL and lateral accelerations are passed to the Low-Pass (LP) linear block, which is responsible for scaling and filtering the low-frequency content of the signals, the so-called sustained accelerations, by means of a second order low-pass filter. The transfer function of this filter in the Laplace domain can be written as follows:

$$\frac{\omega^2}{s^2 + 2\zeta\omega s + \omega^2}, \quad (\text{B.2})$$

where ω is the cut-off angular frequency of the filter and ζ is the damping of the filter. These accelerations are reproduced by tilting the motion system to certain roll and pitch angles. The LP linear block also ensures that the output accelerations do not exceed

the limit value. The parameters used for this block in the experiments described in the Chapters 4 and 5 are reported in Table B.4.

Table B.4: Parameters of the LP linear block of the motion cueing algorithm.

Parameter	Value (Ch.4)	Value (Ch.5)	Unit
LP filter Roll cut-off freq.	-	3	rads ⁻¹
LP filter Roll damping	-	0.9	-
LP filter Roll gain	-	0.5	-
LP filter Pitch cut-off freq.	3	3	rads ⁻¹
LP filter Pitch damping	0.9	0.9	-
LP filter Pitch gain	0.5	0.5	-
Limit value of output accelerations	3	2	ms ⁻²

B.6. HIGH-PASS ROTATIONAL

IN the HP rotational block, the angular accelerations are scaled and then filtered with a third-order high-pass filter. The transfer function of this filter can be written in the Laplace domain as follows:

$$\frac{s^3}{(s^2 + 2\zeta\omega s + \omega^2)(s + \omega_2)}, \quad (\text{B.3})$$

where ω is the cut-off angular frequency of the second order part of the filter, ω_2 is the cut-off angular frequency of the first order part of the filter and ζ is the damping of the filter. The resulting angular accelerations are also limited to a maximum value. The parameters used for the HP rotational block in the experiments described in the Chapters 4 and 5 are reported in Table B.5.

Table B.5: Parameters of the HP rotational block of the motion cueing algorithm.

Parameter	Value (Ch.4)	Value (Ch.5)	Unit
HP filter Roll cut-off freq. (2 nd order)	-	1	rads ⁻¹
HP filter Roll cut-off freq. (1 st order)	-	1	rads ⁻¹
HP filter Roll damping	-	0.8	-
HP filter Roll gain	-	0.5	-
HP filter Pitch cut-off freq. (2 nd order)	2	1	rads ⁻¹
HP filter Pitch cut-off freq. (1 st order)	1	1	rads ⁻¹
HP filter Pitch damping	0.8	0.8	-
HP filter Pitch gain	0.5	0.5	-
HP filter Yaw cut-off freq. (2 nd order)	-	1	rads ⁻¹
HP filter Yaw cut-off freq. (1 st order)	-	1	rads ⁻¹
HP filter Yaw damping	-	0.8	-
HP filter Yaw gain	-	0.5	-
Limit value of output rot. accelerations	3	3	rads ⁻²

B.7. ADAPTIVE ALGORITHM

THE adaptive algorithm takes as input the output generated by the HP linear and the sum of the outputs from the LP linear and the HP rotational blocks and modifies them according to the adaptive cueing strategy. The principle of the adaptive algorithm is to introduce more washout on the linear displacements to ensure that the platform stays within its workspace. Washout is a term used to identify a motion applied to the platform that goes in the opposite direction of the one needed to provide inertial feedback to the simulator user. The washout motion is therefore a false motion cue, which is necessary to avoid the physical limitations of the motion system. The advantage of an adaptive cueing algorithm is that when the required motion is small, the motion system will use more of the available workspace to reproduce more accurately the motion reference. While, when the required motion is very large, the adaptive algorithm will reduce the linear platform displacements keeping the system within its boundaries. The way the additional displacements are calculated is by minimizing a cost function. The factors involved are: actuator position (large positions need to be avoided due to limited actuator lengths), actuator velocity (high velocities require large actuators positions, which is an issue due to limited length) and washout acceleration (washout is a false cue and needs to be minimized). The tuning of the adaptive algorithm requires a trade-off between these three quantities.

B.8. PLATFORM KINEMATICS

THE output of the Adaptive block is then passed to the Platform kinematics block, which translates the requested motion in actuator reference signals to be commanded to the motion system.

REFERENCES

- [1] R. Wade Allen, George D. Park, and Marcia L. Cook. “Simulator Fidelity and Validity in a Transfer-of-Training Context”. In: *Transportation Research Record: Journal of the Transportation Research Board* 2185.1 (Jan. 2010), pp. 40–47. DOI: [10.3141/2185-06](https://doi.org/10.3141/2185-06).
- [2] Federico Barbagli, Diego Ferrazzin, Carlo Alberto Avizzano, and Massimo Bergamasco. “Washout filter design for a motorcycle simulator”. In: *Proceedings IEEE Virtual Reality 2001*. IEEE Comput. Soc, 2001. DOI: [10.1109/vr.2001.913790](https://doi.org/10.1109/vr.2001.913790).
- [3] Mauro Baseggio, Alessandro Beghi, Mattia Bruschetta, Fabio Maran, and Diego Minen. “An MPC approach to the design of motion cueing algorithms for driving simulators”. In: *2011 14th International IEEE Conference on Intelligent Transportation Systems (ITSC)*. IEEE, Oct. 2011. DOI: [10.1109/itsc.2011.6083053](https://doi.org/10.1109/itsc.2011.6083053).
- [4] A. Berthoz, W. Bles, H. H. Bühlhoff, B. J. Correia Grácio, P. Feenstra, N. Filliard, R. Huhne, A. Kemeny, M. Mayrhofer, M. Mulder, H. G. Nusseck, P. Pretto, G. Reymond, R. Schlüsselberger, J. Schwandtner, H. Teufel, B. Vaillieu, M. M. van Paassen, M. Vidal, and M. Wentink. “Motion Scaling for High-Performance Driving Simulators”. In: *IEEE Transactions on Human-Machine Systems* 43.3 (May 2013), pp. 265–276. DOI: [10.1109/tsmc.2013.2242885](https://doi.org/10.1109/tsmc.2013.2242885).
- [5] Erwin R. Boer, Nobuyuki Kuge, and Tomohiro Yamamura. “Affording realistic stopping behaviour: A cardinal challenge for driving simulators”. In: *Proceedings of the 1st Human-Centered Transportation Simulation Conference*. 2001.
- [6] Erwin R. Boer, Tomohiro Yamamura, Nobuyuki Kuge, and Ahna Girshick. “Experiencing the Same Road Twice: A Driver Centered Comparison between Simulation and Reality”. In: *Proceedings of the Driving Simulation Conference, Paris, France*. 2000.
- [7] J. E. Bos, S. N. MacKinnon, and A. Patterson. “Motion sickness symptoms in a ship motion simulator: Effects of inside, outside, and no view”. In: *Aviation, Space, and Environmental Medicine* 76 (2005).
- [8] Stephen P. Boyd and Lieven Vandenbergh. *Convex Optimization*. Cambridge University Press, 2004.
- [9] Johnell O. Brooks, Richard R. Goodenough, Matthew C. Crisler, Nathan D. Klein, Rebecca L. Alley, Beatrice L. Koon, William C. Logan, Jennifer H. Ogle, Richard A. Tyrrell, and Rebekkah F. Wills. “Simulator sickness during driving simulation studies”. In: *Accident Analysis & Prevention* 42.3 (May 2010), pp. 788–796. DOI: [10.1016/j.aap.2009.04.013](https://doi.org/10.1016/j.aap.2009.04.013).

- [10] M. Bruschetta, F. Maran, and A. Beghi. “A fast implementation of MPC-based motion cueing algorithms for mid-size road vehicle motion simulators”. In: *Vehicle System Dynamics* 55.6 (Feb. 2017), pp. 802–826. DOI: [10.1080/00423114.2017.1280173](https://doi.org/10.1080/00423114.2017.1280173).
- [11] Mattia Bruschetta, Carlo Cenedese, and Alessandro Beghi. “A real-time, MPC-based Motion Cueing Algorithm with Look-Ahead and driver characterization”. In: *Transportation Research Part F: Traffic Psychology and Behaviour* 61 (Feb. 2019), pp. 38–52. DOI: [10.1016/j.trf.2017.04.023](https://doi.org/10.1016/j.trf.2017.04.023).
- [12] Katherine S. Button, John P. A. Ioannidis, Claire Mokrysz, Brian A. Nosek, Jonathan Flint, Emma S. J. Robinson, and Marcus R. Munafò. “Power failure: why small sample size undermines the reliability of neuroscience”. In: *Nature Reviews Neuroscience* 14.5 (Apr. 2013), pp. 365–376. DOI: [10.1038/nrn3475](https://doi.org/10.1038/nrn3475).
- [13] E. F. Camacho and C. Bordons. *Model Predictive Control*. Advanced Textbooks in Control and Signal Processing. Springer London, 2007. DOI: [10.1007/978-0-85729-398-5](https://doi.org/10.1007/978-0-85729-398-5).
- [14] Oliver Carsten and A. Hamish Jamson. “Driving Simulators as Research Tools in Traffic Psychology”. In: *Handbook of Traffic Psychology*. Elsevier, 2011, pp. 87–96. DOI: [10.1016/b978-0-12-381984-0.10007-4](https://doi.org/10.1016/b978-0-12-381984-0.10007-4).
- [15] Sergio Casas, Inmaculada Coma, Cristina Portalés, and Marcos Fernández. “Towards a simulation-based tuning of motion cueing algorithms”. In: *Simulation Modelling Practice and Theory* 67 (Sept. 2016), pp. 137–154. DOI: [10.1016/j.simpat.2016.06.002](https://doi.org/10.1016/j.simpat.2016.06.002).
- [16] Sergio Casas, Inmaculada Coma, José Vicente Riera, and Marcos Fernández. “Motion-Cueing Algorithms: Characterization of Users’ Perception”. In: *Human Factors: The Journal of the Human Factors and Ergonomics Society* 57.1 (June 2014), pp. 144–162. DOI: [10.1177/0018720814538281](https://doi.org/10.1177/0018720814538281).
- [17] Sergio Casas, Cristina Portalés, Pedro Morillo, and Marcos Fernández. “A particle swarm approach for tuning washout algorithms in vehicle simulators”. In: *Applied Soft Computing* 68 (July 2018), pp. 125–135. DOI: [10.1016/j.asoc.2018.03.044](https://doi.org/10.1016/j.asoc.2018.03.044).
- [18] Francesco Celiberti and Marco Grotto. *PTW model in safety critical manoeuvres*. Tech. rep. MOTORIST Deliverable 2.1, 2018.
- [19] Francesco Celiberti, Marco Grotto, Maria Di Gesu, Marco Gubitosa, and Stijn Donders. “An Overview on the MOTORIST motorcycle simulator”. In: *Proceedings of Driving Simulation Conference & Exhibition 2016 Europe (DSC 2016 Europe)*. 2016, pp. 219–221.
- [20] Francesco Celiberti, Marco Grotto, Yves Lemmens, and Sikandar Moten. *Simulator based rider modelling*. Tech. rep. MOTORIST Deliverable 2.4a, 2016.
- [21] Sung-Hua Chen and Li-Chen Fu. “Predictive Washout Filter Design Using the Forward Kinematics and a Kalman Filter”. In: *2007 IEEE International Conference on Control Applications*. IEEE, Oct. 2007. DOI: [10.1109/cca.2007.4389267](https://doi.org/10.1109/cca.2007.4389267).

- [22] Shingo Chiyoda, Kenichi Yoshimoto, Daisuke Kawasaki, Yoshifumi Murakami, and Takayuki Sugimoto. “Development of a motorcycle simulator using parallel manipulator and head mounted display”. In: *The Proceedings of the International Conference on Motion and Vibration Control* 6.1.0 (2002), pp. 599–602. DOI: [10.1299/jsmaintmovic.6.1.599](https://doi.org/10.1299/jsmaintmovic.6.1.599).
- [23] David D. Clarke, Patrick Ward, Craig Bartle, and Wendy Truman. “The role of motorcyclist and other driver behaviour in two types of serious accident in the UK”. In: *Accident Analysis & Prevention* 39.5 (Sept. 2007), pp. 974–981. DOI: [10.1016/j.aap.2007.01.002](https://doi.org/10.1016/j.aap.2007.01.002).
- [24] D. Cleij, J. Venrooij, P. Pretto, M. Katliar, H. H. Bülthoff, D. Steffen, F. W. Hoffmeyer, and H.-P. Schöner. “Comparison between filter- and optimization-based motion cueing algorithms for driving simulation”. In: *Transportation Research Part F: Traffic Psychology and Behaviour* 61 (2019), pp. 53–68. DOI: [10.1016/j.trf.2017.04.005](https://doi.org/10.1016/j.trf.2017.04.005).
- [25] D. Cleij, J. Venrooij, P. Pretto, D. M. Pool, M. Mulder, and H. H. Bülthoff. “Continuous rating of perceived visual-inertial motion incoherence during driving simulation”. In: *Driving Simulation Conference & Exhibition*. 2015.
- [26] Diane Cleij, Joost Venrooij, Paolo Pretto, Daan M. Pool, Max Mulder, and Heinrich H. Bülthoff. “Continuous Subjective Rating of Perceived Motion Incongruence During Driving Simulation”. In: *IEEE Transactions on Human-Machine Systems* 48.1 (2018), pp. 17–29. DOI: [10.1109/thms.2017.2717884](https://doi.org/10.1109/thms.2017.2717884).
- [27] Ton J. Cleophas and Aeilko H. Zwinderman. “Statistical Analysis of Clinical Data on a Pocket Calculator”. In: (2011). DOI: [10.1007/978-94-007-1211-9](https://doi.org/10.1007/978-94-007-1211-9).
- [28] Matteo Corno, Sergio Matteo Savaresi, Mara Tanelli, and Luca Fabbri. “On optimal motorcycle braking”. In: *Control Engineering Practice* 16.6 (June 2008), pp. 644–657. DOI: [10.1016/j.conengprac.2007.08.001](https://doi.org/10.1016/j.conengprac.2007.08.001).
- [29] B. J. Correia Grácio, M. Wentink, and A. R. Valente Pais. “Driver Behavior Comparison Between Static and Dynamic Simulation for Advanced Driving Maneuvers”. In: *Presence: Teleoperators and Virtual Environments* 20.2 (2011), pp. 143–161. DOI: [10.1162/pres_a_00040](https://doi.org/10.1162/pres_a_00040).
- [30] V. Cossalter, R. Lot, and A. Doria. “Sviluppo di un simulatore di guida motociclistico”. In: *Proceedings of the 16th AIMETA Congress of Theoretical and Applied Mechanics*. Sept. 2003.
- [31] V. Cossalter, R. Lot, and M. Massaro. “An advanced multibody code for handling and stability analysis of motorcycles”. In: *Meccanica* 46.5 (Aug. 2010), pp. 943–958. DOI: [10.1007/s11012-010-9351-7](https://doi.org/10.1007/s11012-010-9351-7).
- [32] V. Cossalter, R. Lot, M. Massaro, and R. Sartori. “Development and validation of an advanced motorcycle riding simulator”. In: *Proceedings of the Institution of Mechanical Engineers, Part D: Journal of Automobile Engineering* 225.6 (2011), pp. 705–720. DOI: [10.1177/0954407010396006](https://doi.org/10.1177/0954407010396006).

- [33] Vittore Cossalter and Roberto Lot. “A Motorcycle Multi-Body Model for Real Time Simulations Based on the Natural Coordinates Approach”. In: *Vehicle System Dynamics* 37.6 (2002), pp. 423–447. DOI: [10.1076/vesd.37.6.423.3523](https://doi.org/10.1076/vesd.37.6.423.3523).
- [34] Vittore Cossalter, Roberto Lot, and Stefano Rota. “Objective and subjective evaluation of an advanced motorcycle riding simulator”. In: *European Transport Research Review* 2.4 (2010), pp. 223–233. DOI: [10.1007/s12544-010-0041-2](https://doi.org/10.1007/s12544-010-0041-2).
- [35] Elizabeth Crundall, Alex W. Stedmon, Rossukorn Saikayasit, and David Crundall. “A simulator study investigating how motorcyclists approach side-road hazards”. In: *Accident Analysis & Prevention* 51 (Mar. 2013), pp. 42–50. DOI: [10.1016/j.aap.2012.10.017](https://doi.org/10.1016/j.aap.2012.10.017).
- [36] Javier Cuadrado, Daniel Dopico, Miguel A. Naya, and M. Gonzalez. “Real-Time Multibody Dynamics and Applications”. In: *Simulation Techniques for Applied Dynamics*. Springer Vienna, 2008, pp. 247–311. DOI: [10.1007/978-3-211-89548-1_6](https://doi.org/10.1007/978-3-211-89548-1_6).
- [37] M. Dagdelen, G. Reymond, A. Kemeny, M. Bordier, and N. Maïzi. “MPC based Motion Cueing Algorithm: Development and Application to the ULTIMATE Driving Simulator”. In: *Driving Simulation Conference*. 2004.
- [38] Herman J. Damveld, Mark Wentink, Peter M. van Leeuwen, and Riender Happee. “Effects of Motion Cueing on Curve Driving”. In: *Driving Simulation Conference*. 2012.
- [39] Seyed Rasoul Davoodi and Hussain Hamid. “Motorcyclist Braking Performance in Stopping Distance Situations”. In: *Journal of Transportation Engineering* 139.7 (July 2013), pp. 660–666. DOI: [10.1061/\(asce\)te.1943-5436.0000552](https://doi.org/10.1061/(asce)te.1943-5436.0000552).
- [40] Seyed Rasoul Davoodi, Hussain Hamid, Mahdiah Pazhouhanfar, and Jeffrey W. Muttart. “Motorcyclist perception response time in stopping sight distance situations”. In: *Safety Science* 50.3 (Mar. 2012), pp. 371–377. DOI: [10.1016/j.ssci.2011.09.004](https://doi.org/10.1016/j.ssci.2011.09.004).
- [41] E. J. H. de Vries and H. B. Pacejka. “Motorcycle tyre measurements and models”. In: *Vehicle System Dynamics* 29.sup1 (1998), pp. 280–298. DOI: [10.1080/00423119808969565](https://doi.org/10.1080/00423119808969565).
- [42] J. C. F. De Winter, P. M. Van Leeuwen, and R. Happee. “Advantages and Disadvantages of Driving Simulators: A Discussion”. In: *Proceedings of Measuring Behavior, Utrecht, The Netherlands*. 2012.
- [43] Moritz Diehl, Hans Georg Bock, and Johannes P. Schlöder. “A Real-Time Iteration Scheme for Nonlinear Optimization in Optimal Feedback Control”. In: *SIAM Journal on Control and Optimization* 43.5 (Jan. 2005), pp. 1714–1736. DOI: [10.1137/s0363012902400713](https://doi.org/10.1137/s0363012902400713).
- [44] C. G. Drury and P. Pietraszewski. “The motorists’ perception of the bicyclists’ hand signals”. In: *Ergonomics* 22.9 (Sept. 1979), pp. 1045–1057. DOI: [10.1080/00140137908924679](https://doi.org/10.1080/00140137908924679).

- [45] ukasz Dziuda, Marcin P. Biernacki, Paulina M. Baran, and Olaf E. Truszczyski. “The effects of simulated fog and motion on simulator sickness in a driving simulator and the duration of after-effects”. In: *Applied Ergonomics* 45.3 (May 2014), pp. 406–412. DOI: [10.1016/j.apergo.2013.05.003](https://doi.org/10.1016/j.apergo.2013.05.003).
- [46] H. Ecker, J. Wassermann, G. Hauer, R. Ruspekhofer, and M. Grill. “Braking Deceleration of Motorcycle Riders”. In: *International Motorcycle Safety Conference*. 2001.
- [47] H. Ecker, J. Wassermann, R. Ruspekhofer, G. Hauer, and M. Winkelbauer. “Brake Reaction Times of Motorcycle Riders”. In: *International Motorcycle Safety Conference* (2001).
- [48] Simos Evangelou. “The Control and Stability Analysis of Two-wheeled Road Vehicles”. PhD thesis. Imperial College London, 2003.
- [49] Zhou Fang and Andras Kemeny. “An efficient Model Predictive Control-based motion cueing algorithm for the driving simulator”. In: *SIMULATION* 92.11 (Oct. 2016), pp. 1025–1033. DOI: [10.1177/0037549716667835](https://doi.org/10.1177/0037549716667835).
- [50] D. Ferrazzin, F. Barbagli, C. A. Avizzano, G. Di Pietro, and M. Bergamasco. “Designing new commercial motorcycles through a highly reconfigurable virtual reality-based simulator”. In: *Advanced Robotics* 17.4 (Jan. 2003), pp. 293–318. DOI: [10.1163/156855303765203010](https://doi.org/10.1163/156855303765203010).
- [51] D. Ferrazzin, F. Salsedo, F. Barbagli, C. A. Avizzano, G. Di Pietro, A. Brogni, M. Vignoni, M. Bergamasco, L. Arnone, M. Marcacci, L. Masut, and A. Benedetti. “The MORIS Motorcycle Simulator: an overview”. In: *SAE Technical Paper Series*. SAE International, Dec. 2001. DOI: [10.4271/2001-01-1874](https://doi.org/10.4271/2001-01-1874).
- [52] D. Ferrazzin, F. Salsedo, and M. Bergamasco. “The MORIS simulator”. In: *8th IEEE International Workshop on Robot and Human Interaction. RO-MAN '99 (Cat. No.99TH8483)*. IEEE, 1999. DOI: [10.1109/roman.1999.900329](https://doi.org/10.1109/roman.1999.900329).
- [53] Hans Joachim Ferreau, Christian Kirches, Andreas Potschka, Hans Georg Bock, and Moritz Diehl. “qpOASES: a parametric active-set algorithm for quadratic programming”. In: *Mathematical Programming Computation* 6.4 (Apr. 2014), pp. 327–363. DOI: [10.1007/s12532-014-0071-1](https://doi.org/10.1007/s12532-014-0071-1).
- [54] Martin Fischer, Håkan Sehamar, and Göran Palmkvist. “Applied Motion Cueing Strategies for Three Different Types of Motion Systems”. In: *Journal of Computing and Information Science in Engineering* 11.4 (Dec. 2011). DOI: [10.1115/1.4005454](https://doi.org/10.1115/1.4005454).
- [55] Martin Fischer and Julia Werneke. “The new time-variant motion cueing algorithm for the DLR dynamic driving simulator”. In: *Driving Simulation Conference 2008*. 2008.
- [56] Donald L. Fisher, Matthew Rizzo, Jeffrey Caird, and John D. Lee, eds. *Handbook of Driving Simulation for Engineering, Medicine, and Psychology*. CRC Press, Apr. 2011. DOI: [10.1201/b10836](https://doi.org/10.1201/b10836).

- [57] Nikhil J.I. Garrett and Matthew C. Best. “Model predictive driving simulator motion cueing algorithm with actuator-based constraints”. In: *Vehicle System Dynamics* 51.8 (Aug. 2013), pp. 1151–1172. DOI: [10.1080/00423114.2013.783219](https://doi.org/10.1080/00423114.2013.783219).
- [58] Peter R. Grant and Bruce Haycock. “Effect of Jerk and Acceleration on the Perception of Motion Strength”. In: *Journal of Aircraft* 45.4 (2008), pp. 1190–1197. DOI: [10.2514/1.33757](https://doi.org/10.2514/1.33757).
- [59] Peter R. Grant and Lloyd D. Reid. “PROTEST: An Expert System for Tuning Simulator Washout Filters”. In: *Journal of Aircraft* 34.2 (Mar. 1997), pp. 152–159. DOI: [10.2514/2.2166](https://doi.org/10.2514/2.2166).
- [60] Peter Grant, Bruce Artz, Mike Blommer, Larry Cathey, and Jeff Greenberg. “A Paired Comparison Study of Simulator Motion Drive Algorithms”. In: *Driving Simulation Conference 2002*. 2002.
- [61] Peter Grant and Peter Tung Sing Lee. “Motion-Visual Phase-Error Detection in a Flight Simulator”. In: *Journal of Aircraft* 44.3 (2007), pp. 927–935. DOI: [10.2514/1.25807](https://doi.org/10.2514/1.25807).
- [62] Marc Green. ““How Long Does It Take to Stop?” Methodological Analysis of Driver Perception-Brake Times”. In: *Transportation Human Factors* 2.3 (Sept. 2000), pp. 195–216. DOI: [10.1207/sthf0203_1](https://doi.org/10.1207/sthf0203_1).
- [63] S. de Groot, M. Mulder, and P. A. Wieringa. “Nonvestibular Motion Cueing in a Fixed-Base Driving Simulator: Effects on Driver Braking and Cornering Performance”. In: *Presence: Teleoperators and Virtual Environments* 20.2 (Apr. 2011), pp. 117–142. DOI: [10.1162/pres_a_00039](https://doi.org/10.1162/pres_a_00039).
- [64] Marco Grottoli and Francesco Celiberti. *The MOTORIST simulator: design and realization of a modular motorcycle simulator. Presented at: Safe2Wheelers - Accidentology and Motorcycle Simulator Workshop*. Apr. 2016.
- [65] Marco Grottoli, Francesco Celiberti, Maria Di Gesu, Sikandar Moten, and Yves Lemmens. “The MOTORIST Motorcycle Riding Simulator”. In: *Bicycle and Motorcycle Dynamics*. 2016.
- [66] Marco Grottoli, Francesco Celiberti, Anne van der Heide, Yves Lemmens, and Riender Happee. “Motorcycle multibody model validation for Human-in-the-Loop simulation”. In: *Driving Simulation & Virtual Reality Conference & Exhibition*. 2019.
- [67] Marco Grottoli, Francesco Celiberti, Anne van der Heide, Yves Lemmens, and Riender Happee. *Motorcycle multibody model validation for HuiL simulator - Results*. 2019. DOI: [10.4121/uuid:048a3ce0-3cb8-49c5-ad4c-69e15833417e](https://doi.org/10.4121/uuid:048a3ce0-3cb8-49c5-ad4c-69e15833417e).
- [68] Marco Grottoli, Diane Cleij, Paolo Pretto, Yves Lemmens, Riender Happee, and Heinrich H. Bühlhoff. “Objective evaluation of prediction strategies for optimization-based motion cueing”. In: *SIMULATION* 95.8 (Dec. 2018), pp. 707–724. DOI: [10.1177/0037549718815972](https://doi.org/10.1177/0037549718815972).

- [69] Marco Grottooli, Marco Gubitosa, Stijn Donders, Edward Holweg, and Riender Happee. "Objective Comparison of Motion Cueing Algorithms for Driving Simulator". In: *4th Joint International Conference on Multibody System Dynamics*. 2016.
- [70] Marco Grottooli, Anne van der Heide, and Yves Lemmens. "A High Fidelity Driving Simulation Platform for the Development and Validation of Advanced Driver Assistance Systems". In: *Reinventing Mechatronics*. Springer International Publishing, 2020, pp. 93–109. DOI: [10.1007/978-3-030-29131-0_7](https://doi.org/10.1007/978-3-030-29131-0_7).
- [71] Marco Grottooli, Anne van der Heide, and Yves Lemmens. "Impact of vehicle dynamics model fidelity in the development of ADAS". In: *NAFEMS World Congress*. 2019.
- [72] Marco Grottooli, Alessandro Toso, Marco Gubitosa, Edward Holweg, and Riender Happee. "High-Fidelity Multibody Model for a Powered-Two-Wheeler Driving Simulator". In: *ECCOMAS Thematic Conference on Multibody Dynamics*. 2015.
- [73] Marco Grottooli, Anne van der Heide, and Yves Lemmens. "Impact of vehicle dynamics model fidelity in the development of ADAS". In: *NAFEMS World Congress*. 2019.
- [74] S. Guth, M. Geiger, A. Parduži, S. Will, R. Pless, and H. Winner. "Method to Assess the Processing of Optical Information by Non-primary Riding Tasks while Riding a Motorcycle". In: *In Proceedings of Bicycle and Motorcycle Dynamics Conference BMD*. 2016.
- [75] S. Guth, M. Geiger, S. Will, R. Pless, and H. Winner. "Motion cueing algorithm to reproduce motorcycle specific lateral dynamics on riding simulators". In: *Driving Simulation Conference & Exhibition*. 2015.
- [76] Sebastian Guth. "Motorcycle riding simulation to assess instrument and operation concepts and informing riding assistance systems". In: *10th International Motorcycle Conference*. 2014.
- [77] Riender Happee, Arend Schwab, Marco Grottooli, Gustavo Gil, and Maria Di Gesu. *Requirements for volunteer testing of rider behaviour*. Tech. rep. MOTORIST Deliverable 2.2, 2015.
- [78] Sandra G. Hart and Lowell E. Staveland. "Development of NASA-TLX (Task Load Index): Results of Empirical and Theoretical Research". In: *Advances in Psychology*. Elsevier, 1988, pp. 139–183. DOI: [10.1016/s0166-4115\(08\)62386-9](https://doi.org/10.1016/s0166-4115(08)62386-9).
- [79] Edward J. Haug. *Computer aided kinematics and dynamics of mechanical systems. Volume I: Basic methods*. Allyn & Bacon, 1989, p. 498.
- [80] M. Houtenbos, J. C. F. de Winter, A. R. Hale, P. A. Wieringa, and M. P. Hagenzieker. "Concurrent audio-visual feedback for supporting drivers at intersections: A study using two linked driving simulators". In: *Applied Ergonomics* 60 (Apr. 2017), pp. 30–42. DOI: [10.1016/j.apergo.2016.10.010](https://doi.org/10.1016/j.apergo.2016.10.010).

- [81] P. Huertas-Leyva, M. Nugent, G. Savino, M. Pierini, N. Baldanzini, and S. Rosalie. "Identification of emergency braking performance distinguishing level of skills of motorcycle riders in an integrated real-life perceptual-action task". In: *Proceedings of Road Safety and Simulation International Conference*. 2017.
- [82] Pedro Huertas-Leyva, Marilee Nugent, Giovanni Savino, Marco Pierini, Niccolò Baldanzini, and Simon Rosalie. "Emergency braking performance of motorcycle riders: skill identification in a real-life perception-action task designed for training purposes". In: *Transportation Research Part F: Traffic Psychology and Behaviour* 63 (May 2019), pp. 93–107. DOI: [10.1016/j.trf.2019.03.019](https://doi.org/10.1016/j.trf.2019.03.019).
- [83] Richard J. Jagacinski and John M. Flach. *Control Theory for Humans: Quantitative Approaches To Modeling Performance*. CRC Press, 2003.
- [84] Javier Garca de Jalón and Eduardo Bayo. *Kinematic and Dynamic Simulation of Multibody Systems*. Springer New York, 1994. DOI: [10.1007/978-1-4612-2600-0](https://doi.org/10.1007/978-1-4612-2600-0).
- [85] Susan Jamieson. "Likert scales: how to (ab)use them". In: *Medical Education* 38.12 (Dec. 2004), pp. 1217–1218. DOI: [10.1111/j.1365-2929.2004.02012.x](https://doi.org/10.1111/j.1365-2929.2004.02012.x).
- [86] A. H. Jamson and P. Smith. "Are you used to it yet? Braking performance and adaptation in a fixed base driving simulator". In: *Proceedings of the Driving Simulation Conference North America, Detroit, Michigan*. 2003.
- [87] Peter Jonik, Ana Rita Valente Pais, Marinus van Paassen, and Max Mulder. "Phase Coherence Zones in Flight Simulation". In: *AIAA Modeling and Simulation Technologies Conference*. American Institute of Aeronautics and Astronautics, Aug. 2011. DOI: [10.2514/6.2011-6555](https://doi.org/10.2514/6.2011-6555).
- [88] I Kageyama. "Development of a riding simulator for two-wheeled vehicles". In: *JSAE Review* 23.3 (July 2002), pp. 347–352. DOI: [10.1016/s0389-4304\(02\)00202-3](https://doi.org/10.1016/s0389-4304(02)00202-3).
- [89] Tsuyoshi Katayama, Tomoo Nishimi, Takumi Okayama, and Akira Aoki. "A simulation model for rider's control behaviors". In: *JSAE Review* 17.4 (Oct. 1996), p. 441. DOI: [10.1016/s0389-4304\(96\)80545-5](https://doi.org/10.1016/s0389-4304(96)80545-5).
- [90] Mikhail Katliar, Ksander N. de Winkel, Joost Venrooij, Paolo Pretto, and Heinrich H. Bülthoff. "Impact of MPC Prediction Horizon on Motion Cueing Fidelity". In: *Driving Simulation Conference & Exhibition 2015*. Tübingen, Germany, 2015, pp. 219–222.
- [91] Mikhail Katliar, Jörg Fisher, Gianluca Frison, Moritz Diehl, Harald Teufel, and Heinrich H. Bülthoff. "Nonlinear Model Predictive Control of a Cable-Robot-Based Motion Simulator". In: *The 20th World Congress of the International Federation of Automatic Control*. 2017, pp. 10249–10255.
- [92] Robert S. Kennedy, Norman E. Lane, Kevin S. Berbaum, and Michael G. Lilienthal. "Simulator Sickness Questionnaire: An Enhanced Method for Quantifying Simulator Sickness". In: *The International Journal of Aviation Psychology* 3.3 (July 1993), pp. 203–220. DOI: [10.1207/s15327108ijap0303_3](https://doi.org/10.1207/s15327108ijap0303_3).

- [93] Yash Raj Khusro, Yanggu Zheng, Marco Grotoli, and Barys Shyrokau. “MPC-Based Motion-Cueing Algorithm for a 6-DOF Driving Simulator with Actuator Constraints”. In: *Vehicles* 2.4 (Dec. 2020), pp. 625–647. DOI: [10 . 3390 / vehicles2040036](https://doi.org/10.3390/vehicles2040036).
- [94] Natália Kováčsová, Maco Grotoli, Francesco Celiberti, Yves Lemmens, Riender Happee, M. P. Hagenzieker, and J. C. F. De Winter. *Supplementary data for the article: Emergency braking at intersections: A motion-base motorcycle simulator study*. en. 2019. DOI: [10 . 4121 / UUID : 6B1E0FFB - 3606 - 4095 - 9702 - BE34DD3C2D59](https://doi.org/10.4121/UUID:6B1E0FFB-3606-4095-9702-BE34DD3C2D59).
- [95] Natália Kováčsová, Marco Grotoli, Francesco Celiberti, Yves Lemmens, Riender Happee, Marjan P. Hagenzieker, and Joost C. F. de Winter. “Emergency braking at intersections: A motion-base motorcycle simulator study”. In: *Applied Ergonomics* 82 (Jan. 2020), p. 102970. DOI: [10.1016/j.apergo.2019.102970](https://doi.org/10.1016/j.apergo.2019.102970).
- [96] Natália Kováčsová, Marco Grotoli, Francesco Celiberti, Yves Lemmens, Riender Happee, Marjan P. Hagenzieker, and Joost C. F. de Winter. *Report on rider training on a motorcycle test rig*. Tech. rep. MOTORIST Deliverable 1.3, 2018.
- [97] J. D. Lee. “Simulator fidelity: How low can you go?”. In: *Proceedings of the 48th annual meeting of the Human Factors and Ergonomics Society*. 2004.
- [98] Yee Mun Lee and Elizabeth Sheppard. “The effect of motion and signalling on drivers’ ability to predict intentions of other road users”. In: *Accident Analysis & Prevention* 95 (Oct. 2016), pp. 202–208. DOI: [10.1016/j.aap.2016.07.011](https://doi.org/10.1016/j.aap.2016.07.011).
- [99] Luca Leonelli and Nicolò Mancinelli. “A multibody motorcycle model with rigid-rigid tyres: formulation and validation”. In: *Vehicle System Dynamics* 53.6 (Mar. 2015), pp. 775–797. DOI: [10.1080/00423114.2015.1014820](https://doi.org/10.1080/00423114.2015.1014820).
- [100] Rensis Likert. “A technique for the measurement of attitudes”. In: *Archives of psychology* (1932).
- [101] D. J. N. Limebeer, R. S. Sharp, and S Evangelou. “The stability of motorcycles under acceleration and braking”. In: *Proceedings of the Institution of Mechanical Engineers, Part C: Journal of Mechanical Engineering Science*. 2001.
- [102] Régis Lobjois, Virginie Dagonneau, and Brice Isableu. “The contribution of visual and proprioceptive information to the perception of leaning in a dynamic motorcycle simulator”. In: *Ergonomics* 59.11 (Feb. 2016), pp. 1428–1441. DOI: [10.1080/00140139.2016.1149229](https://doi.org/10.1080/00140139.2016.1149229).
- [103] Jan Marian Maciejowski. *Predictive Control with Constraints*. Prentice Hall, 2002.
- [104] MAIDS. *Motorcycle Accident In-depth Study MAIDS: In-depth investigations of accidents involving powered two wheelers*. Tech. rep. The European Association of Motorcycle Manufacturers ACEM, 2009.
- [105] Francesco Migliore. “Sviluppo di modelli motore e veicolo per l’analisi di strategie di controllo in applicazioni Software e Hardware In the Loop”. PhD thesis. Università di Bologna, 2010.

- [106] Yukio Miyamaru, Goro Yamasaki, and Katsuhito Aoki. "Development of a motorcycle riding simulator". In: *JSAE Review* 23.1 (Jan. 2002), pp. 121–126. DOI: [10.1016/s0389-4304\(01\)00147-3](https://doi.org/10.1016/s0389-4304(01)00147-3).
- [107] Arash Mohammadi, Houshyar Asadi, Shady Mohamed, Kyle Nelson, and Saeid Nahavandi. "Future Reference Prediction in Model Predictive Control based Driving Simulators". In: *ACRA 2016: Proceedings of the ARAA Australian Conference on Robotics and Automation*. Brisbane, Qld.: Australian Robotics and Automation Association, 2016, p. 8.
- [108] Arash Mohammadi, Houshyar Asadi, Shady Mohamed, Kyle Nelson, and Saeid Nahavandi. "Optimizing Model Predictive Control horizons using Genetic Algorithm for Motion Cueing Algorithm". In: *Expert Systems with Applications* 92 (Feb. 2018), pp. 73–81. DOI: [10.1016/j.eswa.2017.09.004](https://doi.org/10.1016/j.eswa.2017.09.004).
- [109] Douglas C. Montgomery and George C. Runger. *Applied Statistics and Probability for Engineers*. 3rd Editio. John Wiley & Sons, Inc., Hoboken, NJ, 2003.
- [110] David Moreno Giner, Claudio Brenna, Ioannis Symeonidis, and Gueven Kavadarlic. "MYMOSA: Towards the Simulation of Realistic Motorcycle Manoeuvres by Coupling Multibody and Control Techniques". In: *Volume 17: Transportation Systems*. ASME, 2008. DOI: [10.1115/imece2008-67297](https://doi.org/10.1115/imece2008-67297).
- [111] Umberto Musella, Ludovico Zanellati, Marco Grottoli, Francesco Celiberti, Bart Peeters, Francesco Marulo, and Patrick Guillaume. "Driving a Motion Platform with a Vibration Control Software for Multi-Axis Environmental Testing: Challenges and Solutions". In: *Special Topics in Structural Dynamics, Volume 5*. Springer International Publishing, May 2018, pp. 215–231. DOI: [10.1007/978-3-319-75390-4_20](https://doi.org/10.1007/978-3-319-75390-4_20).
- [112] L. Nehaoua, S. Hima, H. Arioui, N. Seguy, and S. Espie. "Design and Modeling of a New Motorcycle Riding Simulator". In: *2007 American Control Conference*. IEEE, July 2007. DOI: [10.1109/acc.2007.4283070](https://doi.org/10.1109/acc.2007.4283070).
- [113] Alessandro Nesti, Carlo Masone, Michael Barnett-Cowan, Paolo Robuffo Giordano, Heinrich H. Bühlhoff, and Paolo Pretto. "Roll rate thresholds and perceived realism in driving simulation". In: *Driving Simulation Conference 2012*. Paris, France, Sept. 2012, p. 6.
- [114] Alessandro Nesti, Suzanne Nooij, Martin Losert, Heinrich H Bühlhoff, and Paolo Pretto. "Roll rate perceptual thresholds in active and passive curve driving simulation". In: *SIMULATION* 92.5 (Mar. 2016), pp. 417–426. DOI: [10.1177/0037549716637135](https://doi.org/10.1177/0037549716637135).
- [115] Geoff Norman. "Likert scales, levels of measurement and the laws of statistics". In: *Advances in Health Sciences Education* 15.5 (Feb. 2010), pp. 625–632. DOI: [10.1007/s10459-010-9222-y](https://doi.org/10.1007/s10459-010-9222-y).
- [116] Oculus VR. *Oculus Developer Guide: SDK Version 0.4*. Tech. rep. Oculus VR, LLC, 2014.

- [117] Paul L. Olson and Michael Sivak. "Perception-Response Time to Unexpected Roadway Hazards". In: *Human Factors: The Journal of the Human Factors and Ergonomics Society* 28.1 (Feb. 1986), pp. 91–96. DOI: [10.1177/001872088602800110](https://doi.org/10.1177/001872088602800110).
- [118] Chih-Wei Pai. "Motorcycle right-of-way accidents - A literature review". In: *Accident Analysis & Prevention* 43.3 (May 2011), pp. 971–982. DOI: [10.1016/j.aap.2010.11.024](https://doi.org/10.1016/j.aap.2010.11.024).
- [119] Avinash P. Penumaka, Giovanni Savino, Niccolò Baldanzini, and Marco Pierini. "In-depth investigations of PTW-car accidents caused by human errors". In: *Safety Science* 68 (Oct. 2014), pp. 212–221. DOI: [10.1016/j.ssci.2014.04.004](https://doi.org/10.1016/j.ssci.2014.04.004).
- [120] M. Pinto, V. Cavallo, and T. Ohlmann. "The development of driving simulators: toward a multisensory solution". In: *Le travail humain* 71.1 (2008), p. 62. DOI: [10.3917/th.711.0062](https://doi.org/10.3917/th.711.0062).
- [121] Alexander Pollatsek, Vinod Narayanaan, Anuj Pradhan, and Donald L. Fisher. "Using eye movements to evaluate a PC-based risk awareness and perception training program on a driving simulator". In: *Human Factors* 48 (2006), pp. 447–464.
- [122] P. Pretto, M. Ogier, H.H. Bülthoff, and J.-P. Bresciani. "Influence of the size of the field of view on motion perception". In: *Computers & Graphics* 33.2 (Apr. 2009), pp. 139–146. DOI: [10.1016/j.cag.2009.01.003](https://doi.org/10.1016/j.cag.2009.01.003).
- [123] J. D. Prothero. "The role of rest frames invection, presence and motion sickness". PhD thesis. University of Washington, USA, 1998.
- [124] Jerrold D. Prothero, Mark H. Draper, Thomas A. Furness, Donald E. Parker, and Maxwell J. Wells. "Do visual background manipulations reduce simulator sickness?" In: *Proceedings of the international workshop on motion sickness: medical and human factors*. 1997, pp. 18–21.
- [125] Imad Al Qaisi and Ansgar Traechtler. "Human in the loop: Optimal control of driving simulators and new motion quality criterion". In: *2012 IEEE International Conference on Systems, Man, and Cybernetics (SMC)*. IEEE, Oct. 2012. DOI: [10.1109/icsmc.2012.6378073](https://doi.org/10.1109/icsmc.2012.6378073).
- [126] James B. Rawlings and David Q. Mayne. *Model Predictive Control: Theory and Design*. Nob Hill Publishing, 2009.
- [127] Lloyd D. Reid and Meyer A. Nahon. *Flight Simulator Motion-Base Drive Algorithms: Part 1 - Developing and Testing the Equations*. Tech. rep. University of Toronto Institute for Aerospace Studies, 1985.
- [128] Lloyd D. Reid and Meyer A. Nahon. *Flight Simulator Motion-Base Drive Algorithms: Part 2 - Selecting the System Parameters*. Tech. rep. University of Toronto Institute for Aerospace Studies, 1986.
- [129] Gilles Reymond and Andras Kemeny. "Motion Cueing in the Renault Driving Simulator". In: *Vehicle System Dynamics* 34.4 (Oct. 2000), pp. 249–259. DOI: [10.1076/vesd.34.4.249.2059](https://doi.org/10.1076/vesd.34.4.249.2059).

- [130] Gilles Reymond, Andras Kemeny, Jacques Droulez, and Alain Berthoz. “Role of Lateral Acceleration in Curve Driving: Driver Model and Experiments on a Real Vehicle and a Driving Simulator”. In: *Human Factors: The Journal of the Human Factors and Ergonomics Society* 43.3 (Sept. 2001), pp. 483–495. DOI: [10.1518/001872001775898188](https://doi.org/10.1518/001872001775898188).
- [131] Ali Rezajat, Marco Grottole, Yves Lemmens, Tommaso Tamarozzi, and Christophe Liefvooghe. “Influence of internal loads on the accuracy of durability tests of a vehicle on a test rig”. In: *International Conference on Noise and Vibration Engineering*. 2020.
- [132] Ingrid G. Salisbury and David J. N. Limebeer. “Optimal Motion Cueing for Race Cars”. In: *IEEE Transactions on Control Systems Technology* 24.1 (Jan. 2016), pp. 200–215. DOI: [10.1109/tcst.2015.2424161](https://doi.org/10.1109/tcst.2015.2424161).
- [133] Giovanni Savino, Marco Pierini, and Michael G. Lenné. “Development of a low-cost motorcycle riding simulator for emergency scenarios involving swerving”. In: *Proceedings of the Institution of Mechanical Engineers, Part D: Journal of Automobile Engineering* 230.14 (Dec. 2016), pp. 1891–1903. DOI: [10.1177/0954407015624998](https://doi.org/10.1177/0954407015624998).
- [134] Giovanni Savino, Marco Pierini, Jason Thompson, Michael Fitzharris, and Michael G. Lenné. “Exploratory field trial of motorcycle autonomous emergency braking (MAEB): Considerations on the acceptability of unexpected automatic decelerations”. In: *Traffic Injury Prevention* 17.8 (Mar. 2016), pp. 855–862. DOI: [10.1080/15389588.2016.1155210](https://doi.org/10.1080/15389588.2016.1155210).
- [135] Stanley F. Schmidt and Bjorn Conrad. *Motion drive signals for piloted flight simulators*. Tech. rep. Washington: NASA, 1970. DOI: [19700017803](https://doi.org/10.1017/cbo9781107337213).
- [136] Ahmed A. Shabana. *Dynamics of multibody systems*. Cambridge University Press, 2009. DOI: [10.1017/cbo9781107337213](https://doi.org/10.1017/cbo9781107337213).
- [137] Amit Shahar, Virginie Dagonneau, Séphane Caro, Isabelle Israël, and Régis Lobjois. “Towards identifying the roll motion parameters of a motorcycle simulator”. In: *Applied Ergonomics* 45.3 (May 2014), pp. 734–740. DOI: [10.1016/j.apergo.2013.09.013](https://doi.org/10.1016/j.apergo.2013.09.013).
- [138] R. S. Sharp. “Optimal stabilization and path-following controls for a bicycle”. In: *Proceedings of the Institution of Mechanical Engineers, Part C: Journal of Mechanical Engineering Science* 221.4 (Apr. 2007), pp. 415–427. DOI: [10.1243/0954406jmes529](https://doi.org/10.1243/0954406jmes529).
- [139] R. S. Sharp, S. Evangelou, and D. J. N. Limebeer. “Advances in the Modelling of Motorcycle Dynamics”. In: *Multibody System Dynamics* 12.3 (Oct. 2004), pp. 251–283. DOI: [10.1023/b:mubo.0000049195.60868.a2](https://doi.org/10.1023/b:mubo.0000049195.60868.a2).
- [140] Barys Shyrokau, Joost De Winter, Olaf Stroosma, Chris Dijksterhuis, Jan Loof, Rene van Paassen, and Riender Happee. “The effect of steering-system linearity, simulator motion, and truck driving experience on steering of an articulated tractor-semitrailer combination”. In: *Applied Ergonomics* 71 (Sept. 2018), pp. 17–28. DOI: [10.1016/j.apergo.2018.03.018](https://doi.org/10.1016/j.apergo.2018.03.018).

- [141] I. Siegler, G. Reymond, A. Kemeny, and A. Berthoz. "Sensorimotor integration in a driving simulator: contributions of motion cueing in elementary driving tasks". In: *Proceedings of the Driving Simulation Conference*. 2001.
- [142] Florian Soyka, Harald Teufel, Karl Beykirch, Paolo Robuffo Giordano, John Butler, Frank Nieuwenhuizen, and Heinrich Buelthoff. "Does Jerk Have to be Considered in Linear Motion Simulation?" In: *AIAA Modeling and Simulation Technologies Conference*. Reston, Virginia: American Institute of Aeronautics and Astronautics, Aug. 2009, pp. 1381–1388. DOI: [10.2514/6.2009-6245](https://doi.org/10.2514/6.2009-6245).
- [143] A. W. Stedmon, B. Hasseldine, D. Rice, M. Young, S. Markham, M. Hancox, E. Brickell, and J. Noble. "'MotorcycleSim': An Evaluation of Rider Interaction with an Innovative Motorcycle Simulator". In: *The Computer Journal* 54.7 (Aug. 2009), pp. 1010–1025. DOI: [10.1093/comjnl/bxp071](https://doi.org/10.1093/comjnl/bxp071).
- [144] D. Stewart. "A Platform with Six Degrees of Freedom". In: *Proceedings of the Institution of Mechanical Engineers* 180.1 (June 1965), pp. 371–386. DOI: [10.1243/pime_proc_1965_180_029_02](https://doi.org/10.1243/pime_proc_1965_180_029_02).
- [145] Heikki Summala and Mikko Rasanen. "Top-Down and Bottom-Up Processes in Driver Behavior at Roundabouts and Crossroads". In: *Transportation Human Factors* 2.1 (Mar. 2000), pp. 29–37. DOI: [10.1207/sthf0201_5](https://doi.org/10.1207/sthf0201_5).
- [146] Robert J. Telban and Frank M. Cardullo. *Motion Cueing Algorithm Development: Human-Centered Linear and Nonlinear Approaches*. Tech. rep. May. NASA, 2005.
- [147] Geoffrey Underwood, David Crundall, and Peter Chapman. "Driving simulator validation with hazard perception". In: *Transportation Research Part F: Traffic Psychology and Behaviour* 14.6 (Nov. 2011), pp. 435–446. DOI: [10.1016/j.trf.2011.04.008](https://doi.org/10.1016/j.trf.2011.04.008).
- [148] K. Vavryn and M. Winkelbauer. "Braking Performance of Experienced and Novice Motorcycle Riders - Results of a Field Study". In: *Proceedings of the 4th International Conference on Transport and Traffic Psychology*. 2004.
- [149] Joost Venrooij, Max Mulder, Mark Mulder, David A. Abbink, Marinus M. van Paassen, Frans C. T. van der Helm, and Heinrich H. Bülthoff. "Admittance-Adaptive Model-Based Approach to Mitigate Biodynamic Feedthrough". In: *IEEE Transactions on Cybernetics* 47.12 (Dec. 2017), pp. 4169–4181. DOI: [10.1109/TCYB.2016.2601638](https://doi.org/10.1109/TCYB.2016.2601638).
- [150] Carlin Vieri, Grace Lee, Nikhil Balram, Sang Hoon Jung, Joon Young Yang, Soo Young Yoon, and In Byeong Kang. "An 18 megapixel 4.3d^o 1443 ppi 120 Hz OLED display for wide field of view high acuity head mounted displays". In: *Journal of the Society for Information Display* 26.5 (May 2018), pp. 314–324. DOI: [10.1002/jsid.658](https://doi.org/10.1002/jsid.658).
- [151] Willem P. Vlakveld. "A comparative study of two desktop hazard perception tasks suitable for mass testing in which scores are not based on response latencies". In: *Transportation Research Part F: Traffic Psychology and Behaviour* 22 (Jan. 2014), pp. 218–231. DOI: [10.1016/j.trf.2013.12.013](https://doi.org/10.1016/j.trf.2013.12.013).

- [152] Ian Walker. “Signals are informative but slow down responses when drivers meet bicyclists at road junctions”. In: *Accident Analysis & Prevention* 37.6 (Nov. 2005), pp. 1074–1085. DOI: [10.1016/j.aap.2005.06.005](https://doi.org/10.1016/j.aap.2005.06.005).
- [153] Ian Walker and Mark Brosnan. “Drivers’ gaze fixations during judgements about a bicyclist’s intentions”. In: *Transportation Research Part F: Traffic Psychology and Behaviour* 10.2 (Mar. 2007), pp. 90–98. DOI: [10.1016/j.trf.2006.06.001](https://doi.org/10.1016/j.trf.2006.06.001).
- [154] Liuping Wang. *Model Predictive Control System Design and Implementation Using MATLAB®*. Springer London, 2009. DOI: [10.1007/978-1-84882-331-0](https://doi.org/10.1007/978-1-84882-331-0).
- [155] B. E. Westerhof. “Evaluation of the Cruden Motorcycle Simulator”. MA thesis. Delft University of Technology, 2018.
- [156] B. E. Westerhof, E. J. H. de Vries, R. Happee, and A. L. Schwab. “Evaluation of a Motorcycle Simulator”. In: *Proceedings, Bicycle and Motorcycle Dynamics*. 2019.
- [157] Frank Westerhuis and Dick De Waard. “Reading cyclist intentions: Can a lead cyclist’s behaviour be predicted?” In: *Accident Analysis & Prevention* 105 (Aug. 2017), pp. 146–155. DOI: [10.1016/j.aap.2016.06.026](https://doi.org/10.1016/j.aap.2016.06.026).
- [158] Gerald J. S. Wilde. “Social Interaction Patterns in Driver Behavior: An Introductory Review”. In: *Human Factors: The Journal of the Human Factors and Ergonomics Society* 18.5 (Oct. 1976), pp. 477–492. DOI: [10.1177/001872087601800506](https://doi.org/10.1177/001872087601800506).
- [159] Sebastian Will. “A New Approach to Investigate Powered Two Wheelers’ Interactions with Passenger Car Drivers: the Motorcycle Car Multi-Driver Simulation”. In: *UR:BAN Human Factors in Traffic*. Springer Fachmedien Wiesbaden, June 2017, pp. 393–402. DOI: [10.1007/978-3-658-15418-9_22](https://doi.org/10.1007/978-3-658-15418-9_22).
- [160] Sebastian Will. “Development of a presence model for driving simulators based on speed perception in a motorcycle riding simulator”. PhD thesis. Julius-Maximilians-Universität Würzburg, 2017.
- [161] Bob G. Witmer and Michael J. Singer. “Measuring Presence in Virtual Environments: A Presence Questionnaire”. In: *Presence: Teleoperators and Virtual Environments* 7.3 (1998), pp. 225–240. DOI: [10.1162/105474698565686](https://doi.org/10.1162/105474698565686).
- [162] G Yamasaki, K Aoki, Y Miyamaru, and K Ohnuma. “Development of motorcycle training simulator”. In: *JSAE Review* 19.1 (1998), pp. 81–85. DOI: [10.1016/S0389-4304\(97\)00057-X](https://doi.org/10.1016/S0389-4304(97)00057-X).

ACKNOWLEDGEMENTS

This Ph.D. has been a long and challenging experience, which gave me the opportunity to grow both professionally and personally. Receiving this title is a great honor for me, but I would have never made it if it were not for some great people who supported me along the way.

First of all, I would like to thank my promotor, associate prof. Riender Happee. In the years of my Ph.D., many people have supported me for more or less time, but you have been there since the first day. Thanks for your example on how to go ahead with determination and for our open discussions, also when we had different opinions. You have always looked for my interest, even when it was not clear to me. I am very glad to have worked with you. I would also like to thank my second promotor, prof. Max Mulder. You have been my promotor only in the final part of my Ph.D. but you have been a reference for the completion of this thesis and for my growth as a researcher.

I also want to thank the numerous people who have been working with me in Siemens, guiding and supporting me during these years. Alessandro Toso, you have been my first supervisor in Siemens, but you have been for me much more than that. Your technical strengths together with your friendly character towards everyone was a great example for me. Stijn Donders, I want to thank you for teaching me some of your organizational skills, your managing style required some adjustment for me, but we worked well together and we never had an issue. Yves Lemmens, you have been my supervisor in Siemens for the longest time. Together we worked from when I was still a fellow in the MOTORIST until almost the end of my Ph.D., therefore I want to thank you for being with me along the way. Tommaso Tamarozzi, even if you were not technically involved in this thesis, your contribution has been crucial. You helped me to prioritize my responsibilities to focus on completing my Ph.D., and I am grateful to you for that. Christophe Liefoghe, I have had many supervisors during these years, but you were always there. I am grateful for your constant presence and support, even from distance.

I would also like to acknowledge the MOTORIST project, as a fellow of this project I had the opportunity to meet not only great researchers, but great people, with whom I have shared many experiences, including courses, workshops, meetings in different countries and great after work moments. Prof. Marco Pierini, you have been an amazing project coordinator. Giovanni Savino and Niccolò Baldanzini, thanks for your support in the project and your support during the testing activities at the University of Florence. This project gave me the opportunity to focus on what I liked, participate to conferences and find my own way forward.

I am also grateful to have been part of the great team of fellows of the MOTORIST project. Francesco Celiberti (Ciccio), you have been the best team mate that I could ever ask for. Together we built most of the simulator, complementing each other with our skills and having fun at the same time. I want to thank you for always being a companion along the way, from the beginning as a student until the end of the project, and even after

as a friend. Oliver Lee (the Dude), thanks for technical talks about programming and for sharing with me some of the difficulties of being a Ph.D. student, I enjoyed working with you and only wished to have done more together. Natália Kováčsová, thanks for bringing your enthusiasm to our group and for our collaborations during our simulator experiment. Pedro Huertas-Leyva and Marilee Nugent, thanks for your hospitality in Florence and for your support with the measurements on the motorcycle. Thanks also to Maria, George, Gustavo, Siamak, Simon, Nasim, Tomasz, Raul, Sounak for your great research and enthusiasm in the team.

I am thankful to the Max Planck Institute for Biological Cybernetics and in particular to the director Heinrich H. Bülthoff for hosting me for five months in his research institute, where I had the honor to collaborate with great researchers. Paolo Pretto, as the leader of the Motion Perception and Simulation group I had the opportunity to work with you. Between a joke and an espresso, you pushed me to be a better researcher, focusing on the research objective and less on the pure technical challenges. Diane Cleij, thank you for your availability to support my research ideas, your dedication to your work and your great achievements are an example for me and many other researchers. Michael Katliar, thanks for the talks about MPC and for sharing your expertise in modeling and control for motion cueing. Ksander de Winkel, thanks for being an example of scientific integrity. Thanks also to Alessandro Nesti, Daniel Diers, Frank Drop, Mario Olivari, Maria and Johannes Lächele, for the good times at the MPI.

I also want to acknowledge some of the colleague who have helped me with the development of the riding simulator. In particular Oane van der Heide, for your contribution to the motorcycle model and its validation, and Leonardo Cecconi, for your support with simulator electronics. I would also like to acknowledge all the friends who have been close to me during the last years and with who I shared unforgettable moments, between a casual beer and a kicker game. I also want to thank all my volleyball friends of Calypso, for your support and encouragement.

I want to thank my family, my parents Rosa and Vincenzo, for always believing in me and supporting me with your love. Even if we have been physically distant in the last years, I have always known that you were next to me and supporting me in every step of the way. My brother Andrea, who I admire and look up to. My uncles and aunts, my cousins, and my grandparents, to whom I own a lot for being the person I am. I also want to thank Katrien and Ghislain, Delphine and Simon, Valentine and Guillaume, for being my second family in Belgium. You have welcomed me in your home and treated me as a member of the family. Finally, I would like to thank Josephine, for her endless love and support for me since the beginning of this Ph.D., you have been always there for me, especially in the difficult moments, and you have supported me in every possible way.

CURRICULUM VITÆ

MARCO GROTTOLO

Marco Grottoli was born on September 15th, 1989, in Taranto, Italy. Here he attended the scientific high school Giuseppe Battaglini from 2003 and obtained his diploma in 2008, following the experimental curriculum "National Plan of Computer studies".

In 2008, Marco enrolled in a Bachelor of Science degree in Mechanical Engineering at the Politecnico di Milano. For his bachelor's graduation he completed three separate projects: preliminary design of an axial compressor, influence of a tuned-mass damper on the vibrations of a three story building under the influence of an earthquake and the comparison of different modelling techniques to analyze a flanged joint connection with gasket. In 2011, he obtained the bachelor's degree in Mechanical Engineering, finishing the curriculum in nominal time.



In 2011, Marco continued his formation by enrolling in a Master of Science in Mechanical Engineering at the Politecnico di Milano. In 2012, he spent a period of 5 months at the Simon Fraser University of Vancouver, Canada (BC), following the summer term of the Mechatronics System Engineering Major. In 2013, he started an internship of 7 months at LMS International in Leuven, Belgium, where he worked on his master's thesis "Modelling and control techniques for driving simulators". Upon his return to Italy, he completed his last exam on Mechatronics System and graduated in 2014 with the specialization on Mechatronics and Robotics.

In October 2014, Marco was granted the Marie Skodowska-Curie fellowship and started working as an Early Stage Researcher in the EU funded research project MOTORIST on motorcycle rider integrated safety. Within the project he started working for Siemens PLM Software, Belgium, and enrolled in a PhD program at the Technical University of Delft, The Netherlands. He focused on the development and validation of a motion based motorcycle riding simulator for studying rider's behavior and training low speed maneuvering.

In November 2016, Marco started a 5 months secondment period as a Visiting Researcher at the Max Planck Institute for Biological Cybernetics in Tübingen, Germany. During this period, he investigated the limitations of MPC based motion cueing algorithm and the influence of the adopted prediction strategy on the overall perceived inertial motion quality.

Since 2018, he is a Research Engineer in Siemens Digital Industries Software, Belgium. He is involved in research projects funded by the European Commission or the government of the Flemish region of Belgium. His research focuses on: linking change of vehicle design parameters to subjective evaluation of vehicle dynamics performances using a driving simulator; pre-crash simulations of passenger postures in autonomous vehicles; verification and validation of ADAS functionalities in a driving simulator setup; influence of virtual sensing technology on durability studies using time waveform replication.

LIST OF PUBLICATIONS

JOURNAL PUBLICATIONS

1. Marco Grottooli, Diane Cleij, Paolo Pretto, Yves Lemmens, Riender Happee, and Heinrich H. Bülthoff. “Objective evaluation of prediction strategies for optimization-based motion cueing”. In: *SIMULATION* 95.8 (Dec. 2018), pp. 707–724. DOI: [10.1177/0037549718815972](https://doi.org/10.1177/0037549718815972)
2. Natália Kováčsová, Marco Grottooli, Francesco Celiberti, Yves Lemmens, Riender Happee, Marjan P. Hagenzieker, and Joost C. F. de Winter. “Emergency braking at intersections: A motion-base motorcycle simulator study”. In: *Applied Ergonomics* 82 (Jan. 2020), p. 102970. DOI: [10.1016/j.apergo.2019.102970](https://doi.org/10.1016/j.apergo.2019.102970)
3. Yash Raj Khusro, Yanggu Zheng, Marco Grottooli, and Barys Shyrokau. “MPC-Based Motion-Cueing Algorithm for a 6-DOF Driving Simulator with Actuator Constraints”. In: *Vehicles* 2.4 (Dec. 2020), pp. 625–647. DOI: [10.3390/vehicles2040036](https://doi.org/10.3390/vehicles2040036)

BOOK CHAPTERS

1. Marco Grottooli, Anne van der Heide, and Yves Lemmens. “A High Fidelity Driving Simulation Platform for the Development and Validation of Advanced Driver Assistance Systems”. In: *Reinventing Mechatronics*. Springer International Publishing, 2020, pp. 93–109. DOI: [10.1007/978-3-030-29131-0_7](https://doi.org/10.1007/978-3-030-29131-0_7)
2. Umberto Musella, Ludovico Zanellati, Marco Grottooli, Francesco Celiberti, Bart Peeters, Francesco Marulo, and Patrick Guillaume. “Driving a Motion Platform with a Vibration Control Software for Multi-Axis Environmental Testing: Challenges and Solutions”. In: *Special Topics in Structural Dynamics, Volume 5*. Springer International Publishing, May 2018, pp. 215–231. DOI: [10.1007/978-3-319-75390-4_20](https://doi.org/10.1007/978-3-319-75390-4_20)

CONFERENCE PROCEEDINGS

1. Marco Grottooli, Alessandro Toso, Marco Gubitosa, Edward Holweg, and Riender Happee. “High-Fidelity Multibody Model for a Powered-Two-Wheeler Driving Simulator”. In: *ECCOMAS Thematic Conference on Multibody Dynamics*. 2015
2. Marco Grottooli, Marco Gubitosa, Stijn Donders, Edward Holweg, and Riender Happee. “Objective Comparison of Motion Cueing Algorithms for Driving Simulator”. In: *4th Joint International Conference on Multibody System Dynamics*. 2016

3. Marco Grottoli, Francesco Celiberti, Maria Di Gesu, Sikandar Moten, and Yves Lemmens. "The MOTORIST Motorcycle Riding Simulator". In: *Bicycle and Motorcycle Dynamics*. 2016
4. Francesco Celiberti, Marco Grottoli, Maria Di Gesu, Marco Gubitosa, and Stijn Donders. "An Overview on the MOTORIST motorcycle simulator". In: *Proceedings of Driving Simulation Conference & Exhibition 2016 Europe (DSC 2016 Europe)*. 2016, pp. 219–221
5. Marco Grottoli, Francesco Celiberti, Anne van der Heide, Yves Lemmens, and Riender Happee. "Motorcycle multibody model validation for Human-in-the-Loop simulation". In: *Driving Simulation & Virtual Reality Conference & Exhibition*. 2019
6. Marco Grottoli, Anne van der Heide, and Yves Lemmens. "Impact of vehicle dynamics model fidelity in the development of ADAS". in: *NAFEMS World Congress*. 2019
7. Ali Rezajat, Marco Grottoli, Yves Lemmens, Tommaso Tamarozzi, and Christophe Liefoghe. "Influence of internal loads on the accuracy of durability tests of a vehicle on a test rig". In: *International Conference on Noise and Vibration Engineering*. 2020

REPORTS

1. Riender Happee, Arend Schwab, Marco Grottoli, Gustavo Gil, and Maria Di Gesu. *Requirements for volunteer testing of rider behaviour*. Tech. rep. MOTORIST Deliverable 2.2, 2015
2. Francesco Celiberti, Marco Grottoli, Yves Lemmens, and Sikandar Moten. *Simulator based rider modelling*. Tech. rep. MOTORIST Deliverable 2.4a, 2016
3. Natália Kováčsová, Marco Grottoli, Francesco Celiberti, Yves Lemmens, Riender Happee, Marjan P. Hagenzieker, and Joost C. F. de Winter. *Report on rider training on a motorcycle test rig*. Tech. rep. MOTORIST Deliverable 1.3, 2018
4. Francesco Celiberti and Marco Grottoli. *PTW model in safety critical manoeuvres*. Tech. rep. MOTORIST Deliverable 2.1, 2018

WORKSHOP PRESENTATION

1. Marco Grottoli and Francesco Celiberti. *The MOTORIST simulator: design and realization of a modular motorcycle simulator*. Presented at: *Safe2Wheeler - Accidentology and Motorcycle Simulator Workshop*. Apr. 2016

DATASETS AND RELATED DOCUMENTS

1. Marco Grottoli, Francesco Celiberti, Anne van der Heide, Yves Lemmens, and Riender Happee. *Motorcycle multibody model validation for HuiL simulator - Results*. 2019. DOI: [10.4121/uuid:048a3ce0-3cb8-49c5-ad4c-69e15833417e](https://doi.org/10.4121/uuid:048a3ce0-3cb8-49c5-ad4c-69e15833417e)

2. Natália Kováčsová, Maco Grotoli, Francesco Celiberti, Yves Lemmens, Riender Happee, M. P. Hagenzieker, and J. C. F. De Winter. *Supplementary data for the article: Emergency braking at intersections: A motion-base motorcycle simulator study*. en. 2019. DOI: [10.4121/UUID:6B1E0FFB-3606-4095-9702-BE34DD3C2D59](https://doi.org/10.4121/UUID:6B1E0FFB-3606-4095-9702-BE34DD3C2D59)